Nitrogen on Triton and Pluto

Kimberly A. Tryka

In Partial Fulfillment of the Requirements

for the Degree of

Doctor of Philosophy

California Institute of Technology

Pasadena, California

1995

(Submitted December 2, 1994)

To Bob and Priscilla,

From inspirational lecture #317 to fielding panic stricken calls about allergic reactions at midnight, you've endured me well beyond the call of duty, and for that I owe you a great deal.

---Kat

Acknowledgements

First, I must thank Bob Brown for the support and guidance he has offered me during the past two and a half years. Working with Bob has allowed me to explore areas of observational and laboratory research which otherwise would not have been accessible to me. More importantly, he has been willing to share his own experiences, helping me realize that many of the problems which I have found myself facing in the past few years were not unique to myself and that, with patience and perseverance, they could be surmounted.

The observational data which I have used in my thesis work would not have been available to me had it not been for the good graces of Toby Owen, Dale Cruikshank, Bob Brown, Tom Geballe, and Catherine deBergh who allowed me to participate in observations of Triton and Pluto. Additional thanks to Tom who, with great patience, let me help run the telescope (even after bringing the whole system to its knees), and without whom there probably would have been no data at all.

Finally, I thank the faculty for their forbearance while I spent large amounts of time away from campus working with Bob at JPL. That collaboration, and this thesis, could not have happened without their agreement, and I am grateful that I received it.

Abstract

Nitrogen has been detected on the surfaces of two objects in the solar system, Triton and Pluto. To better understand the surfaces of these two bodies I have made measurements of the spectrum of solid nitrogen at temperatures applicable to Triton and Pluto, over a wavelength region which encompasses both the fundamental vibrational transition of N_2, at 4.294 μm, and its first overtone, at 2.148 μm. These measurements show that the appearance of the N_2 bands is a function of temperature. I have used this temperature dependence, in conjunction with observational data and spectral modeling techniques, to determine the temperature of N_2 on Triton and Pluto. The temperature I derive for Triton, 38 ± 1 K, is in agreement with measurements made by the Voyager 2 spacecraft. The temperature determined for Pluto is 40 ± 2 K, slightly warmer than for Triton. Observations of Pluto's thermal flux have not been able to constrain Pluto's temperature well; estimates in the literature run from 30 to 60 K. To determine if the spectroscopically derived temperature for nitrogen on Pluto is consistent with the published thermal fluxes of Pluto I have modeled the expected thermal flux assuming that the N_2 is contained in symmetric polar caps and that the equatorial region is bare of nitrogen. With these assumptions I find that the modeled flux of Pluto fits all the published thermal flux measurements if the polar caps extend to $\pm 20°$ latitude, and if the equatorial region has a bolometric albedo ≤ 0.2.

Table of Contents

List of Figures

Paper 1

Paper 2

Paper 3

Appendix

List of Tables

Paper 3

Preface

This thesis, "Nitrogen in the Outer Solar System," is comprised of three papers, along with supplementary material. The three papers are: "Spectroscopic Determination of the Phase Composition and Temperature of Nitrogen Ice on Triton" by Tryka *et al.*, *Science* **261**, 751-754 (1993) © AAAS, "The Temperature of Nitrogen on Pluto and its Implications for Flux Measurements" by Tryka *et al.*, *Icarus* **112**, 513-527 (1994) © Academic Press, Inc., and "Absorption Coefficients of Nitrogen in the Regions of the Fundamental and First Overtone Bands as a Function of Temperature" by Tryka *et al.*, *Icarus* (1995) © Academic Press, Inc. (volume and page numbers were unavailable at the time of printing this document). The figures from these papers have been edited slightly to fit into the format of this document, but the text is unchanged. I was the first author on each of these works and, although these works have multiple authors, I was responsible for the work reported in them, with the following exceptions. The original idea for the infrared spectroscopic measurements of solid N_2 was Dr. R.H. Brown's. He, Dr. V. Anicich, and Dr. J.R. Green were responsible for designing the laboratory set up and conducting preliminary measurements. The observations of Triton and Pluto which I use in my thesis were made during time awarded to Dr.'s T.C. Owen, D.P. Cruikshank, R.H. Brown, C. deBergh, and T.R. Geballe. Dr. Geballe was responsible for the preliminary reduction of the telescopic data.

The appendix on spectral modeling is intended to be a brief review of spectral modeling techniques, and to demonstrate how varying specific parameters effects the modeled spectrum. Because of space constraints in journals this information was not included in any of the papers making up this thesis, but it may be of interest to the reader.

Introduction

Recently, there have been great advances in our knowledge of Triton and the Pluto/Charon system as a result of unique observational events. The Voyager 2 flyby of Triton gave us a close-up view of that planet, showing us a world which is geologically active, as demonstrated by the plumes seen in the southern hemisphere, and which has many regions of varied appearance. The mutual occultations and eclipses that Pluto and its satellite Charon have recently undergone have transformed those bodies from two inseparable sources to two unique objects with well defined radii and different surface compositions. In this introduction I will review our current knowledge of these two bodies, particularly, those topics relevant to understanding the research which is presented in this thesis.

Triton Background

Triton was discovered by William Lassell in 1846, just a few weeks after the discovery of Neptune. It was soon determined that Triton orbited Neptune in a retrograde orbit, with a period of ≈ 5.8 days. The direction and high inclination of this orbit have given rise to much speculation about the origins of Triton, including various impact and capture scenarios, many involving Pluto. Currently, the most widely accepted scenario is that Triton was captured into its orbit around Neptune (Farinella *et al.* 1980, McKinnon 1984).

Because of Triton's relatively small size and distance from the Earth, it was difficult to determine physical properties, such as radius and albedo, from ground-based observations. Using measurements of Triton's thermal flux, Lebofsky (1979) estimated Triton's radius and bolometric albedo to be 1750 ± 250 km and 0.4, respectively. The mass of Triton had been calculated by

different researchers with differing results (see Cruikshank and Brown 1986 for a summary), in all cases giving a density that was unrealistically high (6 g/cm^{-3} or greater, using the radius determined by Lebofsky (1979)).

Spectroscopic observations identified methane (Cruikshank *et al.* 1979) and possibly nitrogen (Cruikshank *et al.* 1984) on the surface of Triton. Because nitrogen has such weak bands in the infrared, calculations determined that very long pathlengths were needed to produce the observed absorption. This, in conjunction with a temperature for Triton of ≈ 60 K (assuming a bolometric albedo of 0.4 and thermodynamic equilibrium) lead to speculation that Triton was covered by a nitrogen ocean (Cruikshank *et al.* 1984). Lunine and Stevenson (1985) argued that the simplest configuration of volatiles, from the view of phase equilibrium, was for the N_2 and CH_4 to be in solid state.

In August of 1989 Voyager 2 passed by Triton during its flyby of the Neptunian system. Images from the visible camera revealed a unique world with active plumes, wind streaks, many different types of surface structure, and a very bright surface, albedos >0.8 over most of the imaged surface (Smith *et al.* 1989). The radius of the planet was found to be 1350 ± 5 km, and its bulk density was measured at 2.075 g/cm^3. The surface temperature was measured to be 38 (+4, -3) K (Conrath *et al.* 1989) and the surface pressure was inferred to be 14 ± 1 μbar (Broadfoot *et al.* 1989). These values of surface temperature and surface pressure imply a system where nitrogen ice and a nitrogen atmosphere are in vapor pressure equilibrium. One result of such a system is that any surfaces covered with N_2 ice would be buffered to an isothermal temperature, regardless of their position on the planet.

The apparent vapor pressure equilibrium of nitrogen on the surface, combined with images of Triton showing some regions of the surface to be brighter than others, lead researchers to try to understand the transport of volatiles on Triton. Modeling by Spencer *et al.* (1990)

shows that long term volatile transport is toward the poles, which receive the least amount of solar insolation on seasonal timescales. A more complex model by Brown and Kirk (1994), taking into account the viscous spread of N_2 polar caps, demonstrates that, depending on initial volatile inventory, it is possible for Triton to have permanent polar deposits, while seasonal layers of volatiles would increase polar cap extents during winter seasons.

Recently, we have learned more about the surface composition of Triton from ground-based spectral observations. Cruikshank *et al.* (1991, 1993) observed Triton at greatly increased spectral resolution ($\lambda/\Delta\lambda$ of ≈ 300 as opposed to ≈ 50 for previous measurements). The observations resolved methane bands which were previously blended, made possible the identification of CO and CO_2 in the spectrum, and revealed detail in the N_2 band which allowed the temperature of the nitrogen to be determined, based on the shape of the band (Papers 1 and 2 of this thesis).

Pluto Background

Pluto was discovered in 1930 by Clyde Tombaugh at Lowell Observatory. Given its very faint appearance, very little was known about Pluto until advances in telescopic instrumentation in the 1970's made observations more practical. Most of what was known about Pluto centered on its orbital parameters.

The first spectroscopic identification of a component of Pluto's surface was made by Cruikshank *et al.* (1976) when they detected methane in the infrared region of Pluto's spectrum. Methane was also detected later by Fink *et al.* (1980) in the region of 0.6 to 1.0 μm. Some of the bands detected in this region indicated the presence of solid CH_4 on the surface, as well as CH_4 gas in Pluto's atmosphere. Photometric observations of Pluto indicated that its spectrum was

reddish (Bell *et al.* 1979, Barker *et al.* 1980). Because methane ice does not have a reddish color, these observations indicate the presence of an unidentified absorber on Pluto's surface.

In 1978 Pluto's satellite, Charon, was discovered by James Christie, working at the U.S. Naval Observatory. The timing of this discovery fortuitous; calculations of the orbits of the two bodies showed that within the next few years Pluto and Charon would begin to undergo a series of mutual occultations and eclipses (as seen from Earth). These "mutual events" enabled researchers to determine accurate radii and orbital elements (Buie *et al.* 1992) for the two bodies and to map albedo variations on both bodies (Buie *et al.* 1992 , Young and Binzel 1993).

A stellar occultation by Pluto also allowed the determination of the molecular weight of the atmosphere, and the surface pressure and radius of Pluto (Yelle and Lunine 1989, Millis *et al.* 1993, Hubbard *et al* 1990).

The same advances in spectroscopic resolution that allowed the identification of CO and CO_2 on Triton made it possible to identify N_2 and CO on the surface of Pluto (Owen *et al.* 1993).

Although our knowledge of Pluto has greatly increased as a result of the mutual events, there is one quantity which they have not shed light on: the temperature of Pluto. Thermal flux measurements of Pluto at infrared and millimeter wavelengths have yielded conflicting temperature results. The infrared measurements (Sykes *et al.* 1987, Aumann and Walker 1987), made by the Infrared Astronomical Satellite (IRAS), yield relatively warm temperatures (50-60 K) while the millimeter measurements (Altenhoff *et al.* 1988, Stern *et al.* 1993, Jewitt 1994) yield colder temperatures (30-40 K). With the detection of N_2 in the spectrum there is the possibility of determining the temperature of Pluto, in a manner independent of thermal flux measurements. Paper 3 speaks to the issue of determining the temperature of N_2 on Pluto and reconciling this temperature with the various flux measurements discussed above.

References

Altenhoff, W.J., R. Chini, H. Hein, E. Kreysa, P.G. Mezger, C. Salter, and J.B. Schraml 1988. First radio astronomical estimate of the temperature of Pluto. *Astron. and Astrophs.* **190**, 15-17 (letter).

Aumann, H.H. and R.G. Walker 1987. IRAS observations of the Pluto-Charon system. *Astron. J.* **94**, 1088-1091.

Barker, E.S., W.D. Cochran, and A.L. Cochran 1980. Spectrophotometry of Pluto from 3500 to 7350 Angstroms. *Icarus* **44**, 43-52.

Bell, J.F., R.N. Clark, T.B. McCord, and D.P. Cruikshank 1979. Reflection spectra of Pluto and three distant satellites. *Bull. Amer. Astron. Soc.* **11**, 570.

Broadfoot, A.L., S. K. Atreya, J. L. Bertaux, J. E. Blamont, A. J. Dessler, T. M. Donahue, W. T. Forrester, D. T. Hall, F. Herbert, J. B. Holberg, D. M. Hunten, V. A. Krasnopolsky, S. Linick, J. I. Lunine, J. C. McConnell, H. W. Moos, B. R. Sandel, N. M. Schneider, D. E. Shemansky, G. R. Smith, D. F. Strobel, and R. V. Yelle 1989. Ultraviolet spectrometer observations of Neptune and Triton. *Science* **246**, 1459-1466.

Brown, R.H., and R.L. Kirk 1994. Coupling of volatile transport and internal heat flow on Triton. *J. Geophys. Res.* **99**, 1965-1981.

Buie, M.W., D.J. Tholen, K. Horne 1992. Albedo maps of Pluto and Charon: Initial mutual event results. *Icarus* **97**, 211-227.

Conrath, B., F. M. Flasar, R. Hanel, V. Kunde, W. Maguire, J. Pearl, J. Pirraglia, R. Samuelson, P. Gierasch, A. Weir, B. Bezard, D. Gautier, D. Cruikshank, L. Horn, R. Springer, and W. Shaffer 1989. Infrared observations of the Neptunian system. *Science* **246**, 1454-1459.

Cruikshank, D.P., C.B. Pilcher, D. Morrison 1976. Pluto: Evidence for methane frost. *Science* **194**, 835-836.

Cruikshank, D.P., A. Stockton, H.M. Dyck, E.E. Becklin and W. Macy 1979. The diameter and reflectance of Triton. *Icarus* **40**, 104-114.

Cruikshank, D.P., R.H. Brown, and R.N. Clark 1984. Nitrogen on Triton. *Icarus* **58**, 293-305.

Cruikshank, D.P. and R.H. Brown 1986. The outer solar system. In *Satellites*, (J.A. Burns and M.S. Matthews, Eds.), Univ. Arizona Press, Tucson.

Cruikshank, D.P., T.C. Owen, T.R. Geballe, B. Schmitt, C. de Bergh, J-P. Maillard, B.L. Lutz, and R.H. Brown 1991. Tentative detection of CO and CO_2 ices on Triton. *Bull. Amer. Astron. Soc.* **23**, 1208.

Cruikshank, D.P., T.L. Roush, T.C. Owen, T.R. Geballe, C. deBergh, B. Schmitt, R.H. Brown, and M.J. Bartholomew 1993. Ices on the surface of Triton. *Science* **261**, 742-745.

Farinella, P., A. Milani, A.M. Nobili, and G.B. Valsecchi 1980. Some remarks on the capture of Triton and the origin of Pluto. *Icarus* **44**, 810-812.

Fink, U., B.A. Smith, S.C. Benner, J.R. Johnson, H.J. Reitsema, and J.A. Westphal 1980. Detection of a CH_4 atmosphere on Pluto. *Icarus* **44**, 62-71.

Hubbard, W.B., R.V. Yelle, and J.I. Lunine 1990. Nonisothermal Pluto atmosphere models. *Icarus* **84**, 1-11.

Jewitt, D.C. 1994. Heat from Pluto. *Astronomical J.* **107**, 372-378.

Lebofsky, L.A., G.H. Rieke, and M.J. Lebofsky 1979. Surface composition of Pluto. *Icarus* **37**, 554-558.

Lunine, J.I. and D.J. Stevenson 1985. Physical state of volatiles on the surface of Triton. *Nature* **317**, 238-240.

McKinnon, W.B. 1984. On the origin of Triton and Pluto. *Nature* **311**, 355-358.

Millis, R. L., L. H. Wasserman, O. G. Franz, R. A. Nye, J. L. Elliot, E. W. Dunham, A. J. Bosh, L. A. Young, S. W. Slivan, A. C. Gilmore, P. M. Kilmartin, W. H. Allen, R. D. Watson, S. W. Dieters, K. M. Hill, A. B. Giles, G. Blow, J. Priestly, W. M. Kissling, W. S. G. Walker, B. F. Marino, D. G. Dix, A. Page, J. E. Ross, M. D. Kennedy, K. A. Mottram, G. Mayland, T. Murphy, C. C. Dohn, and A. R. Klemola 1993. *Icarus* **105**, 282-297.

Owen, T.C. T.L. Roush, D.P. Cruikshank, J.L. Elliot, L.A. Young, C. deBergh, B. Schmitt, T.R. Geballe, R.H. Brown, and M.J. Bartholomew 1993. Surface Ices and Atmospheric Composition of Pluto. *Science* **261**, 745-748.

Smith, B.A., L.A. Soderblom, D. Banfield, C. Barnet, A.T. Basilevsky, R.F. Beebe, K. Bollinger, J.M. Boyce, A. Brahic, G.A. Briggs, R.H. Brown, C. Chyba, S.A. Colling, T. Colvin, A.F. Cook II, D. Crisp, S.K. Croft, D. Cruikshank, J.N. Cuzzi, G.E. Danielson, M.E. Davies, E. De Jong, L. Dones, D. Godfrey, J. Goguen, I. Greinier, V.R. Haemmerle, H. Hammel, C.J. Hansen, C.P. Helfenstein, C. Howell, G.E. Hunt, A.P. Ingersoll, T.V. Johnson, J. Kargel, R. Kirk, D.I. Kuehn, S. Limaye, H. Masursky, A. McEwen, D. Morrison, T. Owen, W. Owen, J.B. Pollack, C.C. Porco, K. Rages, P. Rogers, D. Rudy, C. Sagan, J. Schwartz, E.M. Shoemaker, M Showalter, B. Sicardy, D. Simonelli, J. Spencer, L.A. Sromovsky, C. Stoker, R.G. Strom, V.E. Suomi, S.P. Synott, R.J. Terrile, P. Thomas, W.R. Thompson, A. Verbiscer, J. Veverka 1989. Voyager 2 at Neptune: Imaging science results. *Science* **246**, 1422-1449.

Spencer, J.R. 1990. Nitrogen frost migration on Triton: A historical perspective. *Geophys. Res. Let.* **17**, 1769-1772.

Stern, S.A., D.A. Weintraub, M.C. Festou 1993. Evidence for a low surface temperature on

Pluto from millimeter-wave thermal emission measurements. *Science* **261**, 1713-1716.

Sykes M.V., R.M. Cutri, L.A. Lebofsky, and R.P. Binzel 1987. IRAS serendipitous survey of observations of Pluto and Charon. *Science* **237**, 1336-1340.

Yelle, R.V. and J.I. Lunine 1989. Evidence for a molecule heavier than methane in the atmosphere of Pluto. *Nature* **339**, 228-290.

Young, E.F. and R.P. Binzel 1993. Comparative mapping of Pluto's sub-Charon hemisphere: Three least squares models based on mutual event lightcurves. *Icarus* **102**, 134-149.

Paper 1:

Near-Infrared Absorption Coefficients of Solid Nitrogen as a Function of Temperature

Kimberly A. Tryka
Division of Geological and Planetary Science
California Institute of Technology
MS 170-25
Pasadena, California 91125

Robert H. Brown
Jet Propulsion Laboratory
4800 Oak Grove Drive
MS 183-501
Pasadena, California 91109

Vincent Anicich
Jet Propulsion Laboratory
4800 Oak Grove Drive
MS 183-601
Pasadena, California 91109

Abstract

We present the results of laboratory measurements characterizing the near infrared spectrum of solid nitrogen at temperatures between 35 and 60 K. The measurements show that the appearance of the spectrum in the regions of both the fundamental vibrational transition, and its first overtone, are temperature dependent. The temperature dependence of the spectrum in the overtone region provides a means to determine the temperature of N_2 ice on solar system objects using ground based spectroscopy.

Introduction

Solid nitrogen has multiple phases (Scott, 1976), two of which are relevant to outer solar system objects. The ß phase exists at temperatures between 35.6 K and 63.15 K (the triple point of N_2) and is a hexagonal solid. The higher density, cubic α phase exists at temperatures below 35.6 K.

N_2 is a symmetric linear molecule and has no allowed dipole transitions. However, when a dipole moment is induced, N_2 shows a fundamental vibrational transition at 4.294 μm, with the first overtone in the region of 2.15 μm. The overtone region falls in a transparent portion of the telluric spectrum, whereas ground-based observations of the fundamental are prohibited by CO_2 absorption in the Earth's atmosphere. Therefore, N_2 can only be identified spectroscopically, from the ground, on the basis of the absorption seen in the overtone region.

Previous work has shown that, in the α-phase, N_2 shows significant absorption, due to vibron-phonon interactions (Jodl *et al.* 1987), near the fundamental vibrational transition, and that the appearance of the bands in this region is temperature dependent (Löwen *et al.* 1990). Raman

studies of the same temperature and wavelength region confirm this result (Pangilinan *et al.* 1989, Löwen *et al.* 1990). In these studies neither the ß phase (i.e. temperatures above 35.6 K) nor the wavelength region of the first overtone were examined.

Infrared measurements of the overtone region (Green *et al.* 1991) have shown that as the N_2 passes from the ß to the α phase, the appearance of the spectrum changes drastically. In the ß phase the band at 2.148 μm is shallow ($\approx$ 2% absorption) and broad (FWHM $\approx$ 60 cm^{-1}), while in the α phase it is much deeper ($\approx$ 12% absorption) and narrower (FWHM $\approx$ 1 cm^{-1}).

Ground-based spectroscopy has identified solid nitrogen on the surfaces of two bodies in the outer solar system: Triton (Cruikshank *et al.* 1984, Cruikshank *et al.* 1993) and Pluto (Owen

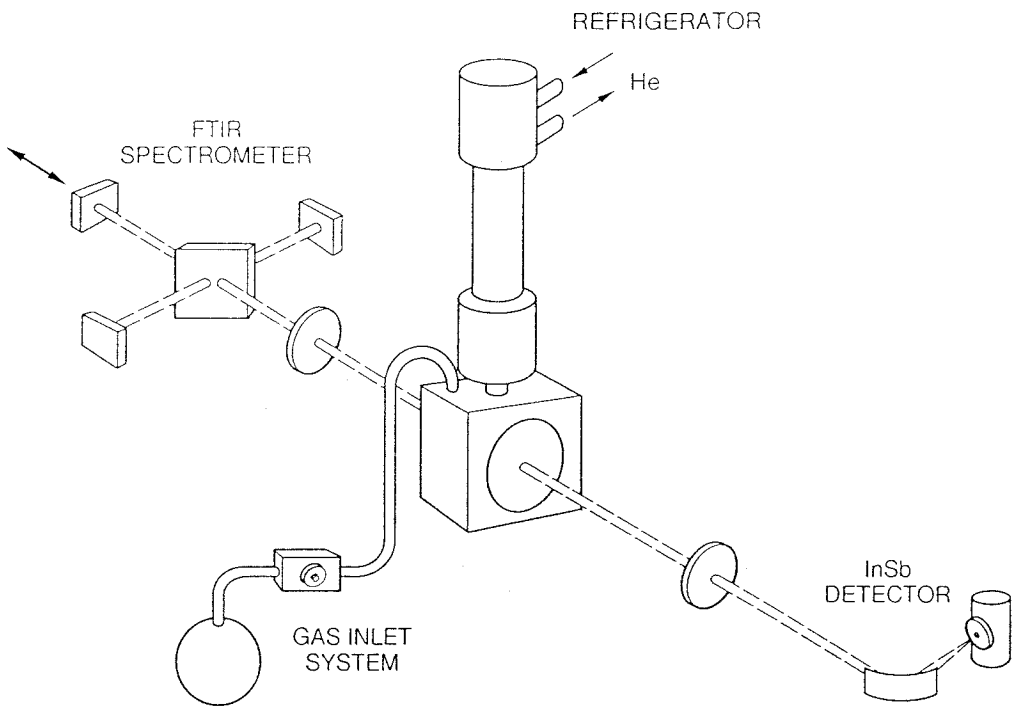

Figure 1. A schematic representation of the laboratory set up for measuring the infrared spectrum of solid nitrogen. More specific information, regarding the instruments and the conditions during the measurements are given in the text.

et al. 1993). For both bodies, the identification of N_2 was based on the presence of a weak absorption at ≈ 2.15 μm, corresponding to the first vibrational overtone of nitrogen. Although the temperature of Triton, 38 K, was determined by the Voyager 2 spacecraft (Conrath *et al.* 1989), estimates of the temperature of Pluto cover a broad range, 30-60 K (Sykes *et al.* 1987, Altenhoff *et al.* 1988, Stern *et al.* 1993, Jewitt 1994). The laboratory measurements presented here were made in the hope of being able to determine the phase of nitrogen on Triton and Pluto, based on their spectral signatures. For Triton this determination would be an independent confirmation of the Voyager temperature results, while for Pluto the determination of the phase of N_2 would be an important step in determining the temperature of the planet. To that end, we have measured the spectrum of N_2 from 1-5 μm over the range of 35-60 K. Similar measurements were made simultaneously by Grundy *et al.* (1993), and are in agreement with our data.

Experimental Apparatus

The laboratory work presented here was carried out at the Extraterrestrial Ice Facility at the Jet Propulsion Laboratory in Pasadena, California. The equipment consisted of a Fourier transform spectrometer, a closed-cycle helium refrigerator, a temperature controller and a vacuum chamber. Figure 1 shows a schematic representation of the experimental setup.

The spectrometer was a Mattson Galaxy Series Fourier transform spectrometer, capable of operation from the ultraviolet to the far infrared. We measured the transmission spectrum of N_2 in the near infrared region, from 2000-10000 cm^{-1} (1-5 μm). The data were recorded every 0.5 cm^{-1}, resulting in a resolution of 1 cm^{-1} (0.00046 μm at 2.15 μm). To optimize the measurements in the region of the N_2 overtone, the spectrometer was outfitted with a CaF_2

beamsplitter, a quartz halogen lamp, and an InSb detector.

A plot of the instrument response function is shown in Fig. 2. This measurement was made with an empty sample cell, cooled to 50 K. The response is relatively smooth and peaks in the region of the first overtone band of N_2, then drops off rapidly in the region of the fundamental, mostly due to detector and light source rolloff. Because the fundamental is much stronger than the overtone, the drop in instrument response at longer wavelengths does not compromise the measurement of the fundamental. The broad features, such as that between 2.5 and 3.0 μm, are characteristic of the system and are easily removed during the background correction. Small narrow features, such as those at $\approx$ 2.6 μm, are due to imperfect purging of atmospheric gases from the path of the beam, and are time variable. However, they do not fall in the region of the overtone, and those near the fundamental, being weaker, cause no confusion.

Because the N_2 overtone is very weak, spectra cannot be measured through a thin film of N_2 ice on a cold window, as is the case for more absorbing substances. Rather, we used a long copper cell which gave an optical pathlength of 2.54 cm through the sample. The cell was cooled by a He refrigerator, and the temperature was regulated by a Lake Shore DRC-93CA temperature controller and a 50 Ω heater. A platinum resistance thermometer was mounted on the exterior of the cell to measure the temperature of the sample.

Because it wasn't possible to place the temperature probe in the sample, there was a slight difference between the temperature of the probe and the temperature of the sample. To quantify this difference the temperature controller was calibrated using two points: the triple point of nitrogen (63.15 K) and the temperature of the α-ß phase transition (35.6 K). The triple point reading was determined by condensing a small amount of nitrogen in the cell and raising and lowering its temperature, choosing the triple point reading on the basis of the vapor pressure and appearance (liquid or solid) of the nitrogen. We used the appearance of the first overtone band

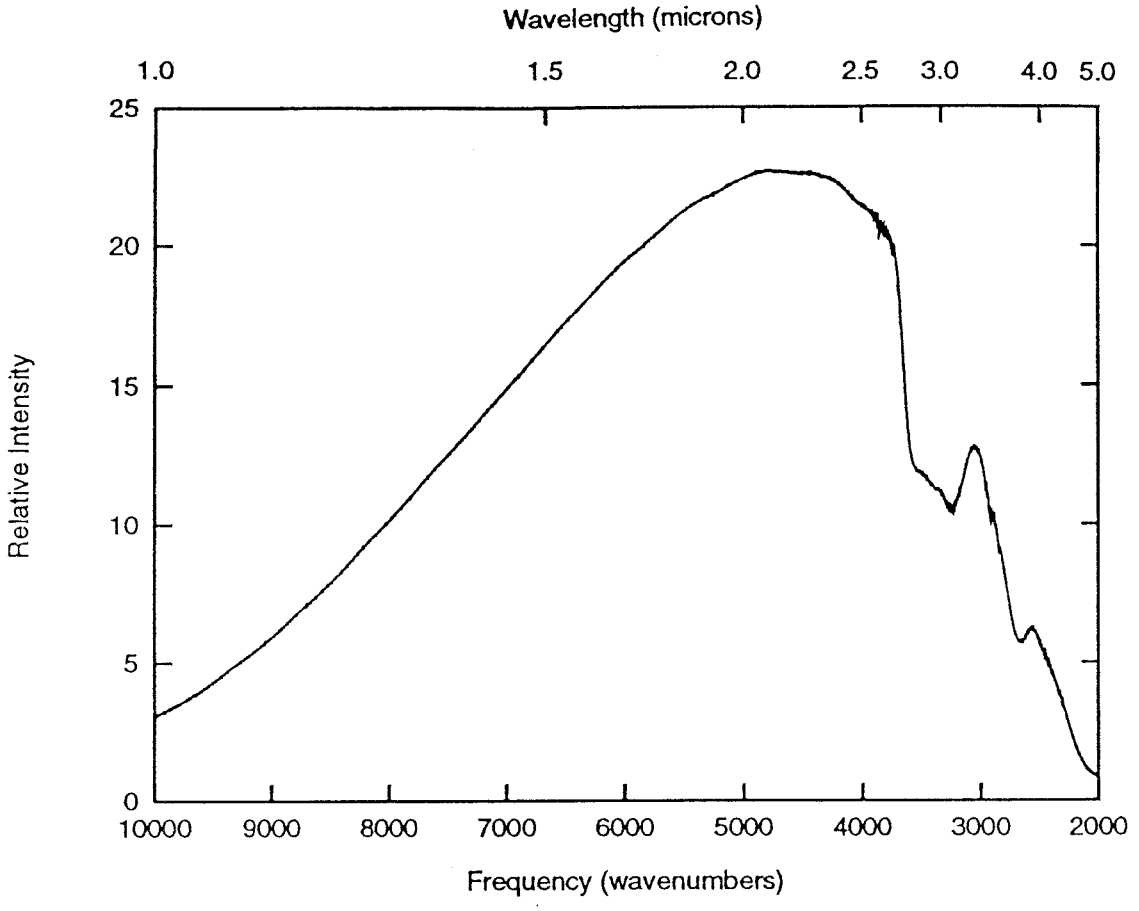

Figure 2. Plot of the instrument response function between 1-5 μm. The measurement was made under the same conditions as the measurements of nitrogen, except that the sample cell was empty.

to determine when the sample had transitioned from ß to α. Given an intermediate reading, a linear extrapolation between these two reference points determined the temperature of the sample.

The nitrogen used to form the sample was supplied by Alphagaz and was quoted as being 99.999% contaminant free. Because helium, of lower purity was introduced into the system (as will be described later) we inserted a cold trap in the line leading to the sample cell, to filter out contaminants. If impurities were included in the sample they were not spectrally significant.

Samples of solid N_2 were formed by first cooling the cell to $\approx$ 65 K and condensing liquid N_2 in the cell. In order to keep the input line from being blocked with solid N_2 as the

sample was cooled, the cell was not completely filled.

To cool the sample through the triple point and form an optically clear solid we had to pressurize the cell with approximately an atmosphere of helium. Without this overpressure, as the sample began to freeze inward from the cell walls, it would also begin to freeze around the void space at the top of the sample. From this void space a hollow tube would form, growing in length, and changing direction at obstacles, as the sample continued freezing. Such a sample had an optically clear edge, but the bulk of the sample was opaque. When we pressurized the cell with helium before starting the cooling, a void space formed in the sample, but was confined to a small area at the top of the sample, leaving the remaining portion of the sample optically clear.

There are many reports in the literature (Scott, 1976) which describe the difficulty of cooling a sample of solid N_2 through the α-ß phase transition without cracking it. These reports suggest that slow cooling rates mitigate the problem. We cooled our sample at a rate of 0.02 K per minute and, even at this slow cooling rate, the sample began to show discrete cracks at 45 K, while remaining optically clear. These fractures became more extensive as the temperature was lowered until, below the α-ß phase transition temperature, the sample had a translucent appearance in transmitted light and appeared dark in reflected light. As the sample became more fractured, light was scattered out of the path of the detector (i.e., scattering caused the output beam to diverge), resulting in an increased noise level, which is apparent in the plots of the data.

Results

The results of our measurements are shown in Fig. 3(a and b), for the region of the fundamental, and Fig. 4(a-d), for the overtone region. For all of these figures the relative

absorption coefficient is plotted as a function of wavelength, for the indicated temperatures. Because of the large number of data points, error bars are not shown. Rather, we have included portions of the continuum on each side of the nitrogen bands. The scatter in the continuum is indicative of the noise level of the data.

The absorption coefficients were derived from our transmission data by first normalizing the data to be 1 in the continuum region. This normalization is what makes the final absorption coefficient a relative, rather than an absolute, quantity. Transmittance was converted to absorption coefficient using the relation

$$I(\lambda) = I_0(\lambda) e^{-\alpha(\lambda)x}$$

where I_0 is the initial intensity of the signal, I is the signal at the detector, α is the absorption coefficient, and x is the thickness of the sample.

As stated previously, when the nitrogen sample was at low temperatures, particularly below the α-ß phase transition temperature, it contained many more scattering centers than it had at higher temperatures. This raises the question of whether the measurements at lower temperatures are an accurate representation of the absorption coefficient of the sample. The absorption coefficient is related to the extinction coefficient, ξ, which includes all possible means of attenuation, through the bolometric hemispheric albedo, A,

$$\alpha(\lambda) = \frac{(1-A)}{(1+A)} \xi(\lambda).$$

If the value of A is small (i.e. little radiation is reflected from the sample) the absorption coefficient and the extinction coefficient are nearly identical. Our sample was dark in reflected light indicating that the scattering occurring in the sample is primarily forward scattering. Such scattering will primarily act to diverge the exit beam, resulting in a less intense signal at the detector, but will add little additional pathlength to the average photon's travel. Thus, even in

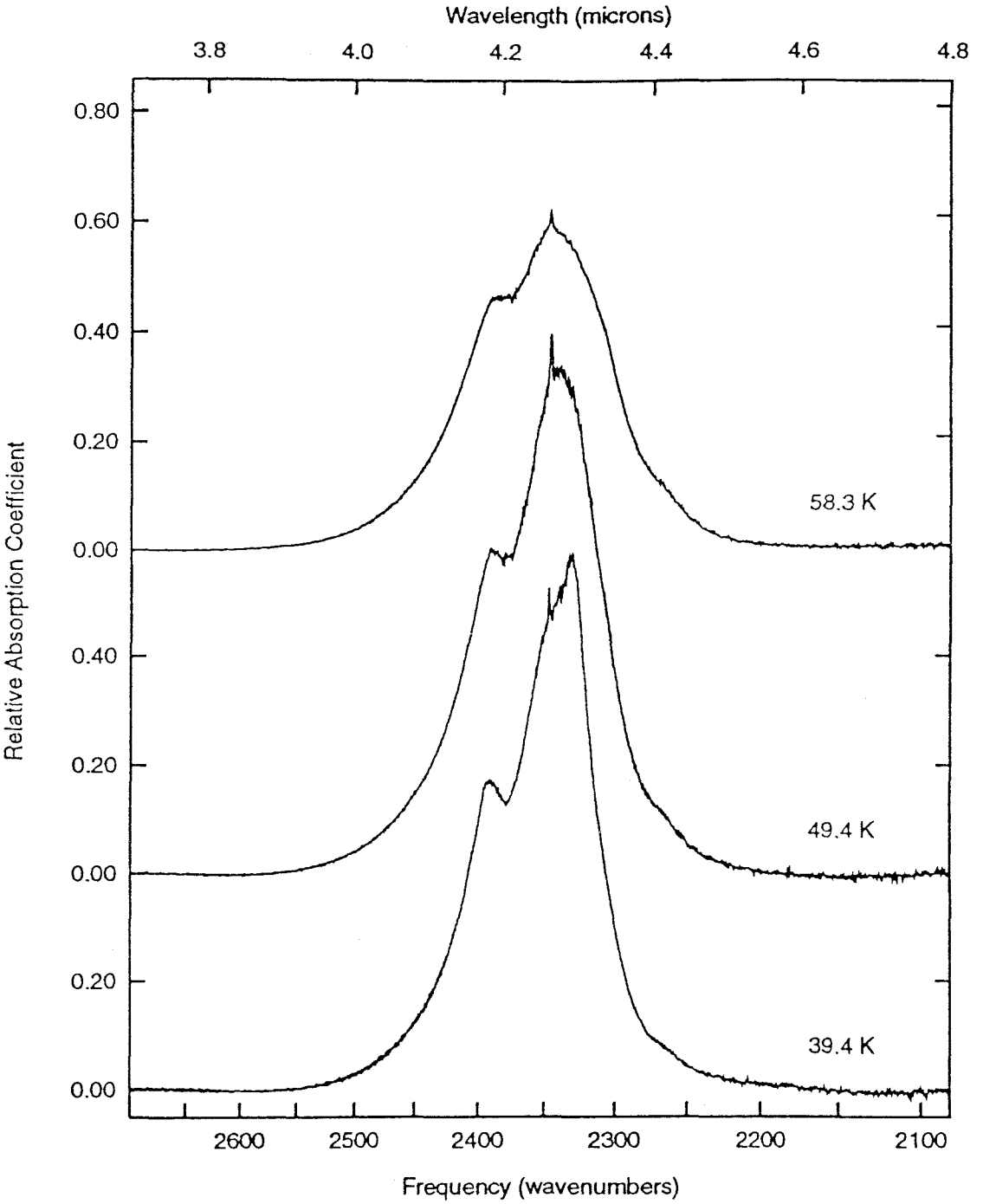

Figure 3(a)

Figure 3. The absorption coefficient for the region around the fundamental vibrational transition (4.294 μm) of solid N_2. Part (a) temperatures of 58.3, 49.4, and 39.4 K. Part (b) temperatures of 36.8, 35.7, and 35.6 K.

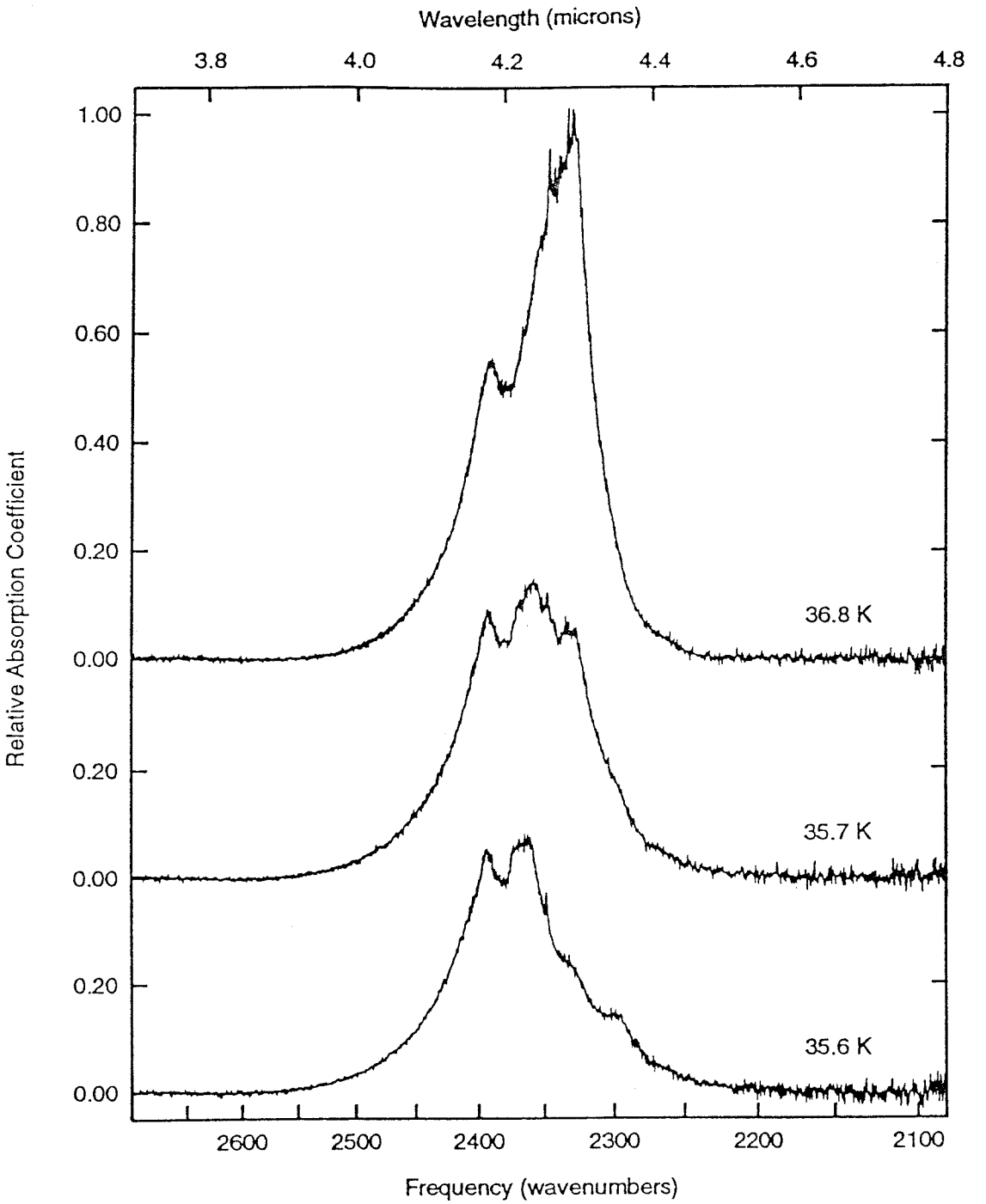
Wavelength (microns)
3.8
4.0
4.2
4.4
4.6
4.8
1.00
0.80
0.60
0.40
0.20
0.00
0.20
0.00
0.20
0.00
Relative Absorption Coefficient
36.8 K
35.7 K
35.6 K
2600
2500
2400
2300
2200
2100
Frequency (wavenumbers)

Figure 3(b)

samples showing large amounts of fracturing, we believe that the absorption coefficient presented here is an accurate representation of the true absorption coefficient.

Figure 3 shows the relative absorption coefficient spectrum of the fundamental region for temperatures ranging from 60 to 35 K. The increase in the noise level at longer wavelengths is due to the rapid decrease of the instrument response function at these wavelengths (Fig. 2). There is very little overlap in temperature coverage between our data and the infrared data presented by Löwen *et al.* (1990), but at 37 K (the highest temperature data they present) their data show two broad bands, the stronger one located at 2330 cm^{-1} (4.292 μm) and the weaker at $\approx$2400 cm^{-1} (4.167 μm). Our data (at slightly higher and lower temperatures) show two broad bands in the same locations. As temperatures drop, the Löwen *et al.* (1990) data indicate that the band at 2330 cm^{-1} weakens, but then becomes a stronger, narrower absorption at colder temperatures (20 K). Our data were not taken at such low temperatures, but they do show that the band at 2330 cm^{-1} begins to weaken below the α-ß phase transition temperature. Above 37 K our data show that the two bands at 2400 and 2330 cm^{-1} become broader as the temperature of the sample rises, with the 2330 cm^{-1} band diminishing in intensity.

Also present in the plots in Fig. 3 is a feature at about 2345 cm^{-1} (4.264 μm), most easily seen in the 58.3 K spectrum. The wavelength of the feature shifts slightly from spectrum to spectrum. The intensity of the feature is not constant: it is a maximum in the 49.4 K spectrum, is similar in intensity to many other features in the 36.8 K spectrum, and is nearly in the noise of two lowest temperature spectra. The wavelength of this feature is near that of a CO_2 absorption. Because of the variability of the feature we are not convinced that it is due to CO_2, but we admit the possibility that it could be. If it is, we do not believe that it is a contaminant within the N_2 sample, but rather that it is due to atmospheric gas condensed on the outside of the cell windows. A small layer could build up on the outside of the cell because of the long time

which the sample was kept frozen in the cell (sometimes as long as 36 hours). Such a layer outside the cell would produce a small absorption in addition to the N_2 absorption, but would not affect the N_2 spectrum.

Figure 4 shows a series of spectra taken in the overtone region, over a temperature range of 35-60 K. These data confirm the change in band shape as the nitrogen passes from the ß to the α phase. More interesting is that, like the bands in the region of the fundamental, the shape of the bands in the overtone region change with temperature while in the ß phase. This change is gradual, compared to the abrupt change at the phase transition, but it indicates that the shape of the N_2 band at 2.148 μm can be used as a thermometer to determine the N_2 temperature on solar system objects if telescopic spectra of sufficient resolution are available. Additionally, the data show a sideband at $\approx$ 2.16 μm (4630 cm $^{-1}$), appearing over a limited temperature range, $\approx$ 41 K and 35.6 K.

Comparison of our measurements of the overtone region with measurements of ß nitrogen made by Grundy *et al.* (1993) show the two data sets to be quite similar. The same authors also present spectra of α N_2, mostly taken at temperatures colder than our measurements, showing structure in the regions of 4700 cm^{-1} (2.128 μm) and 4620 cm^{-1} (2.165 μm). Our data (lowest temperature 35.5 K) do not show such structure, but, as the bands in the Grundy *et al.* (1993) data are temperature dependent, growing stronger with decreasing temperature, we feel that the two data sets are consistent.

Spectral observations (Cruikshank *et al.* 1993) show that the 2.16 μm sideband is present in the Triton spectrum. Analysis of that data shows that the temperature of the N_2 on Triton is 38.0$\pm$1 K (Tryka *et al.* 1993, 1994). Using similar data for Pluto, Tryka *et al.* (1994) have determined that the temperature of N_2 on that body is 40.0$\pm$2 K.

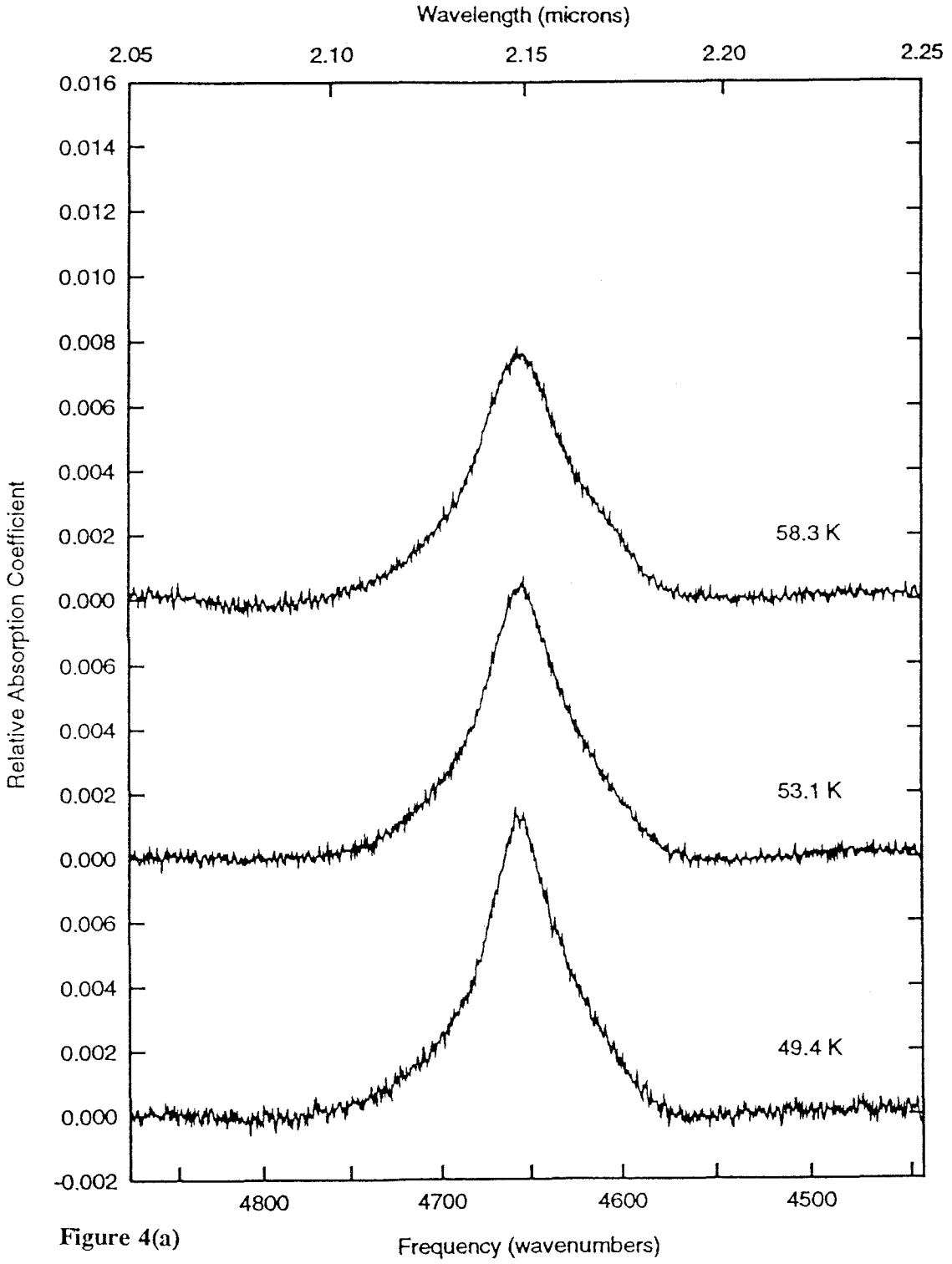

Figure 4(a)

Figure 4. The absorption coefficient in the region around the first overtone band of N_2 (2.148 μm). Temperatures of (a) 58.3, 53.1, and 49.4 K (b) 44.2, 41.4, and 39.4 K (c) 38.1, 37.5, and 36.8 K (d) 35.7 and 35.6 K. Notice that the peak absorption increases as temperature decreases, while the width of the absorption decreases as temperature decreases. Also a side band ($\approx$ 2.16 μm) is visible at temperatures between 36.6 and 41 K.

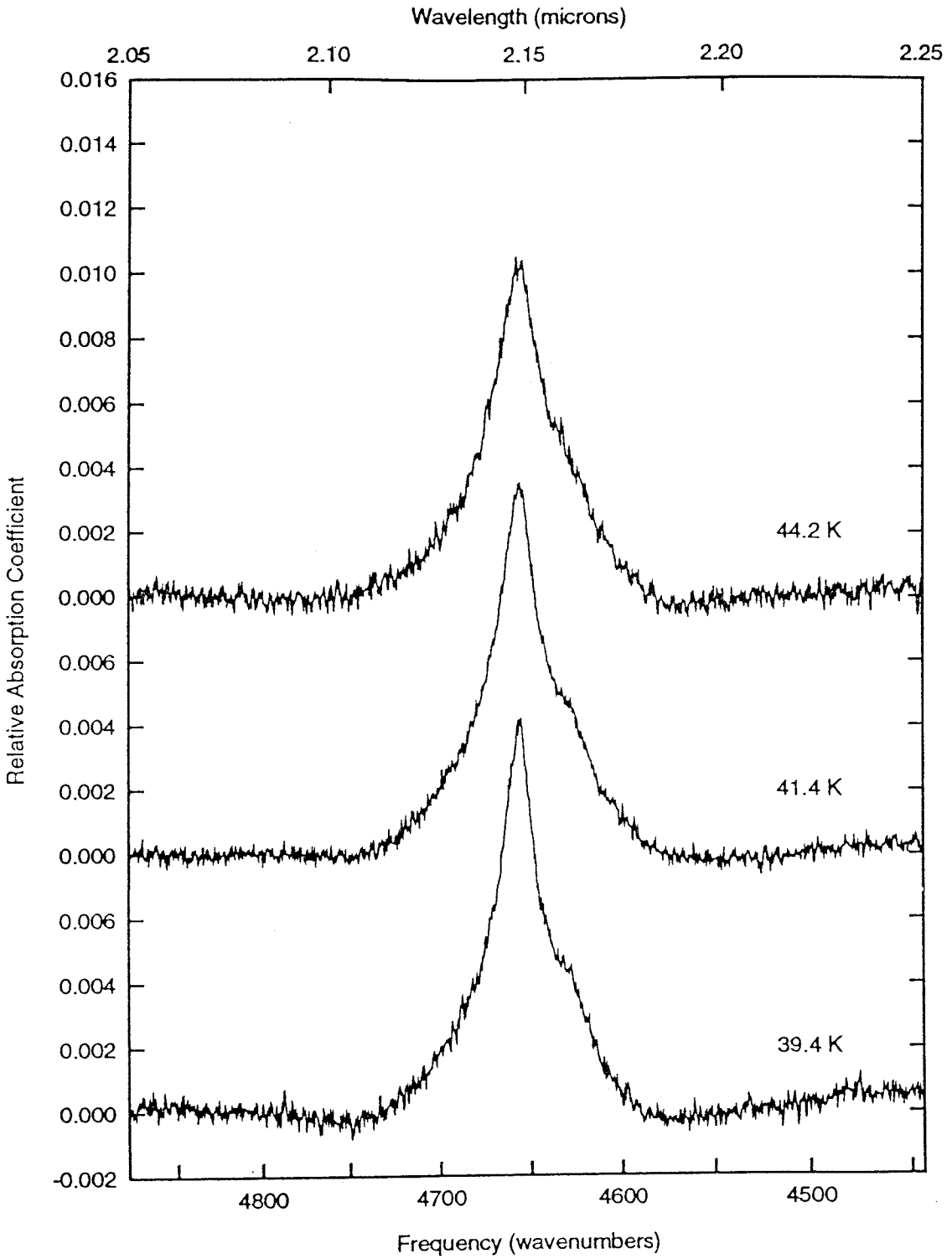
Wavelength (microns)
2.05
2.10
2.15
2.20
2.25
0.016
0.014
0.012
0.010
0.008
0.006
0.004
0.002
0.000
0.006
0.004
0.002
0.000
0.006
0.004
0.002
0.000
-0.002
Relative Absorption Coefficient
44.2 K
41.4 K
39.4 K
4800
4700
4600
4500
Frequency (wavenumbers)

Figure 4(b)

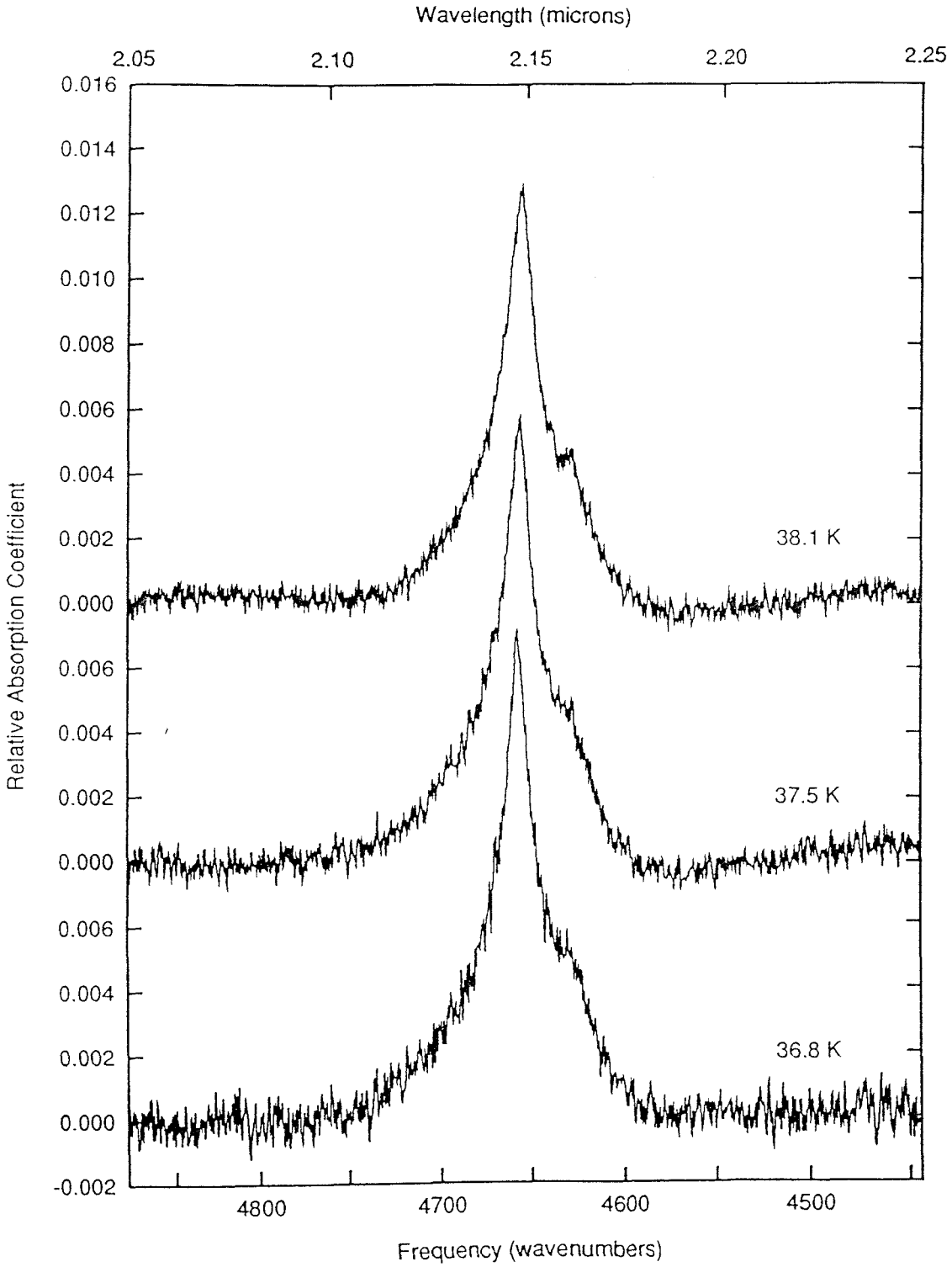
Wavelength (microns)
2.05
2.10
2.15
2.20
2.25
0.016
0.014
0.012
0.010
0.008
0.006
0.004
0.002
0.000
0.006
0.004
0.002
0.000
0.006
0.004
0.002
0.000
-0.002
Relative Absorption Coefficient
38.1 K
37.5 K
36.8 K
4800
4700
4600
4500
Frequency (wavenumbers)

Figure 4(c)

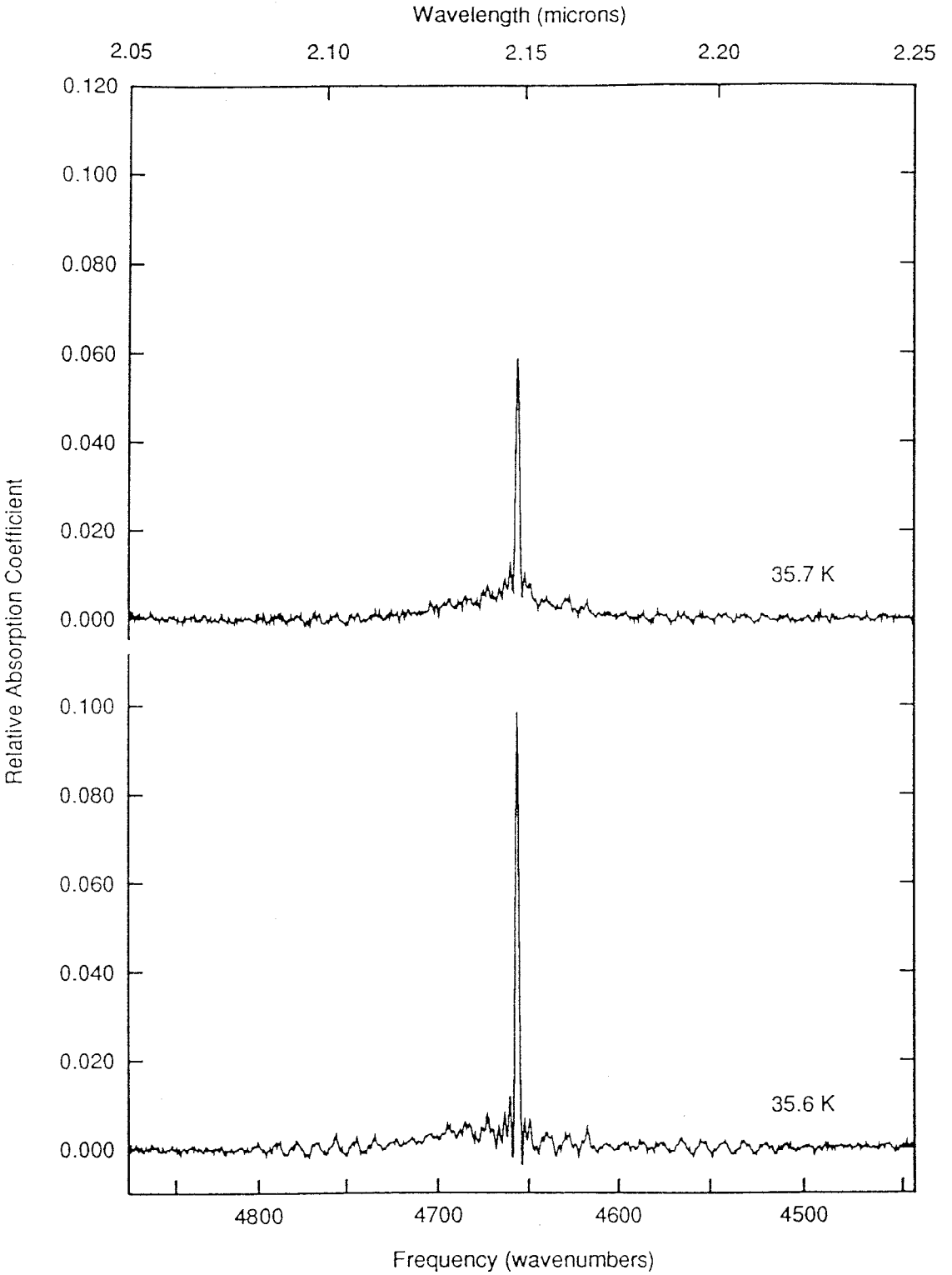
Wavelength (microns)
2.05
2.10
2.15
2.20
2.25
0.120
0.100
0.080
0.060
0.040
0.020
0.000
35.7 K
0.100
0.080
0.060
0.040
0.020
0.000
35.6 K
Relative Absorption Coefficient
4800
4700
4600
4500
Frequency (wavenumbers)

Figure 4(d)

Summary

We have presented absorption coefficients of solid nitrogen in the regions of the fundamental vibrational transition and its overtone over a temperature range of 35-60 K, obtained from laboratory transmission measurements. We find that the bands in both regions are temperature dependent in the ß phase, and that there is a large, abrupt change in the appearance of the band in the overtone region as the sample passes from the ß to the α phase. Additionally, the overtone has a sideband at $\approx$ 2.16 μm which can be identified in spectra of Triton and Pluto. The data for the overtone region can be used in conjunction with ground-based spectroscopic measurements to determine the temperature of nitrogen on solar system objects.

Acknowledgements

We would like to thank Roger Clark and Bernard Schmitt for their reviews of this paper. This paper is contribution 5515 of the Division of Geological and Planetary Sciences, California Institute of Technology, Pasadena, California, 91125.

References

Altenhoff, W.J., R. Chini, H. Hein, E. Kreysa, P.G. Mezger, C. Salter, and J.B. Schraml 1988. First radio astronomical estimate of the temperature of Pluto. *Astron. and Astrophs.* **190**, 15-17 (letter).

Conrath, B., F. M. Flasar, R. Hanel, V. Kunde, W. Maguire, J. Pearl, J. Pirraglia, R. Samuelson, P. Gierasch, A. Weir, B. Bezard, D. Gautier, D. Cruikshank, L. Horn, R. Springer, and W. Shaffer 1989. Infrared observations of the Neptunian system. *Science* **246**, 1454-1459.

Cruikshank, D.P., R.H. Brown, and R.N. Clark 1984. Nitrogen on Triton. *Icarus* **58**, 293-305.

Cruikshank, D.P., T.L. Roush, T.C. Owen, T.R. Geballe, C. de Bergh, B. Schmitt, R.H. Brown, and M.J. Bartholomew 1993. Ices on the surface of Triton. *Science* **261**, 742-745.

Green, J.R., R.H. Brown, D.P. Cruikshank, and V. Anicich 1991. The absorption coefficient of nitrogen with application to Triton. *Bull. Amer. Astron. Soc.* **23**, 1208.

Grundy W.M., B. Schmitt, and E. Quirico 1993. The temperature dependent spectra of α and ß nitrogen ice with application to Triton. *Icarus* **105**, 254-258.

Jewitt, D.C. 1994. Heat from Pluto. *Astronomical J.* **107**, 372-378.

Jodl, H.J., W. Loewen, and D. Griffith 1987. FTIR-spectra of solid O_2, N_2, and CO. *Solid State Commun.* **61**, 503-506.

Löwen, H.W., K.D. Bier, and H.J. Jodl 1990. Vibron-phonon excitations in the molecular crystals N_2, O_2, and CO by Fourier transform infrared and Raman studies. *J. Chem. Phys.* **93**, 8565-8575.

Owen, T.C., T.L. Roush, D.P. Cruikshank, J.L. Elliot, L.A. Young, C. de Bergh, B. Schmitt,

T.R. Geballe, R.H. Brown, and M.J. Bartholomew 1993. Surface ices and atmospheric composition of Pluto. *Science* **261**, 745-748.

Pangilinan, G., G. Guelachvili, R. Sooryakumar, K. Narahari Rao, and R.H. Tipping 1989. Raman study of the $\alpha \rightarrow ß$ structural phase transition of solid N_2. *Phys. Rev. B* **39**, 2522-2525.

Scott, T.A. 1976. Solid and liquid nitrogen. *Phys. Rep.* **27**, 89-157.

Stern, S.A., D.A. Weintraub, M.C. Festou 1993. Evidence for a low surface temperature on Pluto from millimeter-wave thermal emission measurements. *Science* **261**, 1713-1716.

Sykes M.V., R.M. Cutri, L.A. Lebofsky, and R.P. Binzel 1987. IRAS serendipitous survey of observations of Pluto and Charon. *Science* **237**, 1336-1340.

Tryka, K.A., R.H. Brown, V. Anicich, D.P. Cruikshank, T.C. Owen 1993. Spectroscopic determination of the phase composition and temperature of nitrogen on Triton. *Science* **261**, 751-754.

Tryka, K.A., R.H. Brown, D.P. Cruikshank, T.C. Owen, and T.R. Geballe. The temperature of nitrogen ice on Pluto and its implications for flux measurements. *Icarus* **112**, in press.

Paper 2:

Spectroscopic Determination of the Phase Composition and Temperature of Nitrogen Ice on Triton

Kimberly A. Tryka
Division of Geological and Planetary Sciences
California Institute of Technology,
Pasadena, CA 91125

Robert H. Brown, Vincent Anicich
Jet Propulsion Lab
MS 183-501, 4800 Oak Grove Drive,
Pasadena, CA 91109

Dale P. Cruikshank
NASA Ames Research Center
MS 245-6
Moffett Field, CA, 94035-1000

Tobias C. Owen
Institute for Astronomy, University of Hawaii
2680 Woodlawn Dr.
Honolulu, HI 96822

Abstract

Laboratory spectra of the first overtone band (2.148 μm, 4655.4 cm^{-1}) of solid nitrogen show additional structure at 2.162 μm (4625.8 cm^{-1}) over a limited temperature range. The spectrum of Triton shows the N_2 overtone band as well as the temperature sensitive component. The temperature dependence of this band may be used in conjunction with ground-based observations of Triton as an independent means of determining the temperature of surface deposits of nitrogen ice. The surface temperature of Triton is found to be $38.0^{+2.0}_{-1.0}$ K, in agreement with previous temperature estimates and measurements. There is no spectral evidence for the presence of α-nitrogen on Triton's surface, indicating that there is less than 10% carbon monoxide in solid solution with the nitrogen on the surface.

The presence of molecular nitrogen on the surface of Triton was identified from telescopic spectra obtained by Cruikshank *et al.* (1) on the basis of a weak absorption band at 2.148 μm, although the physical state of the nitrogen was unclear. The presence of nitrogen was also deduced from emission lines in Triton's atmospheric spectrum seen by the UV Spectrometer experiment on the Voyager 2 spacecraft during its 1989 flyby (2). Thermal measurements made by the Voyager infrared spectrometer indicated a surface temperature of 38^{+3}_{-4} K (3), and a surface pressure of 14 μbar was derived from measurements by the UV Spectrometer (2). As the triple point temperature of N_2 is 63.15 K (4), Voyager showed that N_2 is present in Triton's atmosphere and exists on the surface as a solid. The close correspondence of the basal temperature and

pressure of Triton's atmosphere to that of vapor-pressure equilibrium (14 μbar at 37.5 K [5]) also suggests that the gas is in vapor-pressure equilibrium with the surface ice.

Since the Voyager 2 encounter with Triton, new infrared spectrometers have become available, making possible significant advances in our understanding of the composition , physical state and distribution of the major components of Triton's surface. In this report we analyze recent ground-based observations of Triton that have yielded spectra of higher resolution than was previously available, and which show additional structure near the N_2 band center, including an unidentified absorption at 2.162 μm (6). From these ground-based data, and high-precision laboratory measurements of the transmission spectrum of N_2 ice reported here, both the temperature and the phase of N_2 ice on Triton can be determined. In addition, the 2.162-μm absorption feature in Triton's spectrum can now be identified.

At pressures and temperatures relevant to Triton solid nitrogen exists in two distinct phases. The ß phase is a low density phase with a hexagonal crystal structure and exists above 35.6 K (at zero pressure). The α phase is a high-density phase with a cubic structure and exists below 35.6 K at zero pressure (4). A third known phase of solid N_2, the γ phase, exists only at high pressures, and is not of interest here. The temperature of the α-ß transition is strikingly close to the measured surface temperature of Triton. In addition, seasonal volatile transport on Triton causes large fluctuations in Triton's globally-averaged temperature on time scales of decades to centuries (7,8,9). The temperatures are such that Triton's surface ices are continuously cycled through the α-ß phase transition (10). Therefore, based on thermodynamic arguments alone, it has not been not possible to rule out the presence of either the α or ß phases of N_2 ice on Triton.

N_2 exhibits a sparse spectrum of near-infrared absorptions caused by an induced-dipole transition (4) and it is expected that changes in the proximity of neighboring N_2 molecules

brought about by changes in temperature and crystal structure will have measurable effects on the near-infrared transmission spectrum of N_2 ice.

Preliminary laboratory work indeed suggests that the shape and strength of both the fundamental vibrational transition at 4.294 μm (2328.7 cm^{-1}) and its first overtone at 2.148 μm change substantially as N_2 goes through the α-ß phase transition (11). This work led us to conclude that better quality laboratory measurements combined with higher precision spectra of Triton, might lead to an identification of the specific phase of N_2 on Triton.

Transmission spectra of solid N_2 were measured at the Extraterrestrial Ice Facility at the Jet Propulsion Laboratory (12, 13). Similar measurements have recently been made by Grundy *et al.* (14). To form an optically clear sample of ß N_2, liquid N_2 was slowly cooled through the triple point as suggested by previous experimenters (4). A typical sample freezes optically clear using this method, though a small void space in the center of the sample forms as the nitrogen contracts during cooling. To minimize the well-documented cracking that occurs in samples of solid nitrogen as they are cooled through the α-ß phase transition (4), our samples were cooled at a rate of 0.02 K per minute. As a result, the nitrogen ice remained clear until reaching about 45 K, where the sample began to show some limited cracking. After passing through the α-ß phase transition, samples became extensively cracked on length scales of several tens of μm, and had a translucent, white appearance. Although the signal transmitted through the cracked sample was considerably less (by a factor of $\approx$25) than the signal through the clear sample, it was adequate for spectral measurements.

Each measurement of the transmission of a given sample was divided by a measurement of the transmission of the empty cell to remove the spectrometer response function. Because a typical sample was left in the cell for a period of days, measurements of the empty-cell transmission were taken both before the sample was formed and after it was evaporated.

To facilitate direct comparisons of our laboratory data with observations of Triton several steps were taken. First the transmittance data were normalized in the continuum to correct for void space and scattering in the sample and to provide a common reference level for the separate measurements (15). The normalized transmittance for three different temperatures is shown in Figures 1A, B, and C. A second band, seen at 2.16 μm in Figure 1B appears only over a limited range of temperatures (41 K to just above the phase transition temperature). Absorption coefficients were derived from the normalized transmittance data by converting transmittance to absorbance and then dividing the absorbance by the cell length to yield absorption coefficients. Because the resolution of the laboratory and observational data were not the same, the lab data were degraded to the resolution of the observational data. This was accomplished by convolving the laboratory data with a gaussian of the appropriate half-width and amplitude. The resulting absorption-coefficient spectrum was used to model the radiance coefficient (16) of particulate N_2 ice, for comparison with the Triton spectrum. The radiance coefficient is the ratio of the reflectance of a surface to the reflectance of a Lambert surface identically illuminated. To calculate this quantity an index of refraction of 1.2 was used (17). Isotropic scattering was assumed, along with surface-normal illumination and reflection. Parameters specifying the opposition effect and macroscopic roughness of a surface were ignored.

The remaining two parameters to be specified are single-scattering albedo and particle size. In the case of an optically thin medium, single-scattering albedo is a function of the absorption coefficient and particle size (16,18). The absorption coefficient spectrum as a function of temperature is determined by our laboratory measurements, leaving particle size as the other free parameter in the model fitting process. The effect of increasing particle size, for a given set of absorption coefficients, is to deepen and broaden the band being modeled. Representative results of the model fits are shown by the lines in Figures 2A and B.

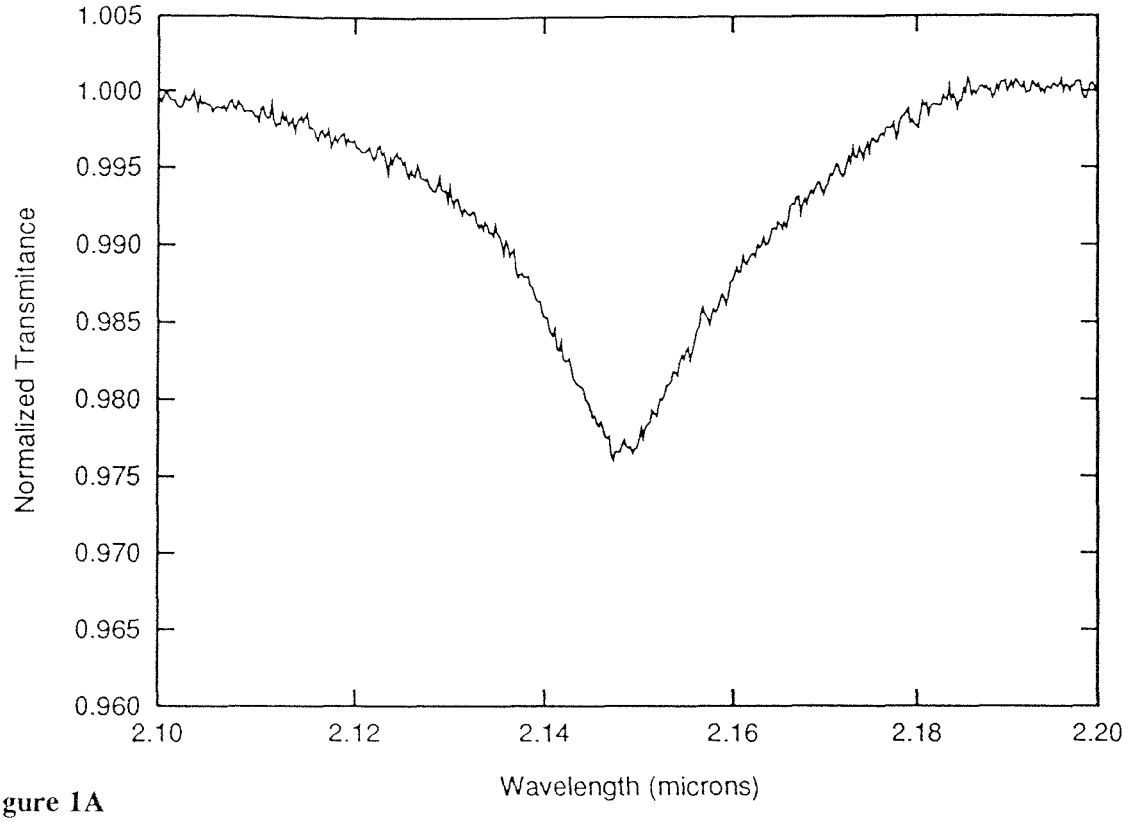

Figure 1A

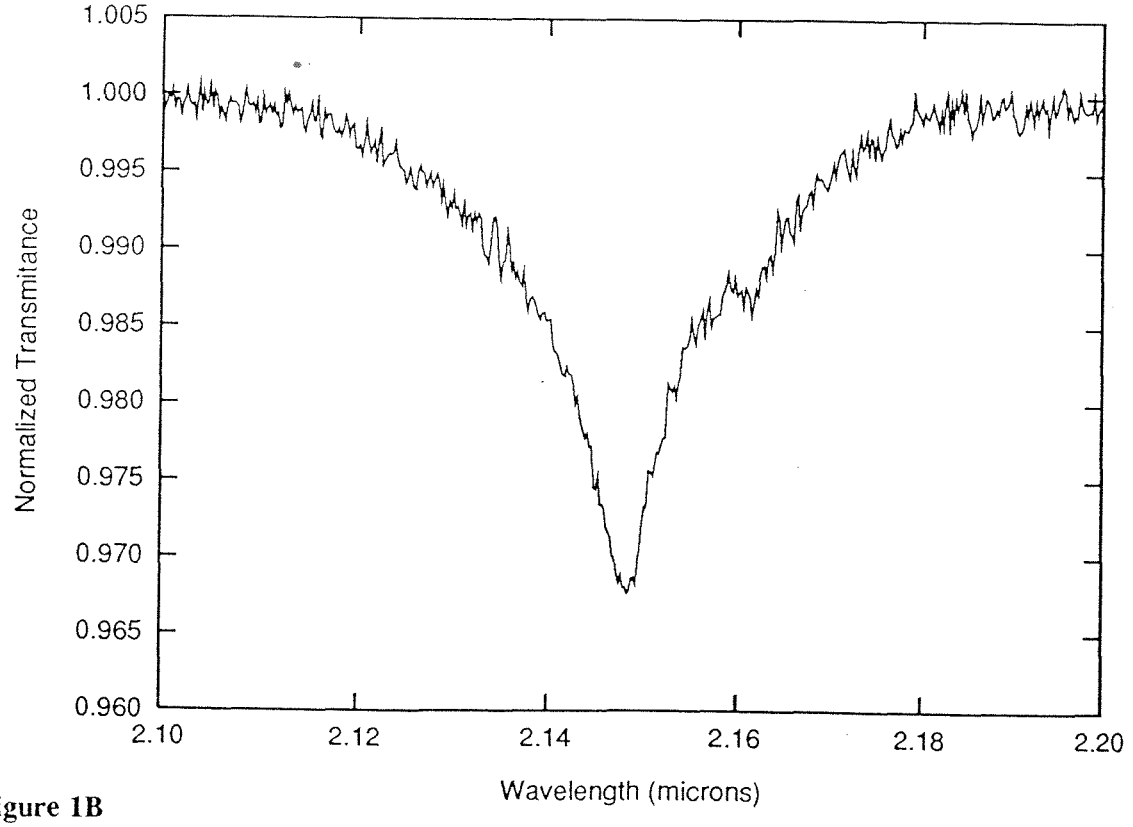

Figure 1B

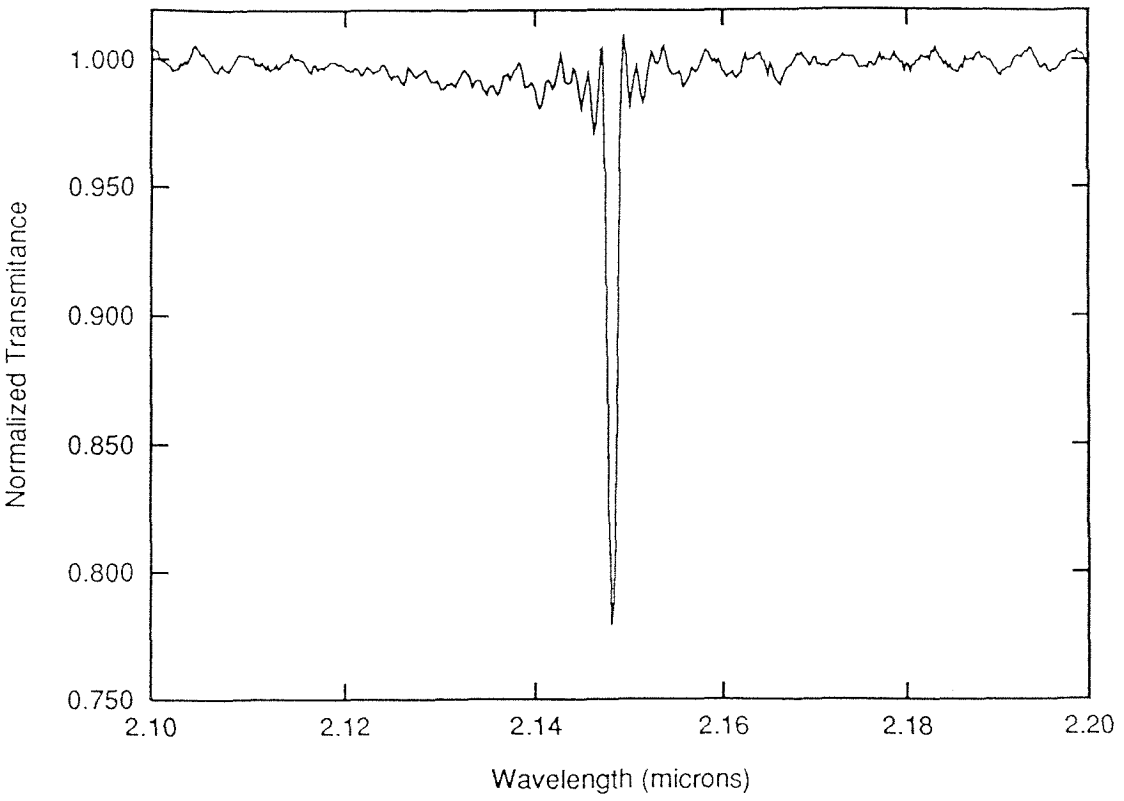

Figure 1C

Figure 1: Normalized transmittance spectra of solid N_2, 2.10-2.20 μm, at temperatures of (**A**) 49.4, (**B**) 39.1, and (**C**) 35.5 K. Note the presence of a second band at 2.16 μm in the 39.1 K spectrum which does not appear in the other spectra.

In both figures the discrete points are observations of Triton taken in May of 1992 (1), with the bars representing the point-to-point scatter of the data. The data are normalized to 1.0 in the continuum and the 2.2-μm CH_4 absorption band was removed to isolate the nitrogen band. The removal of the CH_4 absorption was accomplished by modeling it as a combination of two gaussians and dividing the spectrum by these gaussians. We note that removal of the CH_4 band does not affect the data shortward of 2.175 μm, it merely corrects the downturn of the long wavelength portion of the N_2 band which occurs because of its being superposed on the CH_4 band.

Figure 2A shows the four temperatures which best match the observational data, as

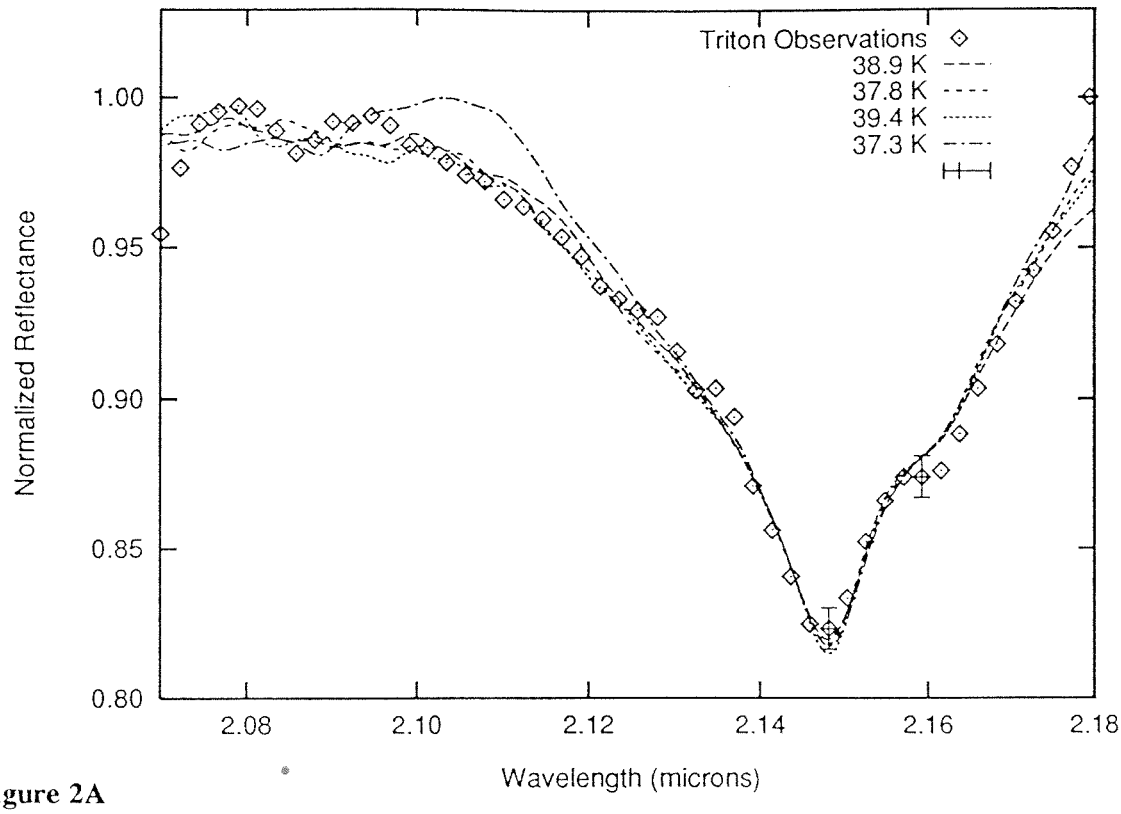

Figure 2A

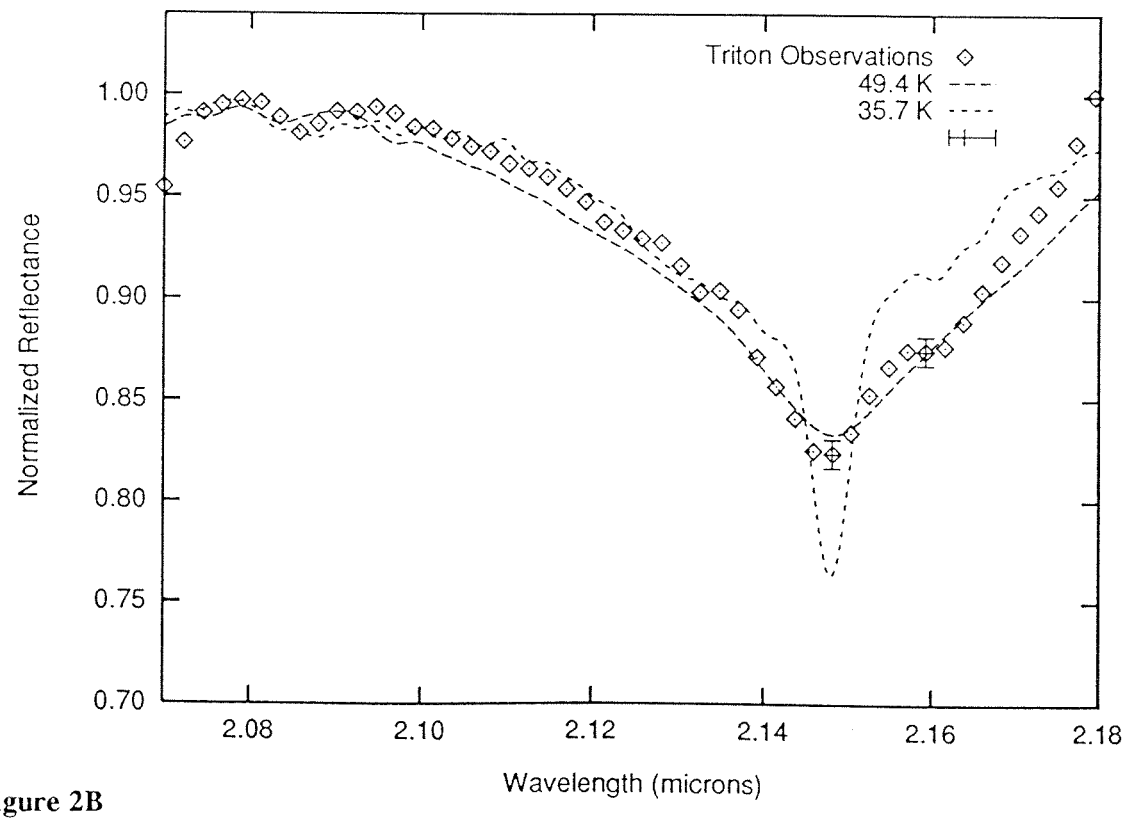

Figure 2B

determined by least-squares fits. Notice that these models match the width and intensity of the broad 2.15-μm band, and display a band at 2.16 μm, although it is weaker than that seen in the observational data. One explanation of this mismatch involves contamination of N_2. It is unlikely that N_2 exists as an isolated substance on the surface of Triton; rather it will be contaminated by small amounts of volatile species such as CO and CH_4 (6). If that is the case, it is possible that the presence of these other species may influence the spectral signature of N_2. Since absorption coefficients for these mixtures have not been measured, we assume, for this discussion, that the spectral line in question is produced by pure N_2.

The best fit is for a temperature of 38.9 K and a particle diameter of 0.43 cm. The next best fits correspond to temperature/size combinations of 37.8 K and 0.41 cm, 39.4 K and 0.45 cm. and 37.3 K and 0.42 cm. The χ^2 of the best fit is 6.67×10^{-3}, the next best fits give a χ^2 in the range of 7.20×10^{-3} to 8.00×10^{-3}. Other models had a χ^2 significantly outside the range quoted above ($> 8.60\times10^{-3}$). We therefore conclude that the range $38.0^{+2.0}_{-1.0}$ K encompasses the temperature of N_2 ice on Triton. These limits are not based on statistical arguments; they only represent the point at which the χ^2 indicates a significantly worse fit. The quoted range of temperatures includes the point at which the equilibrium vapor pressure of N_2 is 14 μbar. As such, our result supports the assumption that N_2 gas in the lower atmosphere of Triton is in vapor pressure equilibrium with the solid on the surface.

Figure 2B demonstrates that N_2 ice at temperatures outside this range does not display the

Figure 2: The infrared spectrum of Triton (points), 2.07-2.18 μm, and models of the spectrum from transmission measurements of solid N_2 as described in the text. The Triton observations are normalized to 1.0 in the continuum and the modeled spectra have been normalized so that the average value in the range 2.07-2.10 μm matches the average continuum value of the observational data in the same region. The error bars represent the point-to-point scatter in the observational data. (**A**) The four models shown are for temperature/particle size combinations of 38.9 K and 0.43 cm, 37.8 K and 0.41 cm, 37.3 K and 0.42 cm, and 39.4 K and 0.45 cm. Models for temperatures of 49.4 and 35.6 K and a particle size of 0.45 cm.

spectral line shape seen in the Triton spectrum. The two models shown are for temperatures of 49.4 and 35.6 K, with a particle size of 0.45 cm. The model spectrum for the higher temperature sample has a width and depth similar to the band on Triton, but lacks the additional structure at 2.16 μm. The model for the lower temperature sample shows a deep, narrow absorption characteristic of α N_2, which is not seen in the Triton spectrum. Thus, there is no spectral evidence for the presence of α N_2 on Triton.

It is known that N_2 and CO are soluble in all proportions and that the addition of CO in N_2 has the effect of raising the α-ß transition temperature (4), as well as lowering the vapor pressure. This, along with the lack of a the spectral signature of α N_2 in the Triton spectrum, can be used to place an upper limit to the amount of CO that might be present in solid solution with N_2 on Triton's surface. If the N_2 temperature is no higher than 40 K, then the phase diagram of the CO-N_2 solid solution series shows that there must be less than $\approx$ 10% CO in solution with the N_2, otherwise Triton's spectrum would display the deep, narrow signature of α N_2. This upper limit is far higher than the 0.1% abundance of CO inferred by Cruikshank *et al.* (6) based on model fits to the 2.35-μm band in Triton's spectrum.

Another paper in this issue (18) identifies nitrogen in the spectrum of Pluto. If spectra of higher resolution and precision can be obtained, an estimate of the temperature of N_2 on Pluto can be made using the same technique used here for Triton. If N_2 is the largest component of the atmosphere and surface of Pluto, its temperature could be very close to the actual surface temperature of the planet.

References and Notes

(1) D. P. Cruikshank, R. H. Brown, and R. N. Clark, *Icarus* **58**, 293 (1984).

(2) A. L. Broadfoot *et al.*, *Science* **246**, 1459 (1989).

(3) B. Conrath *et al.*, *Science* **246**, 1454 (1989).

(4) T. A. Scott *Phys. Rep.* **27**, 89 (1976).

(5) G. N. Brown, Jr. and W. T. Ziegler, *Adv. Cryogenic Engineering* **25** (K. D. Timmerhaus and H. A. Snyder, eds.), 662 (1980).

(6) D. P. Cruikshank, T. L. Roush., T. C. Owen, T. R. Geballe, C. de Bergh, B.Schmitt, R. H. Brown, and M. J. Bartholomew, *Science*, submitted.

(7) J. R. Spencer, *Geophys. Res. Let.* **17**, 1769-1772 (1990).

(8) R. H. Brown, *Bull. Amer. Astron. Soc.* **24**, 966 (1992).

(9) R. H. Brown and R. L. Kirk, *J. Geophys. Res., Plan.*, submitted (1993).

(10) N. S. Duxbury and R. H. Brown, *Science*, submitted (1993).

(11) J. R. Green, R. H. Brown, D. P. Cruikshank, and V. Anicich, *Bull. Amer. Astr. Soc.*, **23**, 1208 (1991).

(12) Our data were taken using a Fourier-transform spectrometer. The spectrometer was fitted with a CaF_2 beamsplitter, a tungsten source, and an InSb detector. Data were taken between 1 and 5 μm (2000 and 10000 cm^{-1}), and spanned a temperature range of 35 to 60 K. The spectral resolution was 5 x 10^{-4} μm at 2.15 μm (1 cm^{-1}). Our integration period was 4 minutes. Backgrounds were taken with the same integration period. The nitrogen from which our samples were formed is of research quality (99.9995% pure). A sample of solid N_2 was held in a cell attached to a cold finger, cooled by a closed-cycle He refrigerator. The temperature controller used in the experiments is capable of mK resolution and able to hold a sample at a constant temperature ($\pm$ 0.02 K) for a period of several hours.

(13) K.A. Tryka, R.H. Brown, and V. Anicich (in preparation).

(14) W.M. Grundy, B. Schmitt, and E. Quirico, *Icarus*, submitted (1993).

(15) The continuum absorption of N_2 is $<1\%$ in this wavelength region making an accurate measurement of this quantity extremely difficult. Since it is the relative depths of the bands which are the important quantity, we chose to normalize the transmittance data to 1 in the continuum providing a common reference level from which to quote results.

(16) B. Hapke *J. Geophys. Res.* **86**, 3039 (1981).

(17) R.C. Weast, Ed., *CRC Handbook of Chemistry and Physics* (CRC Press Inc., Boca Raton, 1980). Since there is no measurement of the index of refraction of solid N_2 in the literature we used the index of refraction of liquid N_2 as given in this reference.

(18) R. N. Clark and T. L. Roush, *J. Geophys. Res.* **89**, 6329 (1984).

(19) Owen, T. C. *et al.*, *Science*, submitted.

(20) We would like to thank two anonymous referees for their useful comments. This is contribution number 5281 of the Division of Geological and Planetary Sciences, California Institute of Technology.

Paper 3:

The Temperature of Nitrogen Ice on Pluto and Its Implications for Flux Measurements

Kimberly A. Tryka
Division of Geological and Planetary Sciences
California Institute of Technology
MS 170-25
Pasadena, CA 91125

Robert H. Brown
Jet Propulsion Laboratory
4800 Oak Grove Drive
MS 183-501
Pasadena, CA 91109

Dale P. Cruikshank
NASA Ames Research Center
MS 245-6
Moffett Field, CA 94035-1000

Tobias C. Owen
Institute for Astronomy
University of Hawaii
2680 Woodlawn Drive
Honolulu, HI 96822

Thomas R. Geballe
Joint Astronomy Centre
660 North Aohoku Place
University Park
Hilo, HI 96720

Catherine deBergh
Observatoire de Paris
5 Jules Janssen
92195 Meudon Cedex, France

Abstract

Previous work by Tryka *et al.* (*Science* **261**, 751-754, 1993) has shown that the profile of the 2.148 μm band of solid nitrogen can be used as a "thermometer" and determined the temperature of nitrogen ice on Triton to be 38 (+2,-1) K. Here we reevaluate that data and refine the temperature value to 38 ± 1 K. Applying the same technique to Pluto we determine that the temperature of the N_2 ice on that body is 40 ± 2 K. Using this result we have created a non-isothermal flux model of the Pluto/Charon system. The model treats Pluto as a body with symmetric N_2 polar caps, and an equatorial region devoid of N_2. Comparison to the infrared and millimeter flux measurements show that the published fluxes are consistent with models incorporating extensive N_2 polar caps (down to $\pm 15°$ or $\pm 20°$ latitude) and an equatorial region with a bolometric albedo ≤ 0.2.

Introduction

Although the mutual occultations and eclipses that Pluto has recently undergone with its satellite Charon have increased our knowledge of the system tremendously, there is one question which the mutual events have been unable to address: what is the temperature of Pluto? One approach to answering this question is to make thermal flux measurements of Pluto and then attempt to find a temperature which fits the results. Several flux measurements of the Pluto/Charon system have been made. Observations made by the Infrared Astronomical Telescope (IRAS) (Aumann and Walker 1987, Sykes *et al.* 1987) predict a warm (55-60 K) Pluto while flux measurements in the millimeter region (Altenhoff *et al.* 1988, Stern *et al.* 1993, Jewitt 1994) yield a lower (30-44 K) temperature.

In this paper we determine the temperature of solid nitrogen on Pluto using a spectroscopic technique. The method is based on the result that the shape of the 2.148-μm N_2 band changes with temperature (Tryka *et al.* 1993). Using the temperature result we then construct a simple model of the Pluto/Charon system and compute the flux from such a system. We compare our model flux with all the observational flux data in an attempt to reconcile the various measurements.

Determination of Nitrogen Temperature from Spectral Measurements

At temperatures and pressures relevant to planetary surfaces solid nitrogen exists in two different phases (Scott 1976) referred to as α and ß. At 0 pressure the cubic α phase exists at temperatures below 35.6 K. The lower density ß phase has an hexagonal structure and exists at temperatures above 35.6 K at 0 pressure. A third form of N_2, γ nitrogen, is also known to

exist, but only at very high (kilobar) pressures.

Nitrogen has a very sparse spectrum in the near infrared region. The fundamental vibrational transition, seen at 4.294 μm, is produced by an induced dipole transition. However, it is the first overtone of this transition, at 2.148 μm, which is of interest to ground-based observers as it falls in a transparent region of the telluric spectrum. On the basis of this overtone band nitrogen has been identified in the spectrum of Triton (Cruikshank *et al.* 1984) and, more recently, in the spectrum of Pluto (Owen *et al.* 1993a).

Laboratory measurements by Green *et al.* (1991) demonstrated that as solid N_2 is cooled from the ß to the α phase the appearance of the 2.148 μm band changes dramatically. In the ß phase the band is broad and shallow, while in the α phase the band is very narrow and much deeper. The change in band appearance is a direct result of the change in lattice structure of the N_2.

Further laboratory measurements, utilizing higher resolution spectrometers and better temperature controllers, have been performed by Tryka *et al.* (1993) and Grundy *et al.* (1993). Both studies demonstrate that the appearance of the 2.148 μm band in ß nitrogen is temperature dependent. Tryka *et al.* (1993, 1994). made transmittance measurements through a thick (1 inch) sample of solid nitrogen over a temperature range of 35-60 K and over wavelengths of 1-5 μm (the reader is referred to Tryka *et al.* 1994 for a detailed description of the laboratory measurements). Representative results for the region of the first overtone band are shown in Fig. 1. There are no error bars shown in this figure, but the continuum on either side of the band is representative of the noise in the system. We do not present results here for the fundamental transition because it is not observable from the ground. As N_2 cools toward the α-ß transition temperature, the band becomes deeper and narrower in a regular fashion, reflecting the fact that the N_2 matrix is becoming more ordered. Figure 1 also shows the presence of a second feature

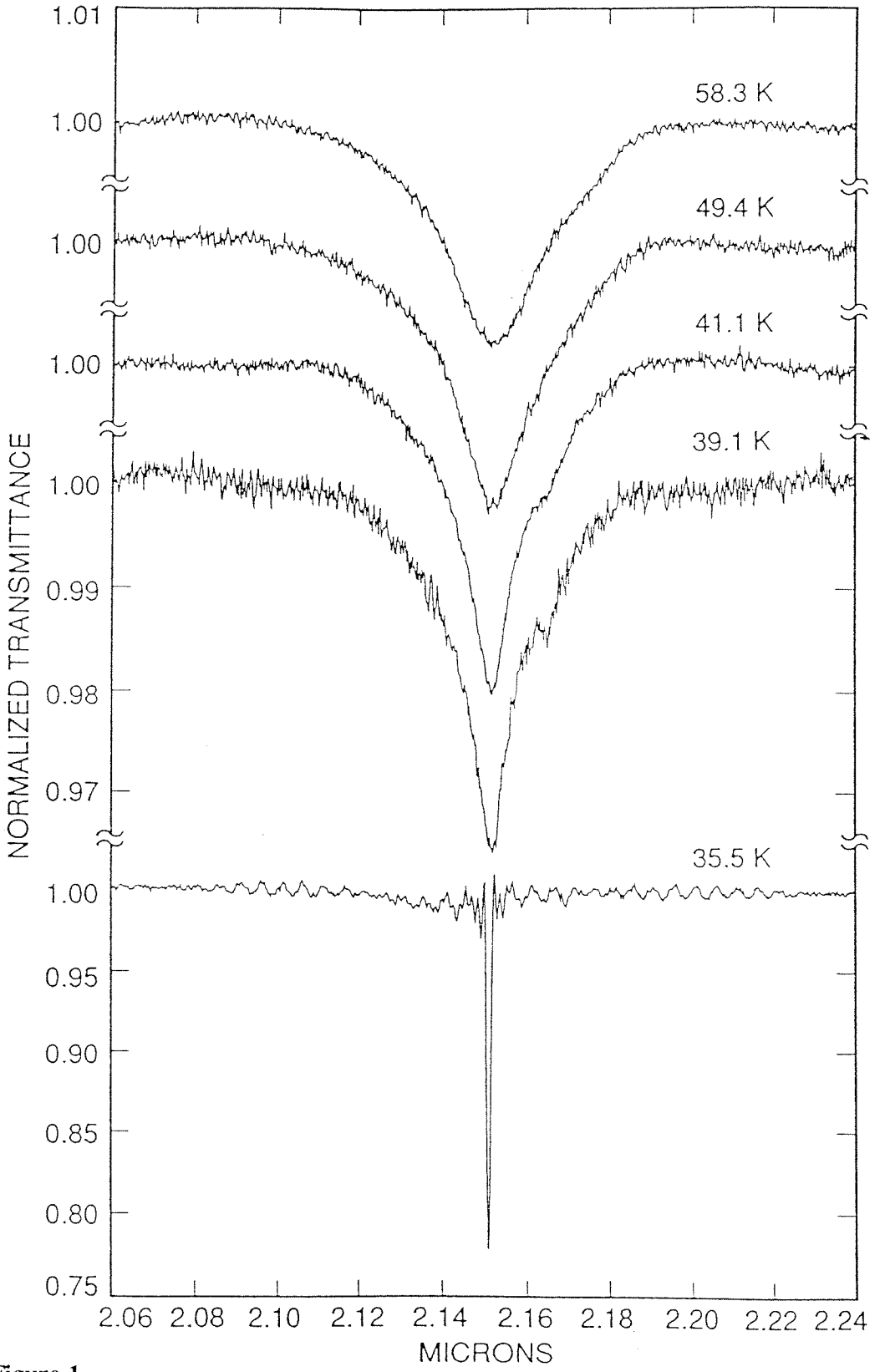
58.3 K
49.4 K
41.1 K
39.1 K
35.5 K
NORMALIZED TRANSMITTANCE
1.01
1.00
1.00
1.00
1.00
0.99
0.98
0.97
1.00
0.95
0.90
0.85
0.80
0.75
2.06 2.08 2.10 2.12 2.14 2.16 2.18 2.20 2.22 2.24
MICRONS

Figure 1

at 2.160 μm over a limited temperature range. The 2.160 μm feature matches a feature seen in a recent spectrum of Triton (Cruikshank *et al.* 1993) as was demonstrated by Tryka *et al.* (1993). Because the profile of the overtone band changes with temperature, careful laboratory measurements of the band provide the basis for an accurate determination of N_2 temperature using spectroscopic observations.

To convert the transmittance data to a synthetic comparison spectrum several steps were taken. The transmittance data were normalized in the continuum to provide a common reference level for separate measurements. Absorption coefficients were derived from the normalized transmittance data by converting transmittance to absorbance and dividing the absorbance by the cell length. The absorption coefficient spectrum was then convolved with a gaussian to produce a spectrum with the same effective resolution as the observational data. The resulting spectrum was then used to model the radiance coefficient (Hapke 1981) of particulate N_2 ice for comparison with the telescopic measurements. The radiance coefficient is the ratio of the reflectance of a surface to the reflectance of a Lambert surface identically illuminated. Isotropic scattering is assumed, along with normal incidence and reflection. Parameters specifying the opposition effect and macroscopic roughness are ignored. Thus the equation for the radiance coefficient is reduced to the form

$$r = \frac{\omega}{4} H^2(\omega, \mu = \mu_0 = 1)$$

where ω is the single scattering albedo, and μ and μ_0 are the cosines of the emission and

Figure 1 - Transmission spectra of solid N_2 in the region of the first overtone. The first overtone band occurs at 2.148 μm. Spectra are shown for five different temperatures; 58.3 K, 49.4 K, 41.1 K, 39.1 K, and 35.5 K. Error bars are not shown on the data, but the continuum region on either side of the band gives an accurate representation of the noise level in the system.

incidence angles. The H's are defined by Chandrasekhar (1960) and are a function of ω, μ, and μ_0.

The unspecified parameter in the equation for the radiance coefficient is the single scattering albedo of the particle being modeled. For the case of an optically thin medium, which we assume for N_2, the single scattering albedo is a function of the absorption coefficient, index of refraction, and particle size (Hapke 1981, Clark and Roush 1984). The absorption coefficient spectrum as a function of temperature is determined by our laboratory experiments, and we assume an index of refraction of 1.2 (Weast 1980), leaving particle size as the only free parameter in the model fitting process. The effect of increasing particle size, for a given set of absorption coefficients, is to deepen and broaden the band being modeled.

Temperature of N_2 on Triton

Before we turn to the case of Pluto, we will demonstrate the validity of this technique by applying it to Triton. The observations of Triton presented here were obtained in May, 1992 at the United Kingdom Infrared Telescope (UKIRT) on Mauna Kea, and the final data have a resolution of $\approx$ 0.007 μm. We previously analyzed these data and determined the N_2 temperature on Triton to be 38 (+2,-1) K (Tryka *et al.* 1993), in agreement with Voyager 2 measurements. In this paper we reanalyze the same data, using a different approach to remove the continuum.

In Tryka *et al.* (1993), the continuum was modeled by fitting straight line segments across obvious absorption bands from high points of the spectrum which were assumed to be in the continuum. For this paper we have modeled the continuum by choosing high points in the same manner, but then fit them with a high order polynomial. Figure 2 compares the isolated N_2 band

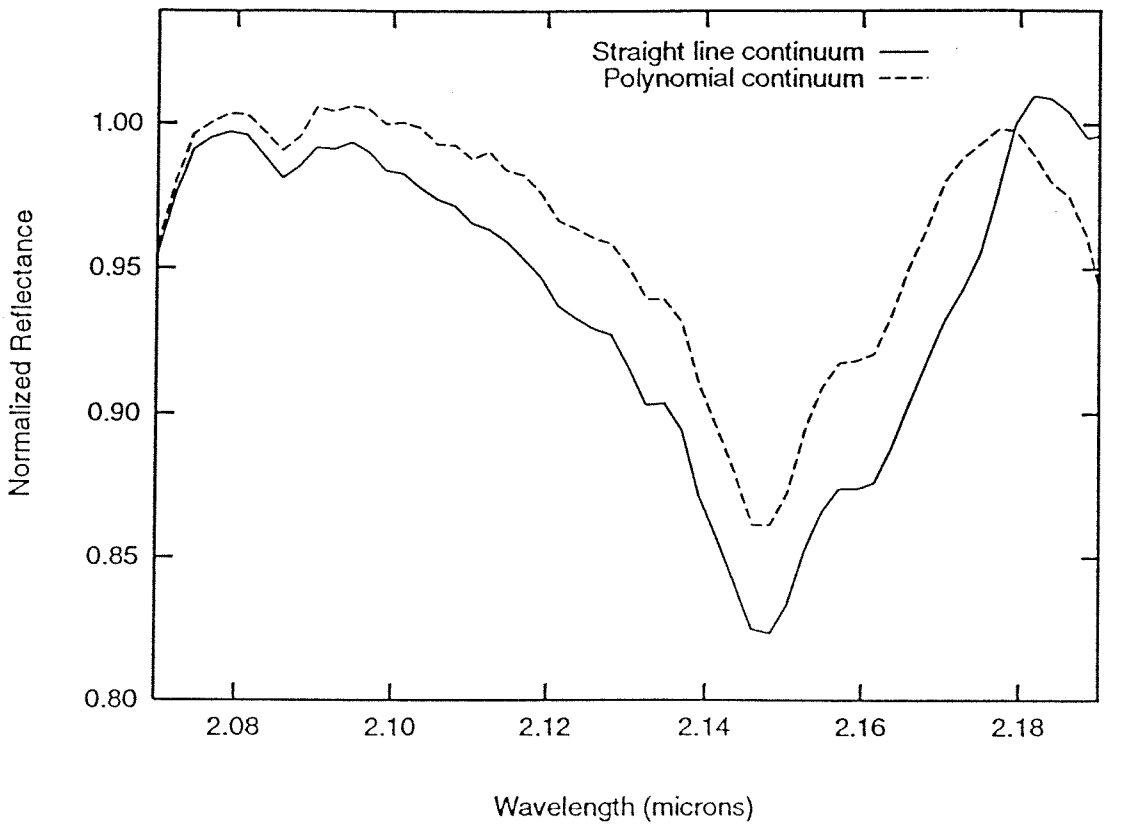

Figure 2. Comparison of the 2.148 μm N_2 band of Triton used in this study (dashed line) and the band used in the previous study by Tryka *et al.* (1993). The difference in the bands' width and depth is a result of different continuum removal techniques. Note that the same features appear in both bands, but that one band is somewhat deeper than the other. The long wavelength absorption (>2.18 μm) in the dashed spectrum is due to CH_4 and can be ignored.

used by Tryka *et al.* (1993) with that used here and shows that the width and depth of the N_2 band is somewhat dependent upon the continuum model used, although the same features are present in each band (e.g., the absorption at 2.160 μm). The downturn in the spectrum longward of 2.18 μm is due to a CH_4 absorption which we did not remove.

Figure 3(a) shows observational data of Triton, represented by points, along with the 4 best-fitting models derived from the laboratory measurements, shown by the lines. The two error bars represent the point-to-point scatter in the observational data. What is most important in these fits is that the width and depth of the band, and the feature at 2.160 μm, are well matched. That the simulated spectrum does not mimic the behavior of the observational data longward of

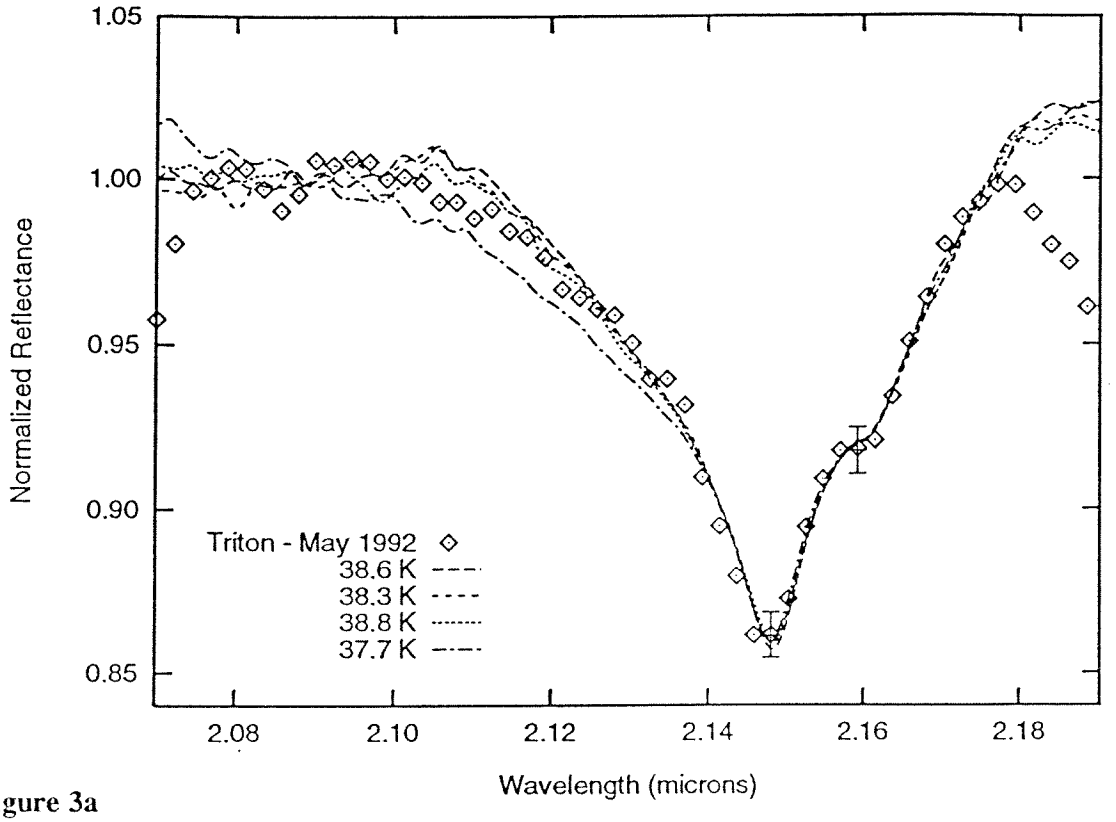

Figure 3a

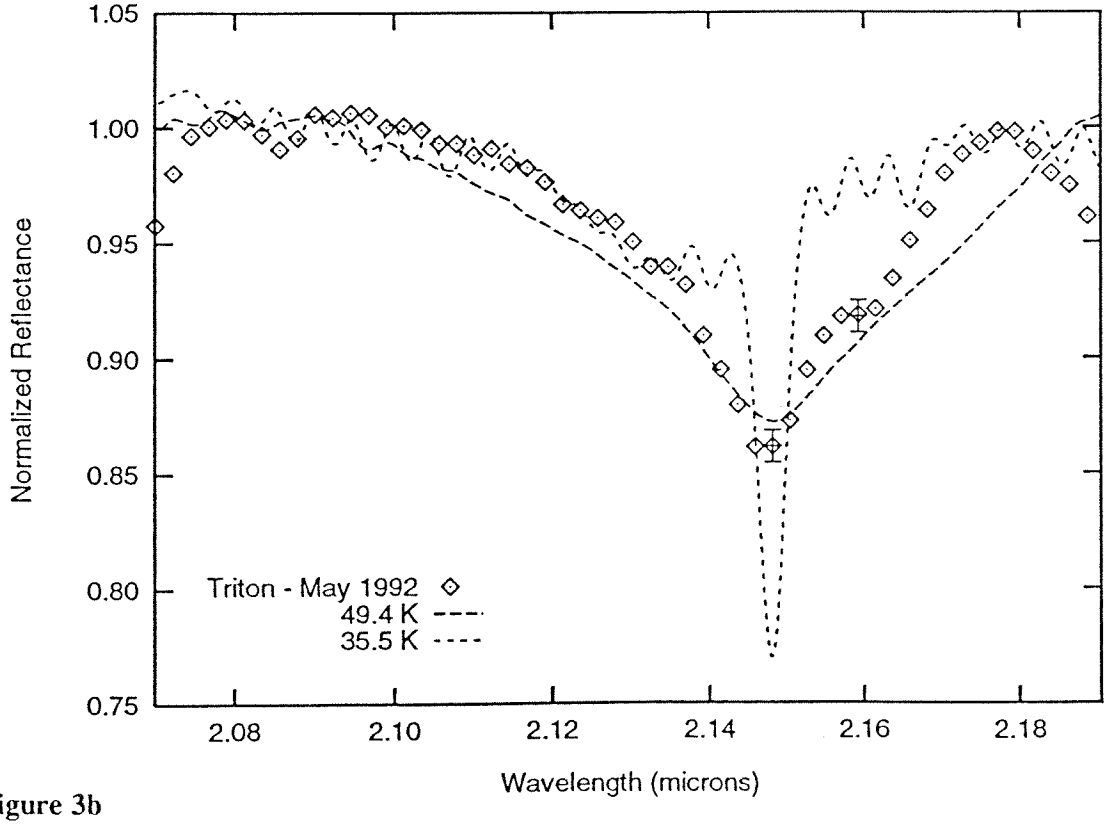

Figure 3b

2.180 μm is to be expected, because of the CH_4 absorption previously mentioned. The choice of the best fits was made using a χ^2 fitting technique, looking only at the area between 2.120 μm and 2.175 μm, to avoid the CH_4 absorption longward of 2.180 μm and other possible absorbers shortward of 2.120 μm. The temperature/particle-diameter combinations represented by the lines are; 38.6 K and 0.33 cm, 38.3 K and 0.31 cm, 38.7 K and 0.30 cm, and 37.7 K and 0.29 cm. From this modeling we determine that the N_2 temperature on Triton is 38 ± 1 K. This temperature result is in agreement with measurements of surface temperature, 38 (+3,-4) K, made by the Voyager 2 infrared spectrometer (Conrath *et al.* 1989). These different temperature determinations, taken in conjunction with the surface pressure inferred by Voyager 2 (Broadfoot *et al.* 1989) indicate that Triton's N_2 is in vapor pressure equilibrium (Brown and Ziegler 1980).

Although the apparent shape of the N_2 spectral band changes as a result of different continuum models, the range of temperatures which fit the two bands are similar. This arises because, in our model, the temperature of the N_2 governs the shape of the spectral band, while the particle size, to first order, scales the band depth. Thus, the particle size needed to fit the nitrogen band which had a polynomial continuum removed is $\approx$0.30 cm, while for the case of a straight line continuum, which resulted in a deeper band, the particle diameter needed to fit the spectral band was $\approx$0.43 cm. Because temperature, not the particle size, is mainly responsible for the band shape, the difference in particle sizes needed to fit the spectral bands is not

Figure 3. Comparison of N_2 band models with the normalized reflectance of Triton. The error bars represent the point to point scatter in the data rather than a formal error. (a) shows the four best fitting models to the observational data. The models are for temperature/particle size combinations of 38.6 K/0.33 cm, 38.3 K/0.31 cm, 38.8 K/0.30 cm, and 37.7 K/0.29 cm. (b) shows two models which do not fit the data. These models are for temperature/particle size combinations of 49.4 K/0.30 cm and 35.5 K/0.30 cm (α phase). This figure demonstrates that it is possible to distinguish between α and ß nitrogen on the basis of the appearance of this spectroscopic band.

significant.

Models which do not fit the data well are shown in Fig. 3(b). The higher temperature model is a poor fit because the main band is too broad and shallow, and it does not show a feature at 2.160 μm (demonstrated by the temperature/particle-size combination of 49.4 K and 0.3 cm). As the temperature falls below the α-ß transition the band becomes much too narrow and deep (as shown by the model for 35.5 K and 0.3 cm). This also demonstrates that, at the resolution of the current data, α and ß nitrogen can easily be differentiated on the basis of the shape of the 2.148 μm band.

Temperature of N_2 on Pluto

Nitrogen has recently been identified on Pluto by Owen *et al.* (1993a). Their data show a shallow N_2 feature at 2.148 μm superimposed upon a very deep methane absorption at 2.2 μm. Additional spectroscopic measurements of Pluto made at UKIRT in May 1993 confirm these earlier observations (Owen *et al.*, 1993b). Both sets of measurements were made with the same instrument and at the same spectral resolution as the Triton data presented in the last section. Pluto was observed at 48 hour intervals over five nights to sample all regions of the planet in an effort to determine whether the surface showed compositional variation. As there were no obvious changes in the region surrounding the nitrogen band with respect to rotational phase, we have coadded the three data sets in order to improve the quality of the spectrum. This spectrum of Pluto from 1993, as well as the Triton data from 1992, is shown in Fig. 4. Neither spectrum in Fig. 4 has had a continuum removed, and both spectra have been normalized to 1 at 1.99 μm.

To determine the temperature of nitrogen on Pluto, we first had to isolate the N_2 band. To do so we removed the continuum by fitting a polynomial to points which we considered to

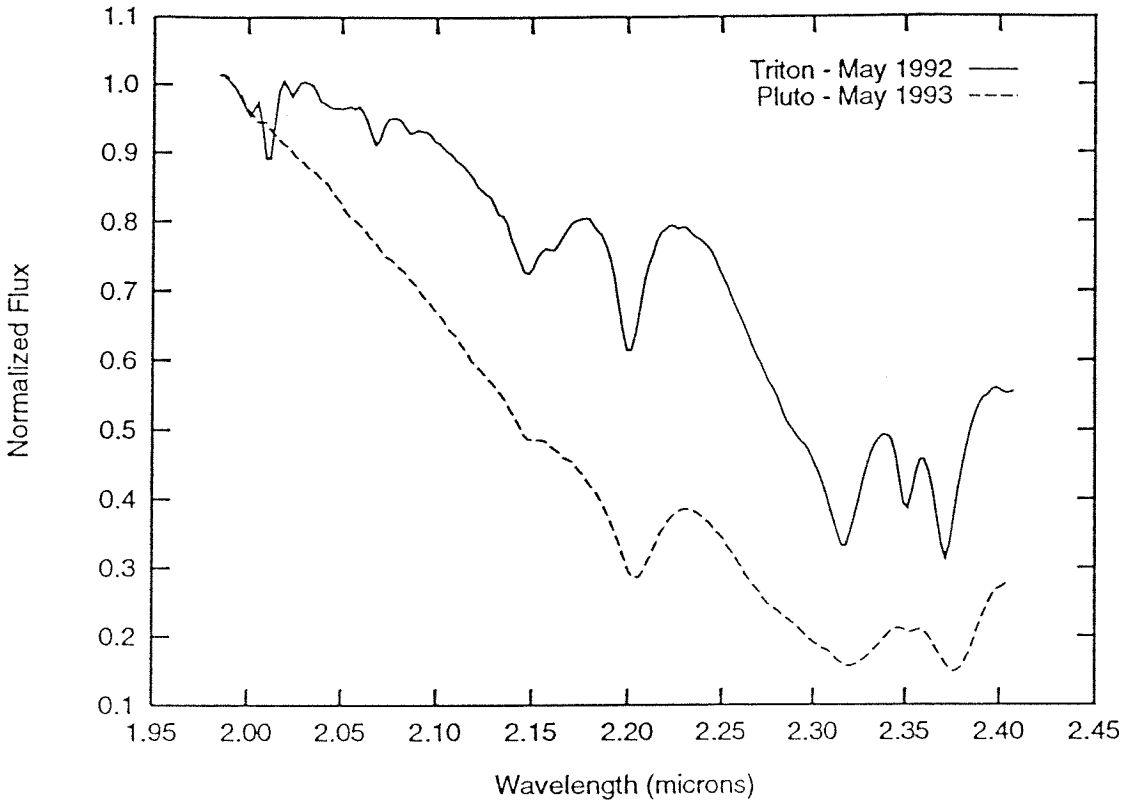

Figure 4. Comparison of the Triton spectrum from May 1992 and the Pluto spectrum from May 1993. The spectra were taken with the same instrument at the same resolution, and neither has had a continuum removed. The Pluto spectrum is the result of data taken on three nights. The spectra were normalized to 1.0 at 1.99 μm.

be in the continuum, removing that model continuum from the full spectrum to yield an intermediate spectrum, and then repeating the process until we had adequately isolated the N_2 band from the other spectral features. Figure 5 shows the result of this continuum removal process for Pluto, along with the N_2 band from Triton for comparison. Notice that the Pluto band is shallower and broader than the Triton band, and that the 2.16-μm feature is not well defined, although there does appear to be an inflection at that wavelength. The general appearance of the band suggests that the nitrogen on Pluto is at a higher temperature than that on Triton.

The three models which best fit the Pluto data (again determined by least squares fitting of the band between 2.13 μm and 2.175 μm) are shown in Fig. 6(a). These models have

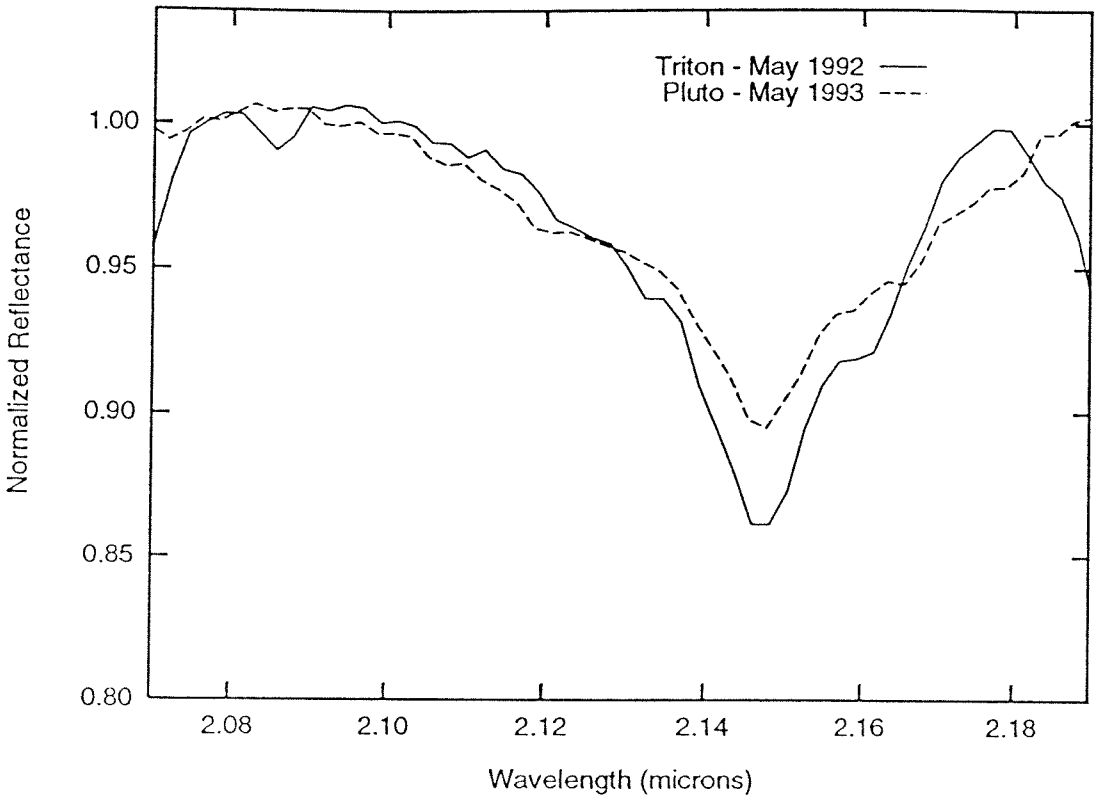

Figure 5. Comparison of the N_2 overtone bands from Triton (May 1992) and Pluto (May 1993). The spectra have been normalized in the continuum.

temperature/particle-diameter combinations of; 38.9 K and 0.16 cm, 39.1 K and 0.16 cm, and 41.1 K and 0.15 cm. Fig. 6(b) shows two models which fit the data poorly; a higher temperature model (at 49.4 K and particle size of 0.15 cm) and a low temperature model (35.5 K and 0.15 cm particles). From the models in Fig. 6(a) we determine that the temperature of N_2 frost on Pluto is 40 ± 2 K. The 2 K error bar may seem large when compared to the temperature spread of the best fit models, but it was chosen, not only to reflect the model fits, but also to reflect the uncertainty in the continuum removal process.

Figure 6. Comparison of N_2 band models with the normalized reflectance of Pluto. The error bars represent the point to point scatter in the data rather than a formal error. (a) shows the three best fit models to the data. The models are for temperature/particle sizes of 38.9 K/0.16 cm, 39.1 K/0.16 cm, and 41.1 K/0.15 cm. (b) shows two models which do not fit the data. These models are for temperature/particle size combinations of 49.4 K/0.15 cm, and 35.5 K/0.15 cm.

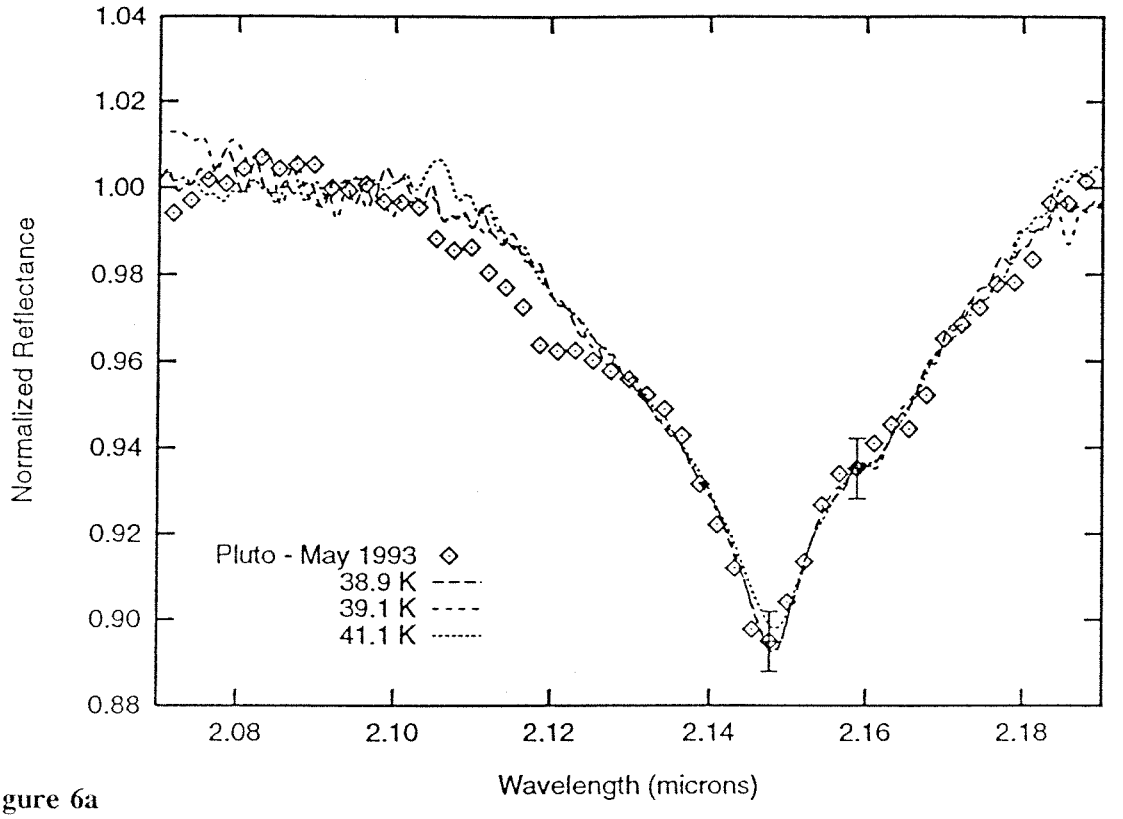

Figure 6a

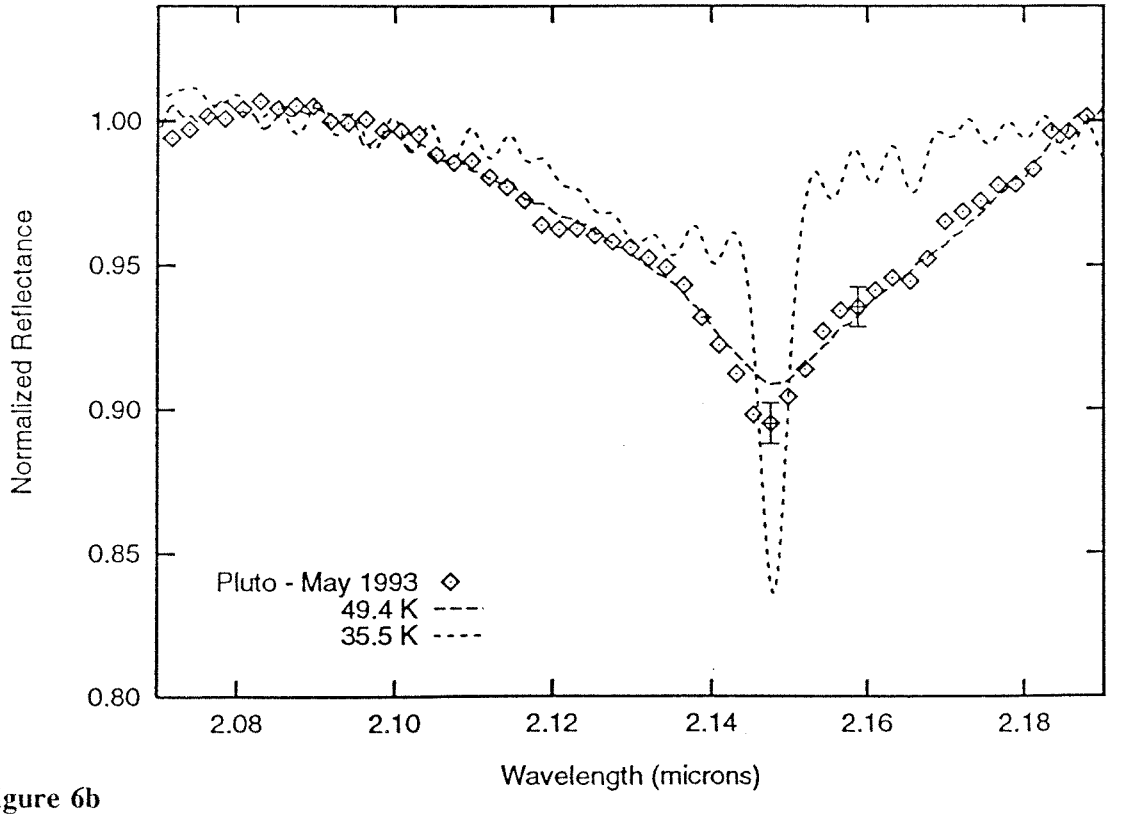

Figure 6b

Also evident in Fig. 6(a) is that none of the models, which reproduce the depth and width of the N_2 band quite well, match the shape of the band in the 2.12 μm region. The absorption in this region is not attributable to nitrogen, or any of the other molecular species identified in the Pluto spectrum (CH_4 and CO). This suggests the presence of an additional infrared absorber on Pluto, which remains unidentified.

If one assumes that the nitrogen in the atmosphere and on the surface of Pluto are in vapor pressure equilibrium, as they appear to be on Triton, then the surface atmospheric pressure on Pluto would be ≈ 60 μbar. This is much higher than the 3-10 μbar value derived by Yelle and Lunine (1989) and Hubbard *et al.* (1990) using stellar occultation data. Such a discrepancy could be caused by the occultation not probing down to the surface of Pluto (Stansberry *et al.* 1994). Also, it is possible that the equilibrium vapor pressure of nitrogen could be altered by the presence of contaminants (such as CO) in its matrix.

Flux Modeling of Pluto/Charon System

Observations and Previous Models

Thermal flux observations of the Pluto/Charon system fall into two categories; infrared measurements made by the Infrared Astronomical Satellite (IRAS), and ground-based millimeter wavelength observations. Table I summarizes these observations, and we will briefly discuss them here.

In 1983 IRAS made two measurements of the Pluto/Charon system. One was made during the all-sky survey resulting in a 60 μm flux determination published by Tedesco *et al.* (1987). The other flux points come from a 'pointed' observation of the Pluto/Charon system.

From these data Aumann and Walker (1987) derived flux measurements at 25 μm, 60 μm, and 100 μm. Sykes *et al.* (1987) also analyzed this data set, reporting fluxes at 60 μm and 100 μm. The Sykes *et al.* (1987) and Aumann and Walker (1987) points at 60 μm and 100 μm agree, although Sykes *et al.* (1987) have published more conservative error bars. The Tedesco *et al.* (1987) point at 60 μm does not agree well with the other observations. Doubts have been raised as to whether the Pluto/Charon system was detected by IRAS. Sykes (personal communication, 1993) has recently reanalyzed the pointed IRAS observations and concludes that there was no error in identifying the system, and that the flux determinations are accurate. For these reasons we adopt the following points for comparison with our models; at 60 μm and 100 μm the data from Sykes *et al.* (1988), and at 25 μm the data point from Aumann and Walker (1988).

Ground-based millimeter measurements have been made at three wavelengths; 800 μm, 1200 μm, and 1300 μm. The earliest observations were reported by Altenhoff *et al.* (1988) at 1200 μm. They measured fluxes on 4 different occasions and averaged them to derive a flux at 1200 μm with very small formal error. In light of recent albedo maps by Buie *et al.* (1992) and Young and Binzel (1993) that show both Pluto and Charon to have large variations in their albedo structure which do not appear to be rotationally symmetric, we choose not to use the averaged value of Pluto's flux reported by Altenhoff *et al.* (1988) because it is not clear that different rotational aspects of Pluto would be expected to produce the same flux distribution. Thus, Table I lists the four separate flux measurements reported by Altenhoff *et al.* (1988) and we use the range of values which encompasses all these measurements, and their reported errors, when comparing our models to these data.

More recently, Stern *et al.* (1993) and Jewitt (1994) have published flux measurements at 800 μm and 1300 μm. Again, since these data were all taken on different days, and thus at different rotational aspects of Pluto, we list all the independent measurements reported by these

authors and use the total range of measurements and errors reported to compare with our models.

As flux measurements have been made, investigators have attempted to determine the temperature of Pluto using various models for the temperature distribution on the planet and its satellite. Sykes *et al.* (1987) used two different techniques to model their flux data. In one case they assumed that the temperature distribution on Pluto would be isothermal along lines of constant latitude, resulting in a subsolar temperature of 59 K for Pluto. Their second model assumed CH_4 polar caps, in vapor pressure equilibrium with a methane atmosphere, and an equatorial region devoid of CH_4. Using this model they determined a temperature of 53 K for the polar caps and a subsolar temperature of 58 K in the equatorial region.

Aumann and Walker (1988) also determined temperatures from their infrared flux measurements. Assuming an isothermal sphere they calculated a temperature of $\approx$ 45 K, while using a standard thermal model they found a subsolar temperature of 60 K. Using their 1200 μm data, Altenhoff *et al.* (1988) determined the temperature of Pluto to be 31-39 K, depending on the radius used to model the planet.

For a planet whose temperature is regulated by nitrogen vapor pressure equilibrium Stern *et al.* (1993) used their data to determine an isothermal temperature for Pluto to be 30-55 K, assuming the emissivity of the surface is 1, and 38-44 K if the emissivity of the surface is 0.7. In an attempt to reconcile all of the data points, Jewitt (1994) explores many different temperature models. In particular he models Pluto as a "two-temperature" system, with N_2 polar caps at 35 K and an isothermal equatorial region, devoid of nitrogen, whose temperature is allowed to vary. He finds that the equatorial region could have temperatures ranging from 52-72 K, depending on the areal coverage of the polar caps.

As is evident from the previous discussion, the infrared and millimeter data, taken in isolation, lead to very different conclusions about the surface temperature of Pluto. Using the

Table I. Summary of Published Flux Measurements

Wavelength (μm)	Flux (mJy)	Flux corrected to IRAS distance (mJy)	Source
25	40 ± 20		Aumann and Walker (1987)
60	420 ± 40	406 ± 38.7	Tedesco *et al.* (1987)
60	594 ± 14		Aumann and Walker (1987)
60	581 ± 58		Sykes *et al.* (1987)
100	727 ± 36.3		Aumann and Walker (1987)
100	721 ± 36		Sykes *et al.* (1987)
800	39 ± 6	35.1 ± 5.4	Jewitt (1994)
800	33 ± 7	32.2 ± 6.8	Stern *et al.* (1993)
1200	15.88 ± 4.53	14.8 ± 4.2	Altenhoff *et al.* (1988)
1200	10.72 ± 5.55	9.8 ± 5.1	Altenhoff *et al.* (1988)
1200	11.89 ± 4.60	10.8 ± 4.2	Altenhoff *et al.* (1988)
1200	15.48 ± 1.57	14.0 ± 1.4	Altenhoff *et al.* (1988)
1300	13 ± 4	11.7 ± 3.6	Jewitt (1994)
1300	12 ± 10	11.8 ± 9.8	Stern *et al.* (1993)
1300	10 ± 6	9.6 ± 5.8	Stern *et al.* (1993)
1300	15 ± 4.8	13.5 ± 4.3	Stern *et al.* (1993)

temperature of nitrogen, determined spectroscopically, we attempt to reconcile all the data with a simple, plausible model of Pluto.

Flux Model

We model Pluto as a spherical planet with symmetric polar caps, an approach suggested by the albedo maps of Pluto published by Buie *et al.* (1992) and Young and Binzel (1993) which show a dark equatorial region surrounded by lighter polar regions. Although neither of these maps show north-south symmetry, we model the caps as rotationally and latitudinally symmetric for simplicity. The polar caps are assumed to be solid N_2, while the equatorial region is bare of N_2. We assume that the nitrogen ice-atmosphere system on Pluto obeys the Leighton-Murray (Leighton and Murray 1966) criterion, implying that all areas covered with N_2 ice are isothermal and that other areas will come to a different equilibrium temperature. We fix the temperature of the N_2 ice to agree with our spectroscopic temperature determination and specify the temperature of the equatorial region by assuming a bolometric albedo for the region and then finding the temperature distribution using an instantaneous equilibrium model (Brown *et al.* 1982). The temperature (in K) is determined as a function of latitude (θ) and longitude (ϕ), and has the following form

$$T(\theta,\phi)=1.523\times10^{9}\left[\frac{1-A}{R^{2}\epsilon_{b}}\right]^{\frac{1}{4}}(\sin\theta\cos\phi)^{\frac{1}{4}}$$

where R is the distance between the object and the sun in centimeters, A is the bolometric albedo of the object, and ϵ_b is the bolometric emissivity of the object. The quantity $\sin\theta\cos\phi$ is the cosine of the incidence angle of the radiation at position (θ,ϕ). This expression is a good

approximation to the temperature distribution on a slowly rotating, spherical body with no atmosphere. Although Pluto has an N_2 atmosphere, we use this expression because the atmosphere is very tenuous and will have little effect on the temperature of regions not covered with nitrogen ice (Stansberry *et al.* 1992).

Some authors (Sykes *et al.* 1987, Stern *et al.* 1993) have chosen to model Pluto with an isothermal latitude model, assuming that Pluto is so cold that it cannot radiate heat efficiently; thus, its temperature distribution will resemble that of a rapid rotator. We have chosen not to use an isothermal latitude model for determining temperatures in the equatorial region for the following reason; one of our coauthors (RHB) has developed a thermal model for airless bodies

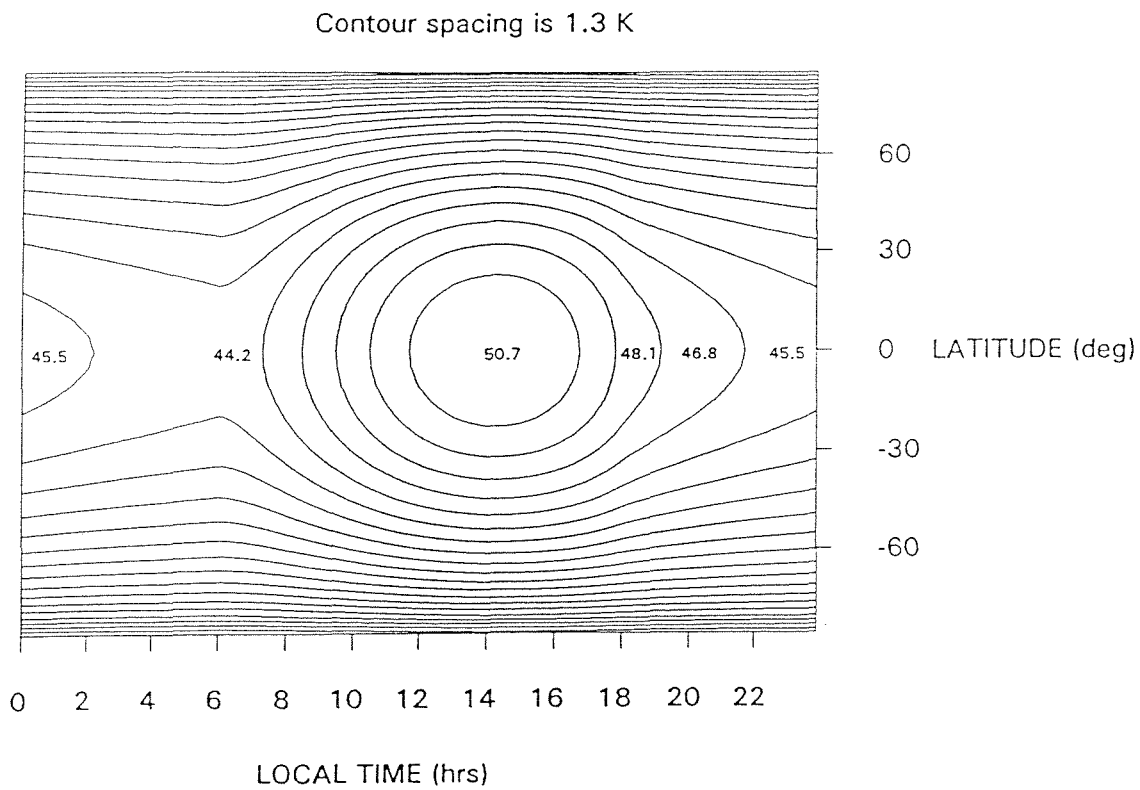

Figure 7. A surface temperature map of Pluto calculated by THERMOD. Note that the temperature is not strictly a function of latitude, but has a well defined thermal bulge at ≈ 2 pm local time.

(THERMOD, cf. Brown and Matson, 1987) which, given such parameters as the heliocentric distance, rotation period, albedo, and thermal inertia of an object, calculates the surface temperature, and temperature at depth, for the object. If we enter thermal parameters similar to those of icy satellites (e.g. a thermal inertia $\approx 3 \times 10^4$ erg $s^{-1/2}$ cm^{-2} K^{-1}) and orbital data relevant to Pluto, we do not find that Pluto shows a temperature distribution dependent only on latitude. Instead, the distribution has a peak temperature at the sub-solar latitude at about 2 pm local time, similar to other icy objects in the solar system (Fig. 7). While an instantaneous equilibrium model does not mimic this behavior exactly (the thermal bulge being at noon rather than 2 pm), it is a better approximation than one in which the temperature depends solely on latitude.

Because Pluto and Charon are not separately resolved in the flux measurements, we must account for the flux from Charon in our model. Little is known about the surface of Charon, aside from the detection of water ice in its spectrum (Buie *et al.* 1987, Marcialis *et al.* 1987), so we model Charon as a spherical uniform body with an albedo typical of the icy Uranian satellites (Veverka *et al.* 1991). Its temperature distribution is then computed using the instantaneous equilibrium equation given above.

Once temperature distributions have been determined for Pluto and Charon the expected flux from the system can be calculated. For these calculations a phase angle of 0° is assumed. This assumption is justified because the Pluto/Charon system is never seen from Earth at a phase angle greater than 1.9°.

The flux received from a spherical planet is

$$F_\lambda = \frac{4\pi h c^2 r^2 \epsilon_\lambda}{D^2 \lambda^5} \int_\phi \int_\theta \frac{\sin^2\theta \cos\phi \, d\theta \, d\phi}{e^{hc/\lambda k T(\theta,\phi)} - 1}$$

where r is the radius of the planet, D is the distance from the planet to the observer, $T(\theta,\phi)$ is

the temperature of the planet at the given θ and ϕ, and ϵ_λ is the emissivity of the object at wavelength λ (Brown *et al.* 1982). For the Pluto/Charon system the total flux is the sum from two spherical bodies, one representing Pluto and the other Charon. The flux integral for Pluto is broken into three portions, one for each polar cap and one for the equatorial region.

Model Parameters

Certain parameters are fixed in our flux modeling. These include the radii of Pluto and Charon, the Pluto-Earth and Pluto-Sun distances, the temperature of the caps, and the emissivities of the caps, the equator, and Charon. The values chosen for these parameters are discussed below.

Although the radius of Pluto is more accurately known from mutual event observations, there is still some debate over its exact value. Buie *et al.* (1992) derive a value for Pluto's radius of 1150 km from analysis of mutual event data, but stellar occultation data yield a value closer to 1180 km (Hubbard *et al.* 1990, Millis *et al.* 1993). For this study we adopt the Buie *et al.* (1992) value in light of recent work by Stansberry (1994) and Stansberry *et al.* (1994) who propose that a strong thermal inversion layer could prevent the underlying atmosphere from being sensed by an occultation. We adopt the value of 593 km for the radius of Charon from the same work.

The distances chosen for the Pluto-Earth and Pluto-Sun separation are those given by Sykes *et al.* (1987) which are appropriate for the time of the IRAS measurements. The millimeter fluxes reported by Altenhoff *et al.* (1988), Stern *et al.* (1993), and Jewitt (1994) were adjusted to the Pluto-Earth distance of the IRAS measurements. Pluto's distance from the Sun also changed between the various observations, but by a small amount which does not

significantly alter the observed fluxes. We assume the Charon-Earth and Charon-Sun distances to be the same as those for Pluto because the separation of Pluto and Charon is small compared to the distance of the system from either the Earth or Sun.

We use the temperature of N_2 on Pluto, 40 K as determined above, as the temperature of the N_2 polar caps. For the emissivity of the N_2 polar caps we use a value of 0.6 based on the analysis of Voyager 2 data of N_2 ice on Triton (Stansberry *et al.* 1990). More recent modeling by Stansberry *et al.* (1992), which takes into account surface-atmosphere interactions, suggests that the emissivity of N_2 on Triton may be 0.75. Because the flux produced by the polar caps in our model is small relative to the total flux of Pluto and Charon (as we will show later) the difference between modeling the caps with an emissivity of 0.75 or 0.6 is negligible. Thus we adopt a constant value of 0.6 for the emissivity of the polar caps.

The emissivities of Charon and the equatorial region of Pluto are set to 0.95 in agreement with measured infrared emissivities of water ice and rocky matter. During our calculations we have assumed that the emissivities are constant over the entire wavelength region being modeled

Table II - Fixed parameters

Pluto Radius[a]	1150 km
Charon Radius[a]	593 km
Pluto-Earth Distance[b]	30.28 AU
Pluto-Sun Distance[b]	29.87 AU
Temperature of Caps	40 K
Emissivity of Caps	0.60
Emissivity of Equator	0.95

[a] Values from Buie *et al.* (1992)
[b] Values at the time of IRAS measurements, from Sykes *et al.* (1987)

(1-3000 μm). Measurements of the icy Galilean satellites and asteroids imply that the effective emissivities of these bodies are lower at centimeter wavelengths than at infrared and visible wavelengths (Ostro and Shoemaker 1990, Muhleman *et al.* 1986, Webster and Johnston 1989). But, as there are no laboratory data which show how the emissivity varies with wavelength, we choose to assume constant emissivities.

Table II summarizes the constant parameters for our flux modeling.

There are three remaining parameters needed to calculate the flux: the equatorial albedo of Pluto, the extent of the polar caps of Pluto, and the albedo of Charon. Because there are no definitive values in the literature for these quantities we vary them to find a set which will fit the observational data.

Albedo maps of Pluto (Buie *et al.* 1992 and Young and Binzel 1993) indicate that the equatorial region is quite dark (normal reflectance of ≈ 0.2). The bolometric albedo associated with this reflectance will depend on the detailed scattering properties of the region, so we have modeled a large range of bolometric albedos to cover the plausible range of values. We vary the albedo of Pluto's equatorial region from 0.1 to 0.6 in increments of 0.1. The sub-solar temperatures which correspond to these albedos, assuming instantaneous equilibrium, are, 71, 69, 67, 64, 61, and 58 K.

Table III - Parameter Space Explored in Flux Modeling

Parameter	Range	Increment
Cap extent	10° - 90°	5°
Equatorial bolometric albedo	0.1 - 0.6	0.1
Charon bolometric albedo	0.3 - 0.5	0.1

As mentioned previously, water ice has been detected on the surface of Charon (Buie *et al.* 1987, Marcialis, *et al.* 1987). Other observations have determined Charon's geometric albedo to be ≈ 0.35 at wavelengths between 0.50 and 1.0 μm (Fink and DiSanti 1988) and 0.15-0.40 in the wavelength region 1.4-2.5 μm (Marcialis *et al.* 1992). Additionally, albedo maps of Charon's Pluto-facing hemisphere show it to be as dark as the equatorial region of Pluto (Buie *et al.* 1992). For these reasons we vary the bolometric albedo over a range similar to those of icy Uranian satellites. We use values of 0.3, 0.4 and 0.5.

The final variable parameter is the extent of the polar caps. As previously mentioned, the caps are modeled as north-south symmetric for simplicity, although it is likely that Pluto's polar caps would have some asymmetry. The largest caps extend to $\pm 10°$ latitude, and we decrease the cap extent by 5° until there are no polar caps.

The ranges of these variable parameters are given in Table III. Our models were run so that the entire parameter space defined by these ranges was explored. The results will be discussed in the next section.

Model Results and Discussion

One of our model runs is compared with observed fluxes in Fig. 8. The model flux (solid line) corresponds to a Pluto with an equatorial albedo of 0.2, polar caps extending to $\pm 20°$ latitude, and a Charon with an albedo of 0.4. As can be seen, this model is consistent with all the data.

Figure 9 shows the contributions of each part of the model, Pluto's caps, Pluto's equator, and Charon, to the total flux from the system. The solid line is the same model shown in the last figure, and the other lines represent, in order of decreasing flux, Pluto's equator, Charon, and

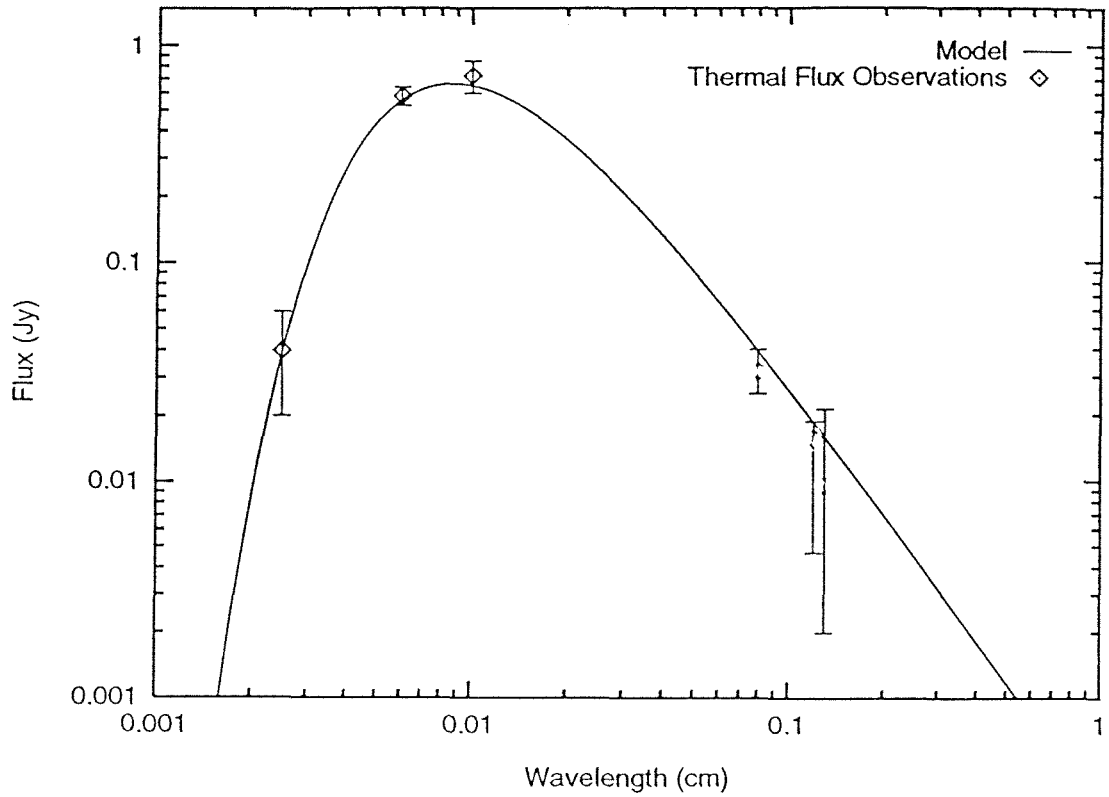

Figure 8. Observations and model of the flux from the Pluto/Charon system. The infrared measurements are represented by points with error bars. The millimeter points are represented by an error bars showing the range of measurements made at that wavelength (see text for details). The line is a model for the total flux from a system with an equatorial albedo of 0.2, polar caps extending down to $\pm 20°$, and a Charon albedo of 0.4.

Pluto's caps. Being colder than the equator, the caps radiate at a longer wavelength and with less intensity. Because of this, as the area of the caps is increased, more flux is removed from the infrared region than is removed from the millimeter region. For example, comparison of the model in Fig. 8 with a model using the same parameters, but no polar caps, shows that the fluxes in a model with caps are smaller by 40% at 60 μm, 35% at 100 μm, and 25% at 800 μm and 1300 μm.

The results of our modeling for three values of Charon's albedo are summarized in Fig. 10. Flux measurements at all wavelengths are satisfied in these models only in the regions of parameter space where the two hatched areas in the figures overlap. This overlap occurs only

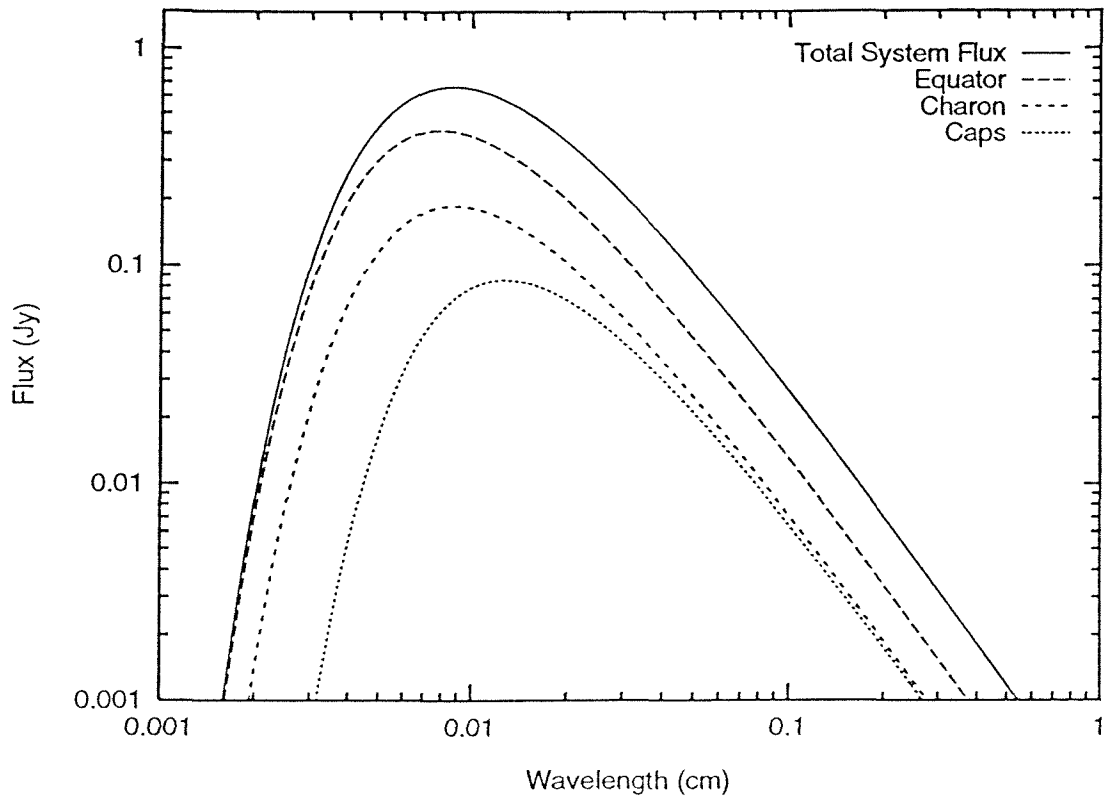

Figure 9. Modeled flux from the Pluto/Charon and contributions from different areas making up the system. The solid line represents the total flux of the system. The other lines represent (in order of decreasing flux) the flux from the equatorial region of Pluto, Charon, and the polar caps of Pluto.

over a very small area of parameter space encompassing bolometric albedos of 0.1 and 0.2, and polar cap extents to $\pm 15°$ and $\pm 20°$ latitude. The figures also illustrate that, regardless of the bolometric albedo of the equator, the millimeter wavelength points demand a very large area of Pluto be covered by a cold region (N_2 ice).

Implicit in the flux model presented here, and previous modeling by other authors, is the assumption that the flux observations at all wavelengths are measuring the same quantity, surface temperature. While the infrared data certainly reflect the surface temperature, millimeter measurements probe deeper into a planet's surface, and may reflect a different temperature regime. To show that the millimeter points represent surface temperature it must be demonstrated that they do not probe much deeper than a diurnal skin depth. Such arguments have been put

forth by Stern *et al.* (1993), and Jewitt (1994).

Stern *et al.* (1993) use a rapid rotator model to model the temperature of Pluto, which implies that the temperature distribution is isothermal along lines of constant latitude. One result of such a model is that the equilibrium temperature, at a given latitude, of the planet does not vary with depth. Thus, measurements at any wavelength will sense temperatures equal to the surface temperature. Jewitt (1994) assumes that Pluto has a large thermal inertia, which if true, results in a diurnal skin depth that is very large compared to the penetration depth of the millimeter radiation. In such a case any temperature variation occurs below the depth that can be sensed.

As mentioned previously, as a result of our own thermal modeling (Fig. 7), we do not believe that Pluto behaves as a rapid rotator. If there are significant temperature variations with longitude on the surface, there will be temperature variations with depth. Using the value of thermal inertia with which we modeled Pluto, and the length of Pluto's diurnal cycle ($\approx$6.5 days) we find that the Pluto's diurnal skin depth is $\approx$3 cm. This is significantly smaller than the skin depth calculated by Jewitt (1994) who assumes a higher thermal inertia. A skin depth of 3 cm is 25 times greater than 1200 μm radiation. This is only 2.5 times the assumed penetration depth of 10λ assumed for millimeter radiation. Thus, it may not be correct to assume that the millimeter points are sensing the surface temperature.

Another factor which could effect the flux measurements is the emissivity of the surface being modeled. While we model the N_2 caps and equatorial region with emissivities constant over all wavelengths, measurements made at centimeter wavelengths suggest that this may not be the case for all objects in the solar system. Thermal measurements of the icy Galilean satellites (Muhleman *et al.* 1986) show that at 2 and 6 cm the effective emissivities of these objects are low, 0.5-0.7, compared to their infrared emissivity, which is close to 0.9. Radar observations of these satellites in the centimeter region show similar results (Ostro and Shoemaker

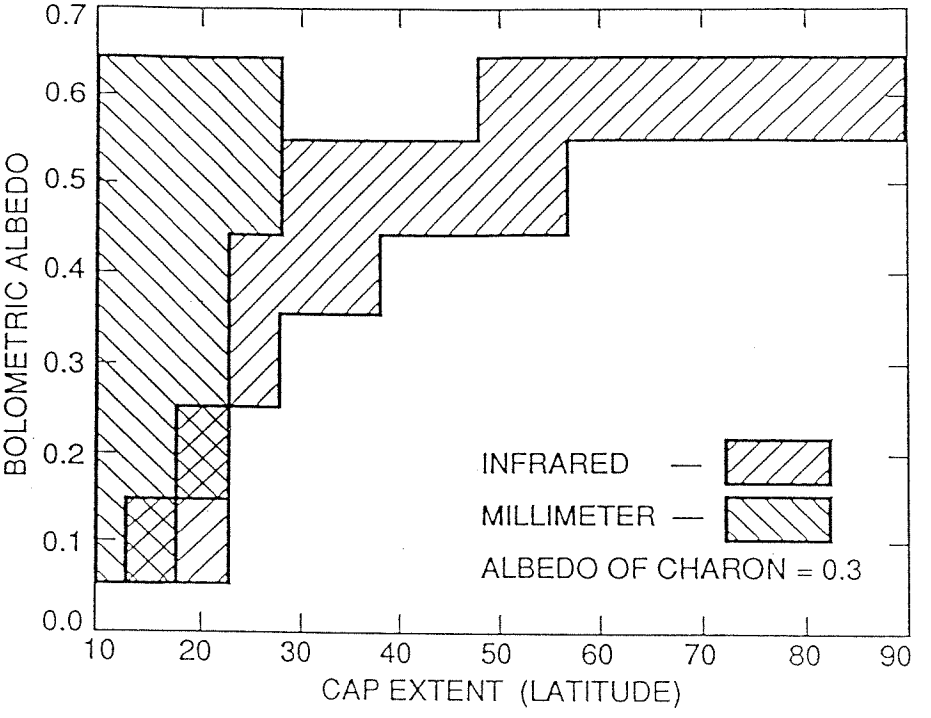

Figure 10a

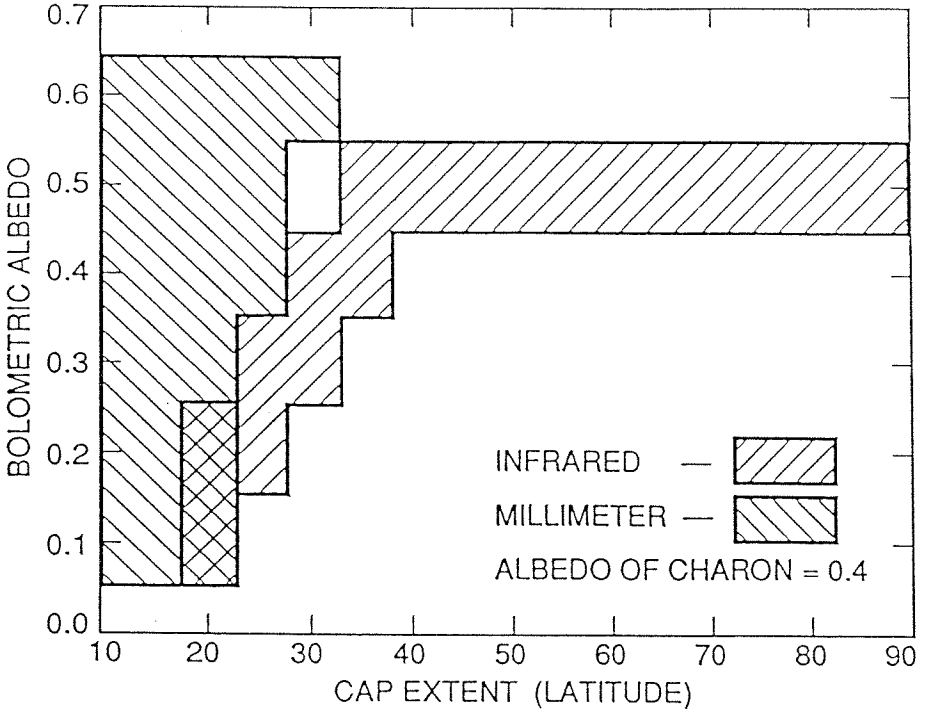

Figure 10b

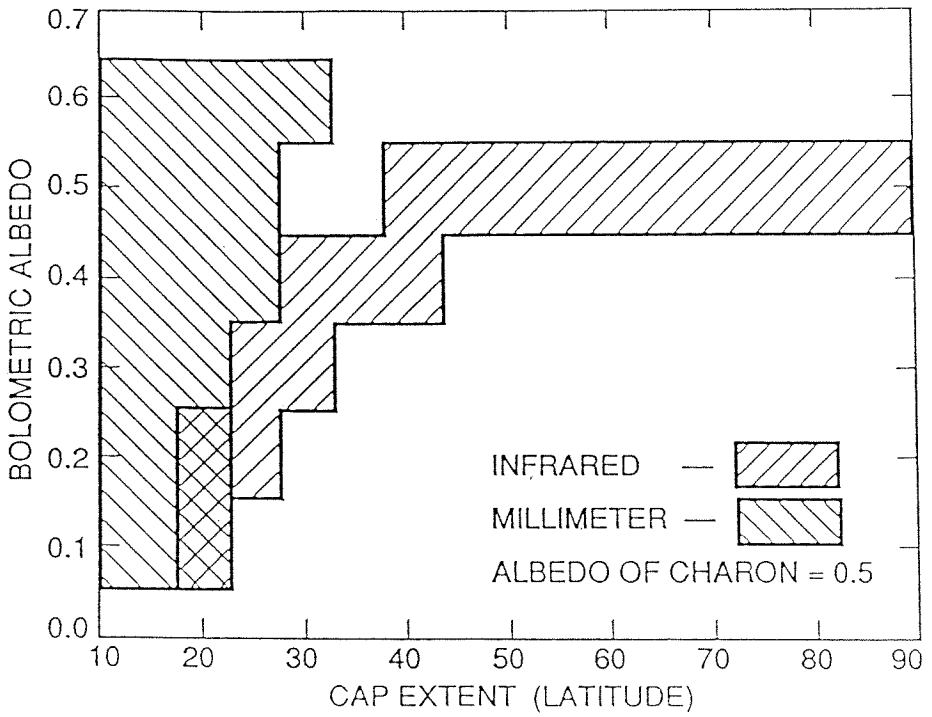

Figure 10c

Figure 10. Plots displaying the bolometric albedo/cap extent parameter space where the flux models fit the observational data. Each part of this figure represents a different bolometric albedo for Charon; (a) 0.3, (b) 0.4, (c) 0.5. Each plot shows two hatched areas, one corresponding to bolometric albedos and polar cap extents where the models match all the infrared measurements, and the other corresponding to the parameters which fit all the millimeter-wave data. Where the hatched ares overlap is the area of parameter space which satisfies all the flux data simultaneously.

1990). Observations of the asteroids 1 Ceres and 4 Vesta show indications of lower emissivities in the centimeter region (Webster and Johnston 1989). Whether these low effective emissivities are indicative of low emissivity materials, or some process, such as multiple scattering, which removes radiation from the observer's line of sight is unclear.

In view of these examples, it is reasonable to assume that Pluto may have lower effective emissivities at long wavelengths. The effect of a smaller emissivities at longer wavelengths would be two-fold. First, and most simply, it would depress the long wavelength fluxes.

Additionally, lower emissivities might also imply that radiation at longer wavelengths is probing deeper into the surface than would otherwise be assumed. Deeper penetration depths would mean that the long wavelength radiation would be even more likely to be probing below the diurnal skin depth, and therefore measuring a temperature more nearly equal to the diurnal-mean temperature rather than the diurnally varying surface temperature.

Summary

We find the temperature of the nitrogen on Pluto's surface to be 40 ± 2 K on the basis of spectroscopic measurements. This is warmer than the temperature determined for Triton (38 ± 1 K) using the same method. If the nitrogen in the atmosphere and on the surface of Pluto were in vapor pressure equilibrium, as appears to be the case for Triton, this would imply a surface pressure of ≈ 60 μbar, much higher then the 3-10 μbar value derived from stellar occultation measurements (Yelle and Lunine 1989, Hubbard *et al.* 1990). This discrepancy could be due to many factors, including contaminants in the nitrogen, or the occultation measurements not probing down to the surface (Stansberry *et al.* 1994).

We modeled the flux expected from the Pluto/Charon system assuming the nitrogen on Pluto is contained in rotationally symmetric polar caps at a temperature of 40 K. Assuming that all flux measurements are indicative of surface temperature, our models show that the IRAS and millimeter wave fluxes are consistent with a Pluto having N_2 polar caps and an equatorial region devoid of N_2. To fit all the observational data, the polar caps must extend to $\pm(15°\text{-}20°)$ latitude, and the bolometric albedo of the equatorial region must be $\leq .2$ (subsolar temperature > 68 K). Examining the millimeter and infrared data separately, we find that the millimeter data can only be fit with an equatorial region having a bolometric albedo ranging from 0.1-0.6, but

only if the polar caps are very large (caps extending down to $\pm 30°$ or larger). The infrared data allow a much larger range of polar cap extents and equatorial albedos, although in this case the larger the albedo, the smaller the polar cap extent.

Larger ranges of these parameters might fit the entire data set if one assume that the millimeter points are sensitive to a temperature other than the surface temperature, or if the emissivity of the surface is dependent upon wavelength (emissivity decreasing as wavelength increases).

Acknowledgements

We wish to thank John Stansberry and an anonymous reviewer for comments which helped improve this paper. TCO would like to acknowledge that his contribution to this work was partially supported by the NASA Planetary Atmospheres Program (NAGW 2650). This is contribution number 5420 of the Division of Geological and Planetary Sciences, California Institute of Technology, Pasadena, California, 91125.

References

Altenhoff, W.J., R. Chini, H. Hein, E. Kreysa, P.G. Mezger, C. Salter, and J.B. Schraml 1988. First radio astronomical estimate of the temperature of Pluto. *Astron. and Astrophs.* **190**, 15-17 (letter).

Aumann, H.H. and R.G. Walker 1987. IRAS observations of the Pluto-Charon system. *Astron. J.* **94**, 1088-1091.

Broadfoot, A.L., *et al.* 1989. Ultraviolet spectrometer observations of Neptune and Triton. *Science* **246**, 1459-1466.

Brown, G.N. and W.T. Ziegler 1980. Vapor pressure and heats of vaporization and sublimation of liquids and solids of interest in cryogenics below 1-atm pressure. *Adv. Cry. Engin.* **25**, 662-670.

Brown, R.H., D. Morrison, C.M. Tedesco, and W.E. Brunk 1982. Calibration of the radiometric asteroid scale using occultation diameters. *Icarus* **52**, 188-195.

Brown, R.H. and D.L. Matson 1987. Thermal effects of insolation propagation into the regoliths of airless bodies. *Icarus* **72**, 84-94.

Buie, M.W., D.P. Cruikshank, L.A. Lebofsky, E.F. Tedesco 1987. Water frost on Charon. *Nature* 329, 522-523.

Buie, M.W., D.J. Tholen, K. Horne 1992. Albedo maps of Pluto and Charon: Initial mutual event results. *Icarus* **97**, 211-227.

Chandrasekhar, S. 1960. *Radiative Transfer*, Dover Publications, Inc., New York.

Clark, R.N. and T.L. Roush 1984. Reflectance spectroscopy: Quantitative analysis techniques for remote sensing applications. *J. Geophys. Res.* **89**, 6329-6340.

Conrath, B., F. M. Flasar, R. Hanel, V. Kunde, W. Maguire, J. Pearl, J. Pirraglia, R.

Samuelson, P. Gierasch, A. Weir, B. Bezard, D. Gautier, D. Cruikshank, L. Horn, R. Springer, and W. Shaffer 1989. Infrared observations of the Neptunian system. *Science* **246**, 1454-1459.

Cruikshank, D.P., R.H. Brown, and R.N. Clark 1984. Nitrogen on Triton. *Icarus* **58**, 293-305.

Cruikshank, D.P., T.L. Roush, T.C. Owen, T.R. Geballe, C. deBergh, B. Schmitt, R.H. Brown, and M.J. Bartholomew 1993. Ices on the surface of Triton. *Science* **261**, 742-745.

Green. J.R., R.H. Brown, D.P. Cruikshank, and V. Anicich 1991. The absorption coefficient of nitrogen with application to Triton. *Bull. Amer. Astron. Soc.* **23**, 1208.

Grundy W.M., B. Schmitt, and E. Quirico 1993. The temperature dependent spectra of α and ß nitrogen ice with application to Triton. *Icarus* **105**, 254-258.

Fink, U. and M.A. DiSanti 1988. Separate spectra of Pluto and its satellite Charon. *Astron. J.* **95**, 229-236.

Hapke, B. 1981. Bidirectional reflectance spectroscopy. *J. Geophys. Res.* **86**, 3039-3054.

Hubbard, W.B., R.V. Yelle, and J.I. Lunine 1990. Nonisothermal Pluto atmosphere models. *Icarus* **84**, 1-11.

Jewitt, D.C. 1994. Heat from Pluto. *Astronomical J.* **107**, 372-378.

Leighton, R.B. and B.C. Murray 1966. Behavior of carbon dioxide and other volatiles on Mars. *Science* **153**, 136-144.

Marcialis, R.L., G.H. Rieke, and L.A. Lebofsky 1987. The surface composition of Charon: Tentative identification of water ice. *Science* **237**, 1349-1351.

Marcialis, R.L., L.A. Lebofsky, M.A. DiSanti, U. Fink, E.F. Tedesco, and J. Africano 1992. The albedos of Pluto and Charon: Wavelength dependence. *Astron. J.* **103**, 1389-1394.

Millis, R. L., L. H. Wasserman, O. G. Franz, R. A. Nye, J. L. Elliot, E. W. Dunham, A. J.

Bosh, L. A. Young, S. W. Slivan, A. C. Gilmore, P. M. Kilmartin, W. H. Allen, R. D. Watson, S. W. Dieters, K. M. Hill, A. B. Giles, G. Blow, J. Priestly, W. M. Kissling, W. S. G. Walker, B. F. Marino, D. G. Dix, A. Page, J. E. Ross, M. D. Kennedy, K. A. Mottram, G. Mayland, T. Murphy, C. C. Dohn, and A. R. Klemola 1993. Pluto's radius and atmosphere - results from the entire 9 June 1988 occultation data set. *Icarus* **105**, 282-297.

Muhleman, D.O., G.L. Berge, D. Rudy, and A.E. Neill 1986. Precise VLA positions and flux-density measurements of the Jupiter system. *Astron. J.* **92**, 1428-1435.

Ostro, S.J. and E.M. Shoemaker 1990. The extraordinary radar echoes from Europa, Ganymede, and Callisto: A geological perspective. *Icarus* 85, 335-345.

Owen, T.C. T.L. Roush, D.P. Cruikshank, J.L. Elliot, L.A. Young, C. deBergh, B. Schmitt, T.R. Geballe, R.H. Brown, and M.J. Bartholomew 1993. Surface ices and atmospheric composition of Pluto. *Science* **261**, 745-748.

Owen, T.C., D.P. Cruikshank, C. de Bergh, T.R. Geballe, T. Roush, M.J. Bartholomew, B. Schmitt, R.H. Brown, J.L. Elliot, L.A. Young, and S. Douté 1993b. New spectra of Pluto in the 1.2-2.5 μm range. *Bull. Amer. Astron. Soc.* **25**, 1128.

Scott, T.A. 1976. Solid and liquid nitrogen. *Phys. Rep.* **27**, 89-157.

Stansberry, J.A., Lunine, J.I., and B. Rizk 1990. The emissivity of nitrogen ice: Implications for Triton. *Bull. Amer. Astron. Soc.* **22**, 1120.

Stansberry, J.A., R.V. Yelle, J.I. Lunine, and A.S. McEwen 1992. Triton's surface-atmosphere energy balance. *Icarus* **99**, 242-260.

Stansberry, J.A. 1994. Surface-atmosphere coupling on Triton and Pluto. University of Arizona, Tucson.

Stansberry, J.A., J.I. Lunine, W.B. Hubbard, R.V. Yelle, and D.M. Hunten 1994. Mirages and

the nature of Pluto's atmosphere. *Icarus* **111**, (in press).

Stern, S.A., D.A. Weintraub, M.C. Festou 1993. Evidence for a low surface temperature on Pluto from millimeter-wave thermal emission measurements. *Science* **261**, 1713-1716.

Sykes M.V., R.M. Cutri, L.A. Lebofsky, and R.P. Binzel 1987. IRAS serendipitous survey of observations of Pluto and Charon. *Science* **237**, 1336-1340.

Tedesco, E.F., G.J. Veeder, R.S. Dunbar, L.A. Lebofsky 1987. IRAS constraints on the sizes of Pluto and Charon. *Nature* **327**, 127-129.

Tryka, K.A., R.H. Brown, V. Anicich, D.P. Cruikshank, and T.C. Owen 1993. Spectroscopic determination of the composition and temperature of nitrogen on Triton. *Science* **261**, 751-754.

Tryka, K.A., R.H. Brown, and V. Anicich. Absorption coefficients of nitrogen in the regions of the fundamental (4.294 μm) and first overtone (2.148 μm) bands as a function of temperature. *In prep.*

Veverka, J., R.H. Brown, and J.F. Bell 1991. Uranus satellites: surface properties. in *Uranus* (J.A. Burns, E.D. Miner, and M.S. Matthews, Eds.), pp 528-560. Univ. of Arizona Press, Tucson.

Weast, R.C. (Ed.) 1980. *CRC Handbook of Chemistry and Physics*. CRC Press, Boca Raton, Florida.

Webster, W.J., and K.J. Johnston 1989. On the wavelength dependence of apparent emissivity of asteroid microwave emissions: Ceres and Vesta. *Pub. Astron. Soc. Pac.* **101**, 122-125.

Yelle, R.V. and J.I. Lunine 1989. Evidence for a molecule heavier than methane in the atmosphere of Pluto. *Nature* **339**, 228-290.

Young, E.F. and R.P. Binzel 1993. Comparative mapping of Pluto's sub-Charon hemisphere: Three least squares models based on mutual event lightcurves. *Icarus* **102**, 134-149.

Summary

Collection of Conclusions

I have made measurements of the near infrared spectrum of solid nitrogen and found that the bands produced by the fundamental vibrational transition, at 4.294 μm, and its first overtone, at 2.148 μm, are temperature dependent. In particular, the first overtone becomes stronger and narrower as the temperature of the sample is lowered. Additionally, a sideband is visible at $\approx$2.16 μm at temperatures between 41 and 35.6 K (the α-ß phase transition temperature). When the temperature of the sample drops below the α-ß phase transition temperature the band abruptly changes its appearance; it becomes very narrow (FWHM $\approx$ 1 cm^{-1}) and much deeper (from 96% transmittance to 75% transmittance).

The N_2 overtone band is seen in the spectra of Triton and Pluto, and my laboratory measurements indicated that, by comparing the laboratory data to the observational data, I would be able to determine the phase, and possibly the temperature, of the N_2 on these objects.

Because the temperature of Triton is known from measurements made by the Voyager 2 spacecraft (Conrath *et al.* 1989), I analyzed the nitrogen overtone band in ground-based observations of Triton to test the accuracy of the technique. Using spectral modeling techniques developed by Hapke (1981) I was able to convert the laboratory transmission data to reflectance for comparison to the observational data. I found that the laboratory data that best fit the observational data of Triton were in the temperature range of 38 ± 1 K, in agreement with Voyager measurements. This result showed that it is possible to accurately derive the temperature of N_2 on an object based on the appearance of the N_2 overtone band in the object's spectrum.

Using the same technique for Pluto I find that the best fitting temperatures are in the range 40 ± 2 K. To determine whether the 40 K temperature could be reconciled with thermal flux observations of Pluto, I modeled the flux from the Pluto/Charon system assuming that Pluto had symmetric nitrogen polar caps at 40 K, and an equatorial region, devoid of N_2, which was in instantaneous equilibrium with the incident solar flux. With these assumptions, I found that all of the observational data could be matched by a Pluto which had polar caps extending to $\pm20°$ latitude, and a very dark equatorial region, bolometric albedo ≤0.2.

Outstanding Problems and Possible Future Research

Assuming that the nitrogen on Pluto is in vapor pressure equilibrium, as it appears to be on Triton, and using the 40 K temperature result, leads to the conclusion that the surface pressure on Pluto is ≈60 μbar. This pressure is much higher than that inferred from observations of a stellar occultation by Pluto, 3-10 μbar (Yelle and Lunine 1989, Hubbard *et al.* 1990). If we again assume vapor pressure equilibrium, the occultation surface pressure would indicate that Pluto's surface temperature was 35-37 K, possibly below the α-ß phase transition temperature. There are many possible ways to explain this apparent discrepancy. One explanation is that the system is not in vapor pressure equilibrium, although the similarities in surface composition and temperature between Triton and Pluto imply that this is a remote possibility. A second possibility is that the N_2 is contaminated by another species, altering the vapor pressure of the system. This idea is supported by laboratory measurements made by Schmitt *et al.* (1993) which demonstrate that if small amounts of CH_4 are in solid solution with N_2, the CH_4 bands are shifted from their positions in pure CH_4. Such shifts in CH_4 bands are observed in the spectra of both Triton and Pluto. Currently the best explanation is that of Stansberry *et al.* (1994), because it also addresses

the discrepancy between the radius of Pluto inferred from the Pluto/Charon mutual events, ≈ 1150 km (Buie *et al.* 1992) and that inferred from the stellar occultation, ≈ 1180 km, (Hubbard *et al.* 1990, Millis *et al.* 1993). They propose that Pluto's atmosphere has a thermal inversion layer which effectively masks the lower atmosphere from detection during a stellar occultation, and makes it appear that the surface is at a greater radius, and lower pressure, than it truly is.

In light of the result that the infrared spectral bands of solid nitrogen are temperature dependent, it is reasonable to consider whether any other molecular solids show this type of behavior. Because the appearance of the nitrogen band is linked to a solid state phase transition, it would be logical to look at molecules which also have solid state phase transitions in temperature regions applicable to the icy satellites. CO, with a phase transition at 61.54 K immediately come to mind. Because CO has much stronger absorptions than nitrogen it is not possible to use the thick cell apparatus that we used to measure the spectrum of nitrogen. Instead, thin samples, deposited on a window in a vacuum chamber, would be necessary. The problem with this technique is that, although CO is stable in vapor pressure equilibrium conditions over a large temperature range, when exposed to vacuum it evaporates quickly except at very cold (< 30 K) temperatures. Such a high evaporation rate will make it hard to determine the absorption coefficients of samples at warmer temperatures, because the thickness of the sample will not be constant while the measurements are being made.

Another process which could change the appearance of spectral bands, and thus the interpretations of those bands, is the presence of contaminants. As mentioned previously, studies by Schmitt *et al.* (1993) have shown that when small amounts of methane are included in a nitrogen matrix the central wavelengths of the methane bands shift from their values in pure methane. Measurements have not yet been made of other possible contaminants in a nitrogen matrix. In particular, it would be interesting to see how CO, which is very similar to N_2 in size

and structure, but which has a dipole moment, might affect the appearance of the N_2 band. In addition to changing the appearance of spectral bands, contaminants can also affect the equilibrium vapor pressure of a sample. N_2/CO mixtures form an ideal solid solution at nearly all temperatures and mixing ratios, so that Raoult's law, relating the partial pressures of the individual vapor components over the solid solution, can be used to determine the vapor pressure. But, for mixtures such as N_2/CH_4, which are not ideal over large ranges of temperature and mixing ratio, Raoult's law is not valid and laboratory measurements are needed to accurately determine vapor pressures (Yelle *et al.* 1995).

There are many reasons to continue observing both Triton and Pluto. As Triton approaches and then recedes from a deep southern summer, and as Pluto moves away from perihelion, it will be interesting to see if there are any changes in the shape of the nitrogen overtone band in either of these planets' spectrum. Changes in the band would allow us to trace the temperature evolution of the surfaces of these bodies and may help constrain volatile transport models. Additionally, there have been observations of both Triton (Cruikshank and Apt 1984) and Pluto (Owen *et al.* 1993) hinting at spectral variability on both objects. To determine whether or not this is the case, both objects will need to be closely monitored in the coming years.

As telescopic instrumentation continues to improve we will be able to take higher resolution spectra of bodies such as Triton and Pluto. Recent spectroscopic measurements of Triton, at higher resolution than those reported in this thesis, show that as resolution is increased, previously unseen bands are revealed. Laboratory measurements suggest that some of these bands can be attributed to isotopic variations of previously identified molecular species (e.g., four bands in the high resolution spectrum of Triton seem to coincide with bands of ^{13}CO measured in the laboratory by Brown *et al.* (1994)). If isotopic ratios can be determined from spectral

observations, it will be possible to speculate about the different fractionation processes which may have lead to such ratios, and thus learn more about the forces that shaped the history of Triton and Pluto.

If current models, proposing that Triton originally formed at a similar distance from the Sun in the solar nebula as Pluto, and was then captured into orbit around Neptune, are correct, then Triton and Pluto become an extremely interesting pair of bodies to study. Forming in the same region of the solar nebula, these objects may have started with very similar compositions and interior structures, but, while Pluto has presumably remained in this primordial state, Triton very likely underwent a great deal of heating while being captured into Neptune's gravitational field. Thus, compositional, and other, differences between Triton and Pluto may be indicative of the unique processes which shaped Triton. A better understanding of the history of Triton can do nothing but add to our understanding of the origins of, and the processes which shaped, the entire solar system.

References

Brown, R.H., V. Anicich, and K.A. Tryka 1994. Heavy isotopes of carbon and nitrogen on Triton and Pluto. *Bull. Amer. Astron. Soc.* **26**, 1176.

Conrath, B., F. M. Flasar, R. Hanel, V. Kunde, W. Maguire, J. Pearl, J. Pirraglia, R. Samuelson, P. Gierasch, A. Weir, B. Bezard, D. Gautier, D. Cruikshank, L. Horn, R. Springer, and W. Shaffer 1989. Infrared observations of the Neptunian system. *Science* **246**, 1454-1459.

Cruikshank, D.P. and J. Apt 1984. Methane on Triton: Physical state and distribution. *Icarus* **58**, 306-311.

Cruikshank, D.P., R.H. Brown, A.T. Tokunaga, R.G. Smith, and J.R. Piscitelli 1988. Volatiles on Triton: The infrared spectral evidence 2.0-2.5 μm. *Icarus* **74**, 413-423.

Hapke, B. 1981. Bidirectional reflectance spectroscopy. *J. Geophys. Res.* **86**, 3039-3054.

Hubbard, W.B., R.V. Yelle, and J.I. Lunine 1990. Nonisothermal Pluto atmosphere models. *Icarus* **84**, 1-11.

Millis, R. L., L. H. Wasserman, O. G. Franz, R. A. Nye, J. L. Elliot, E. W. Dunham, A. J. Bosh, L. A. Young, S. W. Slivan, A. C. Gilmore, P. M. Kilmartin, W. H. Allen, R. D. Watson, S. W. Dieters, K. M. Hill, A. B. Giles, G. Blow, J. Priestly, W. M. Kissling, W. S. G. Walker, B. F. Marino, D. G. Dix, A. Page, J. E. Ross, M. D. Kennedy, K. A. Mottram, G. Mayland, T. Murphy, C. C. Dohn, and A. R. Klemola 1993. *Icarus* **105**, 282-297.

Owen, T.C. T.L. Roush, D.P. Cruikshank, J.L. Elliot, L.A. Young, C. deBergh, B. Schmitt, T.R. Geballe, R.H. Brown, and M.J. Bartholomew 1993. Surface ices and atmospheric composition of Pluto. *Science* **261**, 745-748.

Schmitt, B., E. Quirico, C. deBergh, T.C. Owen, D.P. Cruikshank 1993. The near-infrared spectra of Triton and Pluto: A laboratory analysis of the methane bands. *Bull. Amer. Astron. Soc.* **25**, 1129.

Stansberry, J.A., J.I. Lunine, W.B. Hubbard, R.V. Yelle, and D.M. Hunten 1994. Mirages and the nature of Pluto's atmosphere. *Icarus* **111**, in press.

Yelle, R.V. and J.I. Lunine 1989. Evidence for a molecule heavier than methane in the atmosphere of Pluto. *Nature* **339**, 228-290.

Yelle, R.V., J.I. Lunine, J.B. Pollack, and R.H. Brown 1995. Lower atmospheric structure and volatile transport. To appear in *Neptune*, ed. D.P. Cruikshank and M.S. Matthews. Univ. Arizona Press, Tucson.

Appendix - Spectral Modeling

Introduction

Modeling the reflectance of planetary surfaces is a subject to which many researchers have devoted large portions of their careers. For this reason the spectral modeling techniques I have used are not of my own derivation, but are based on work published by Dr. Bruce Hapke. In particular, the brief review of reflectance modeling in the next section closely follows portions of the paper "Bidirectional Reflectance Spectroscopy: 1. Theory" (Hapke 1981) which will be referred to as Hapke for the remainder of this appendix. Following the review I will discuss the approximations I made for my particular problem, modeling the 2.148 μm-band of N_2, and demonstrate how varying model parameters affects the modeled band.

Review of Reflectance Modeling

Hapke's formulation arose from the desire to describe the reflectance of light from planetary surfaces in terms of the physical parameters of the surface. Empirical expressions, such as Minnaert's law (Minnaert 1941), do not allow an interpretation of this kind, while other theories of light scattering (e.g. Chandrasekhar 1960, Van de Hulst 1963, Hansen and Travis 1974) are not formulated for dense media such as planetary surfaces.

The basic quantity which Hapke derives an equation for is the bidirectional reflectance of a surface, r. The bidirectional reflectance is defined as the ratio of radiant power per unit area per unit solid angle received by a detector viewing a surface at an angle e, measured from the

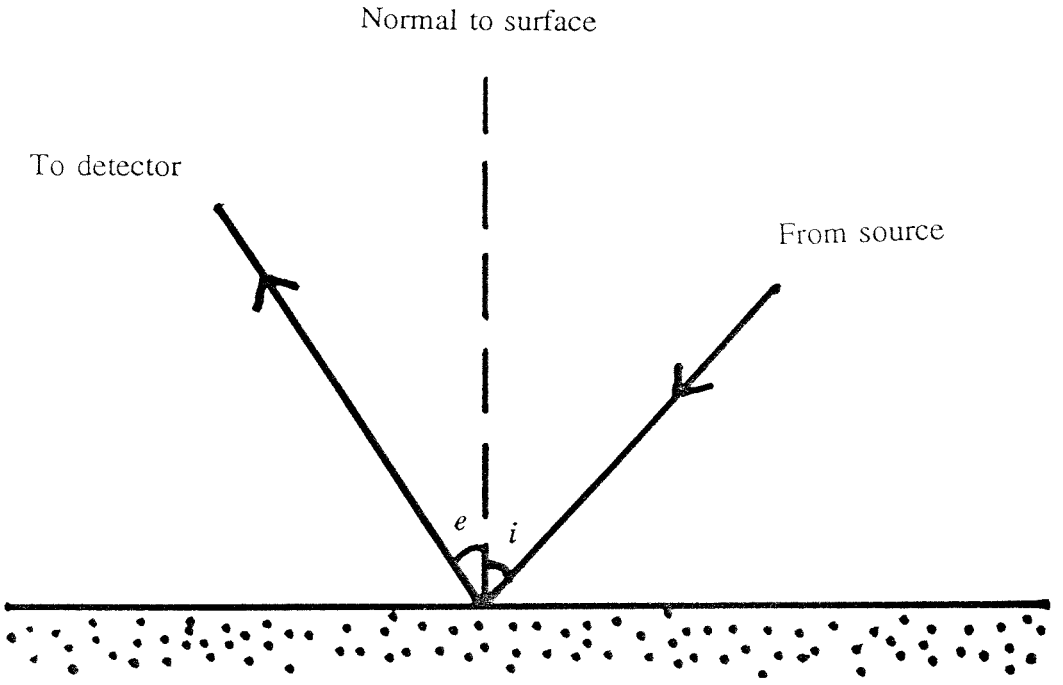

Figure 1 - The geometry used to derive Hapke's bidirectional reflectance coefficient (after Fig. 1, Hapke).

surface normal, to the radiant power per unit area delivered by the source. The source is assumed to be a collimated light, illuminating the surface at an angle *i*, measured from the surface normal, (Fig. 1). The expression for the bidirectional reflectance is

$$r(\mu,\mu_0,g)=\frac{w}{4\pi}\frac{\mu_0}{\mu_0+\mu}\{[1+B(g)]P(g)+H(\mu_0,w)H(\mu,w)-1\}$$

where μ = cos*e*, μ_0 = cos*i*, g is the phase angle between the source of illumination and the observer, and w is the single scattering albedo of the particles which comprise the surface. *P(g)* is the phase function of the surface and *B(g)* is a function which describes the opposition effect. The *H*'s are Chandrasekhar's *H* functions (Chandrasekhar, 1960).

A Lambert surface is one that appears equally bright when viewed from any angle, and reflects all light incident upon it. Hapke shows that the Lambert reflectance, r_L, is

$$r_L=\frac{\mu_0}{\pi}.$$

The quantity which I am interested in modeling is called the radiance coefficient by Hapke, r_c, which I will also refer to as the reflectance. It is defined as the brightness of a surface relative to the brightness of a Lambert surface identically illuminated (or the ratio of the bidirectional reflectance to the Lambert reflectance);

$$r_c = \frac{w}{4}\frac{1}{\mu_0+\mu}\{[1+B(g)]P(g)+H(\mu_0,w)H(\mu,w)-1\}.$$

Assumptions for Modeling the 2.148 μm-band on Triton and Pluto

The term "opposition effect" describes the non-linear increase in log brightness of an object at solar phase angles near 0°. Most icy satellites show such a surge, but, visual observations by Goguen *et al.* (1989) demonstrate that Triton does not display this effect. For this reason I set $B(g) = 0$ when modeling the nitrogen overtone band on Triton. Because of the similarity of the surface compositions of Triton and Pluto, I will also use the same value when calculating spectral band shapes on Pluto.

To simplify the equation for reflectance I have chosen an isotropic phase function ($P(g) = 1.$). For Triton this is shown to be a reasonable choice by the work of Hillier *et al.* (1990) who have analyzed full disk Voyager 2 data of Triton and find that the planet is only very slightly backscattering. As there is no data from Pluto to directly support any value, I again rely on the similarity of Triton and Pluto, and use an isotropic phase function for Pluto as well. Finally, I set $\mu = \mu_0 = 1$, since the majority of the radiation that we receive from both objects will be that which has had near normal incidence and reflection angles.

With these assumptions the equation for the radiance coefficient reduces to

The value of the H function is determined once w and μ are specified, but the evaluation requires

$$r_c = \frac{w}{8} H^2(1,w).$$

numerical techniques. Chandrasekhar (1960) tabulates the values of the H functions for isotropic scattering for certain values of μ and w. For my modeling I have used computer code, provided by Dr. R.N. Clark (personal communication 1993), which interpolates between the values given in Chandrasekhar's tables to determine the values of H.

To use this equation for r_c I must convert the absorption coefficients derived from my laboratory measurements to single scattering albedos. Hapke shows that the single scattering albedo can be represented as

$$w = S_E + \frac{(1-S_E)(1-S_I)e^{-2\alpha D/3}}{1-S_I e^{-2\alpha D/3}}$$

where α is the absorption coefficient of the particle being modeled and D is the particle diameter. S_E and S_I are the external and internal surface scattering coefficients, respectively. These scattering coefficients are functions of the real, n, and imaginary, k, portions of the index of refraction of the material being modeled. The real portion of the index of refraction is assumed to be equal to that of liquid nitrogen (Weast 1980), 1.2. The imaginary portion of the index of refraction is determined by using the absorption coefficient and the relation $\alpha = 4\pi nk/\lambda$. Again, I use a computer code provided by Dr. Roger Clark to evaluate S_E and S_I.

In the region of the 2.148-μm band, nitrogen can be considered an optically thin medium. In this case the equation for the single scattering albedo reduces to

$$w = 1 - \frac{2}{3}\frac{(1-S_E)}{(1-S_I)}\alpha D.$$

The only free parameter in this equation is D.

One final aspect of the modeling which needs to be addressed is that of the difference in

resolution of the laboratory data and the observational data. My laboratory spectra are taken at a higher resolution, 1 cm^{-1}, than the observational data, ≈ 6.5 cm^{-1}. To de-resolve the laboratory data to the resolution of the observational data I convolve the laboratory data with a gaussian having a half width appropriate to the observational data and a depth which makes the area under the gaussian unity. I chose a gaussian for the convolution because the observational data have been smoothed using a gaussian filter.

Modeling Reflectance Spectra

First I could like to demonstrate that small changes in temperature are detectable in the modeled spectra. Figures 2(a) and 2(b) show the N_2 overtone band at various temperatures, all modeled using the same particle diameter, 0.15 cm. The temperatures in part (a) are separated by ≈ 3 K and the models are easily distinguishable from each other by their difference in band depth. Part (b) shows three temperatures, separated by ≈ 0.5 K. In this case, there still is a difference in band depths (the deeper bands being at colder temperatures), but the differences are much smaller. Given these examples I feel confident that temperature information is retained when the transmission data are modeled as reflectance spectra.

Changes in band appearance due to variation of particle size is shown in Fig. 3(a) and (b). Fig. 3(a) shows one set of temperature data converted to reflectance using three different particle sizes. If the middle size particle (0.30 cm) is used as the reference, the smaller particle is 50% smaller (0.15 cm) and the larger particle is 50% larger (0.45 cm). As the figure shows, the band depth changes greatly; the band with 0.30 cm particles is $\approx 35\%$ deeper than the 0.15

Figure 2 - Plots of modeled reflectance spectra for three different temperatures, all using a particle size of 0.15 cm. (a) Temperatures separated by $\approx$ 3.0 K. (b) Temperatures separated by $\approx$ 0.5 K.

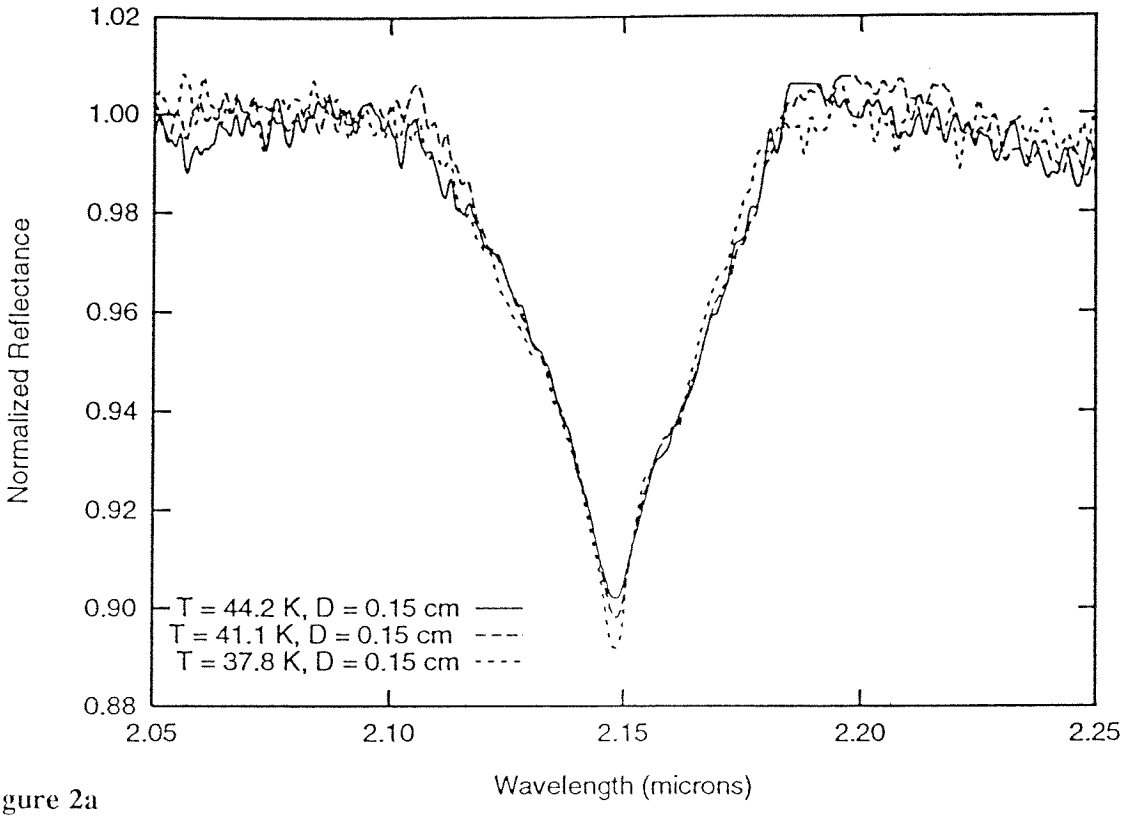

Figure 2a

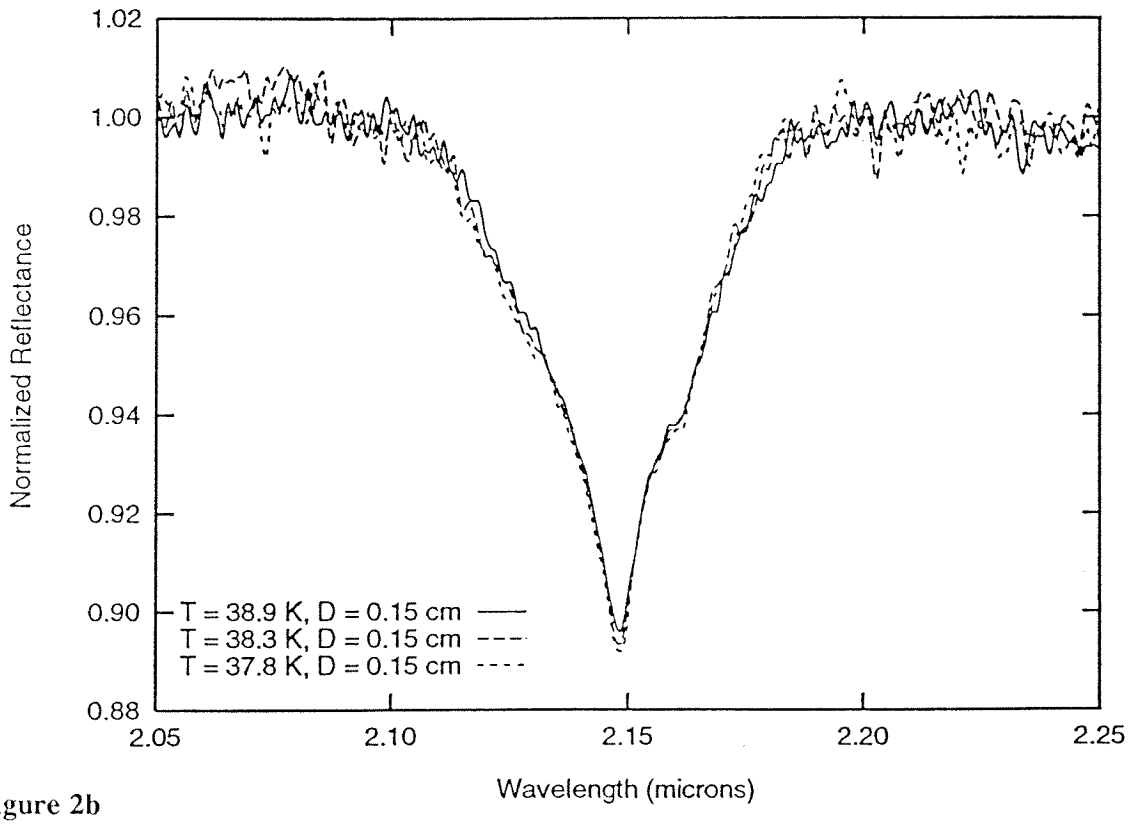

Figure 2b

cm band, while the 0.45 cm band is $\approx$20 % deeper than the 0.30 cm band. Fig 3(a) also shows that as the particle size is increased, details of the band structure are washed out. Notice that some of the small inflections (probably due to noise) on the short wavelength side of the band (near 2.125 μm) are not visible in either of the models incorporating larger particle sizes.

Fig. 3(b) shows three models again, this time with particle sizes differing by 0.01 cm. The differences between the different particle sizes are much smaller. This, combined with the small variation in modeled reflectance between temperatures separated by small amounts, raises the question of whether it is possible to determine a unique temperature/particle size solution when fitting the observational data.

The plots in Figure 4 show attempts to make two modeled spectra, of different temperatures, appear the same by varying their particle size. Figure 4(a) shows two temperatures separated by $\approx$3 K, and in order to match the band depth they had particle sizes differing by 0.02 cm. Fig. 4(b) shows two temperatures separated by $\approx$1 K, and with particle sizes differing by 0.01 cm. For the plots in Fig. 4(a), although the band depths are matched quite well, there is much more deviation in the long wavelength side of the band than there is in the two models shown in Fig. 4(b). Thus, although it is possible to force models with small temperature deviations to be similar by adjusting the particle size parameter, it is not possible to match models with larger temperature differences in this way.

Figure 3 - Plots of modeled reflectance spectra for the same temperature (xx K) for three different particle sizes. (a) particle sizes differing by 0.15 cm. (b) particle sizes differing by 0.01 cm.

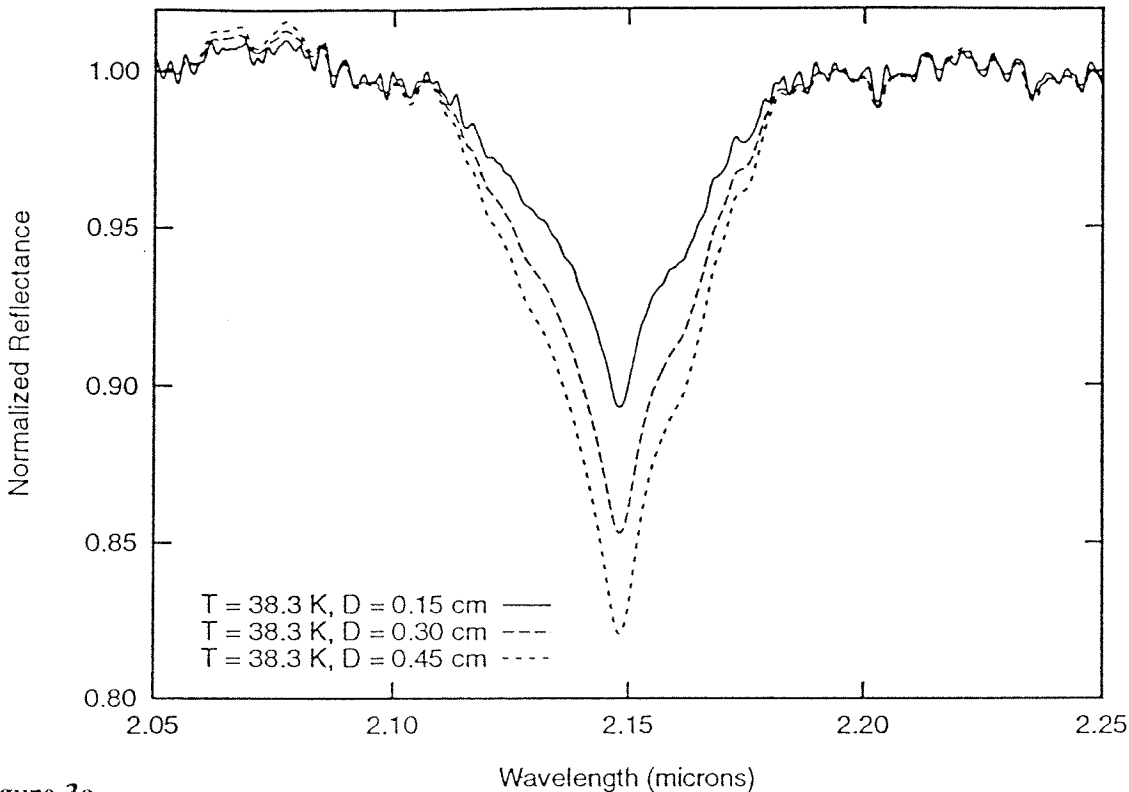

Figure 3a

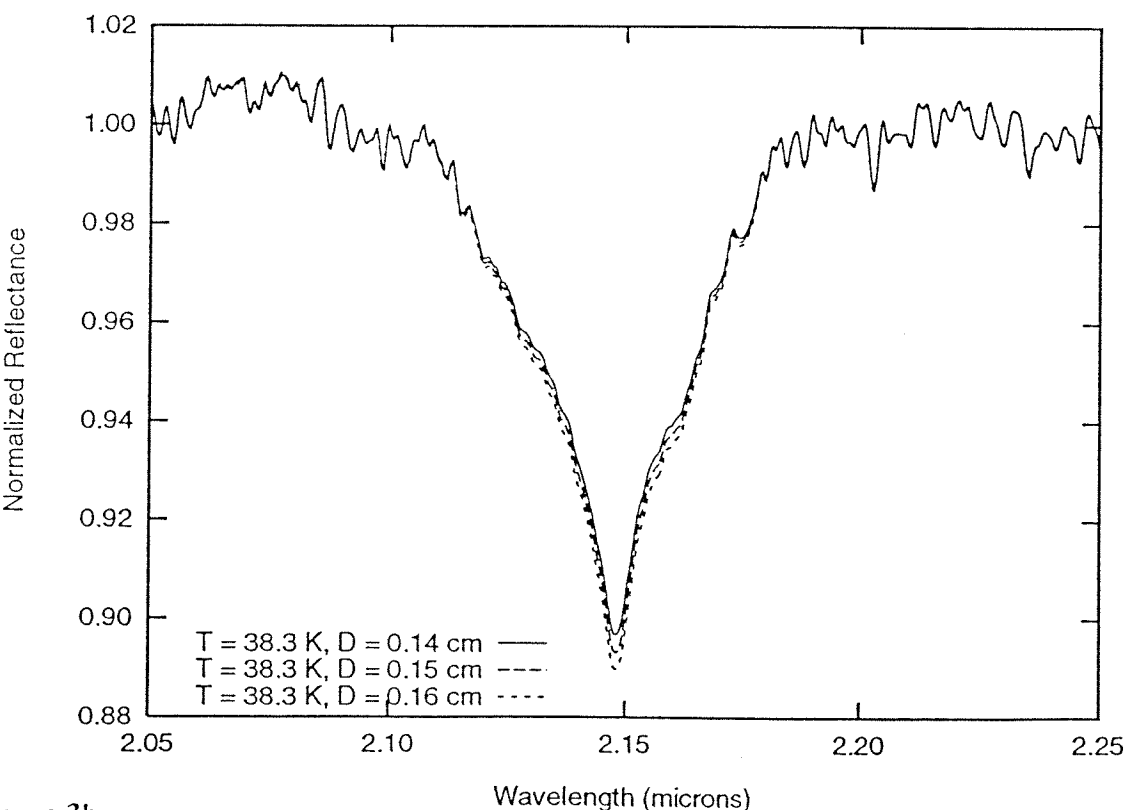

Figure 3b

Summary

This appendix has given a very simple review of how reflectance spectra of planetary bodies can be modeled. It has also explained, in greater detail than in the main text, the assumptions and approximations I used when creating my model spectra.

In addition I have shown that it is possible to distinguish between different temperatures on the basis of the shape of the 2.148 μm nitrogen band. I have also demonstrated how particle size effects the shape of the band, and that it is possible to create models with similar shapes, using different temperatures, by varying the particle size. In light of this I could conclude that this technique is not capable of discerning temperature with an accuracy any greater than ± 1 K.

Figure 4 - Plots of attempts to reproduce identical model results using different temperatures and different particle sizes. (a) Temperature different by $\approx$ 1 K, with particle sizes differing by 0.01 cm. (b) Temperatures differing by $\approx$ 3 K, with particle sizes differing by 0.02 cm.

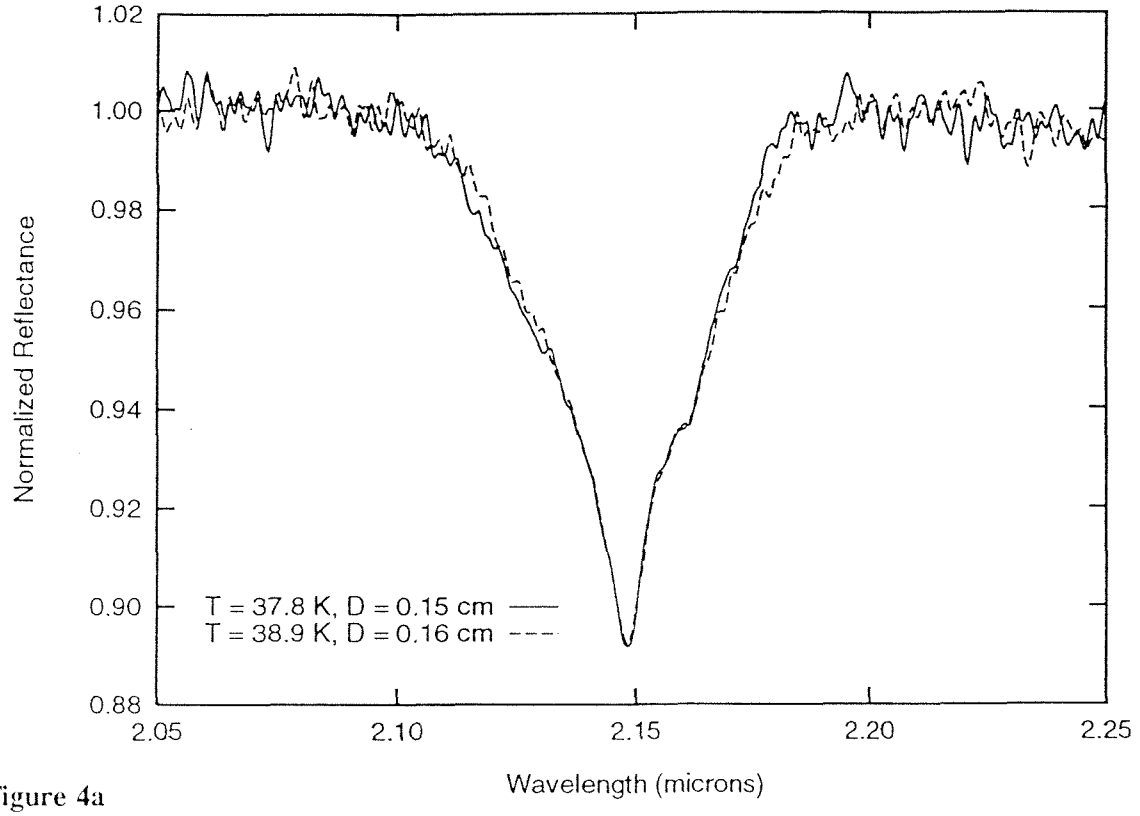

Figure 4a

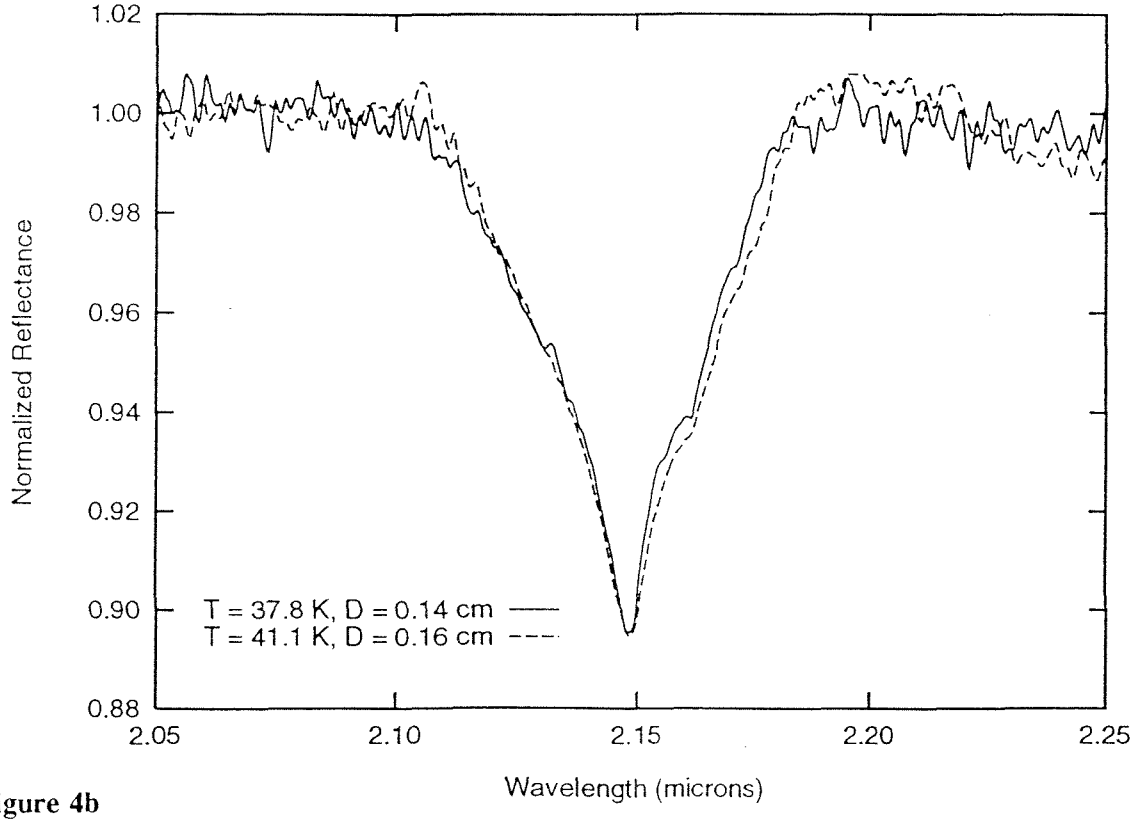

Figure 4b

References

Chandrasekhar, S. 1960. *Radiative Transfer*, Dover Publications, Inc., New York.

Goguen, J.D., H.B. Hammel, and R.H. Brown 1989. V photometry of Titania, Oberon and Triton. *Icarus* **77**, 239-274.

Hansen J.E. and L.D. Travis 1974. Light scattering in planetary atmospheres. *Space Sci. Rev.* **16**, 527-610.

Hapke, B. 1981. Bidirectional reflectance spectroscopy. *J. Geophys. Res.* 86, 3039-3054.

Hillier, J, P. Helfenstein, A. Verbiscer, J. Veverka, R.H. Brown, J. Goguen, and T.V. Johnson 1990. Voyager disk-integrated photometry of Triton. *Science* **250**, 419-421.

Minnaert, M. 1961. Photometry of the Moon. In *Planets and Satellites*, vol. 3 of *The Solar System*, (G.P. Kuiper and M. Middlehurst, Eds.), Univ. Chicago Press, Chicago.

van de Hulst, H.C. 1981. *Light Scattering by Small Particles*. Dover Pub. Inc., New York.

Weast, R.C. 1980. *CRC Handbook of Chemistry and Physics*. CRC Press Inc, Boca Raton, FL.